THE UNIVERSITY *of* EDINBURGH

Studies on the structure, mechanism and inhibition of serine palmitoyltransferase

John Michael Wadsworth

A thesis submitted for the degree of

Doctor of Philosophy

The University of Edinburgh

2014

Declaration

I, John Michael Wadsworth, hereby certify that this thesis has been completed by myself, and that it is a record of my work, and that it has not been accepted in partial or complete fulfilment of any other degree or professional qualification.

John Michael Wadsworth

The University of Edinburgh

2014

Abstract

Sphingolipids and ceramides are essential components of cellular membranes and important signalling molecules. Because of a growing appreciation for their diverse biological roles, understanding of the biosynthesis and regulation of sphingolipids has recently become a key goal in drug discovery. Serine palmitoyltransferase (SPT) is a pyridoxal 5′-phosphate (PLP)-dependent enzyme that catalyses the condensation between L-serine and a long-chain acyl thioester such as palmitoyl-CoA (C_{16}-CoA). This first step in sphingolipid biosynthesis is conserved in all organisms studied to date, from microbes to man.

The fungal natural product myriocin is a potent inhibitor of SPT; however, the molecular details of inhibition are not fully understood. Myriocin contains a long alkyl chain and a polar head group thus it displays features of both SPT substrates. Therefore, the prevailing hypothesis is that inhibition of SPT occurs because myriocin acts as a mimic of a key transition state of the catalytic mechanism. Through a combination of UV-vis spectroscopy, mass spectrometry, x-ray crystallography and enzyme inhibition assays it has been possible to study the interaction between *S. paucimobilis* SPT and myriocin. I have shown that myriocin initially forms an inhibitory PLP:myriocin aldimine complex in the active site that displays a K_i of 967 nM. Interestingly, this complex is susceptible to unexpected, slow enzymatic degradation. The mechanism for myriocin breakdown has been elucidated as a retro-aldol type reaction, which results in cleavage of the C2-C3 bond producing a C18 aldehyde. This aldehyde is then capable of covalently modifying the active site lysine265, forming a second (suicide) inhibitory complex and rendering the enzyme catalytically inactive.

Substitution of the active site lysine produced SPT K265A, an inactive enzyme that did not catalyse the breakdown of the PLP:myriocin complex. However, the determination of the crystal structure of the SPT K265A:PLP-myriocin complex revealed that the myriocin had undergone decarboxylation. Nevertheless, this SPT:PLP:decarboxymyriocin structure revealed details about myriocin's mechanism of inhibition for the first time. The novel mechanism of myriocin degradation has

implications on the structure activity relationship (SAR) and design of drugs targeted towards SPT, the role of feedback regulation by long chain aldehydes and further expands the range of reactions catalysed by this important enzyme.

As well as inhibition studies the structure of bacterial SPT was also examined by preparing an N-terminally truncated *S. paucimobilis* SPT. This version, shortened by 21 amino acids, was ~5-fold slower than the wild-type enzyme and suggests that the N-terminus may play a role in catalysis. Additional work has been undertaken to study an unusual membrane-bound viral SPT, composed of two naturally fused open reading frames (SPT2-SPT1) with the proposed SPT2 domain at the N-terminus and the SPT1 domain at the C-terminus. To study soluble mimics of this interesting fusion I prepared a bacterial *S. paucimobilis* SPT fused wild-type and mutant construct and isolated a fused SPT2-SPT1 with what appears to be single PLP-binding site.

Acknowledgements

I would like to thank Dr Dominic Campopiano for his guidance throughout the course of my PhD and his relentless enthusiasm for all things biochemistry. Secondly thank you to Professor Jim Naismith for collaborating with us on our quest for SPT crystals. Thank you also to Professor Teresa Dunn who supplied us with the SPT clone on which most of this work was carried out and also showed us great hospitality when we visited Washington, D.C.

I was very fortunate to work with some exceptional post-doctorate researchers during my time in Edinburgh who have all taught me a great deal. I would like to thank my friend Dr Dave Clarke for his exceptional mass spectrometry capabilities and openly acknowledge that he undertook all the mass spectrometry analysis detailed within this work. I would also like to thank Dr Jonny Lowther who taught me the intricacies of enzyme kinetics and Dr Stephen McMahon, in St. Andrews, for helping me with the dark art of crystallography.

Research can at times be a relatively lonely field as others struggle to understand the challenges you face. From the outset of my PhD I was lucky to be working with Ashley Beattie who despite her initial hippy tendencies became one of my best friends. Thank you very much for your practical help, your scientific input but most of all thank you for your continued friendship.

I would also like to thank past and present colleagues from lab 229 for their help and humour. With special mention to Chris, Pete, Sam, Scott, Ed, Marine, Lily and Guiomar. A special mentioned should also be made to one of my oldest friends, Martin Wieczysty, who made the move to Edinburgh much more enjoyable by agreeing to share a flat with me.

Finally I would like to thank all my family, both members present before I started my PhD and my beautiful wife and baby who joined me at various stages along this long the way. My parents deserve a special mention as they instilled the importance of learning and working hard from a very young age and for that I am very grateful. Sarah has been a great support to me throughout the last four years and now I look forward to spending the rest of our life together as Dr and Dr Wadsworth.

Contents

List of Figures, Tables and Equations

Abbreviations

AAT	Aspartate aminotransferase
ALAS	5-aminolevulinic acid synthase
AmSPT	American SPT
AONS	8-amino-7-oxononanoate synthase
AOS	α-oxoamine synthase
atm	Atmosphere – unit of pressure. 1 atm = 101325 Pa
BCA	Bicinchoninic acid
BSA	Bovine serum albumin
CFE	Cell free extract
CγL	Cystathionine-γ-lyase
CγS	Cystathionine-γ-synthase
CoA	Coenzyme A
CoASH	Free Coenzyme A
CHO	Chinese Hamster Ovary
CID	Collision induced dissociation
CqsA	Cholera CAI-1 synthase
CTLL-2	IL-2 dependent cytotoxic T-cells
DMSO	Dimethyl sulfoxide
DNA	Deoxyribonucleic acid
doxSAs	Deoxysphingolipids
deaza-PLP	Deazapyridoxal 5´-phosphate
DNA	Deoxyribonucleic acid
DTNB	5,5'-dithiobis-(2-nitrobenzoic acid)
EDTA	Ethylenediaminetetraacetic acid
ER	Endoplasmic reticulum
ESI	Electrospray ionisation
FLAG®	A proprietary purification system developed by Sigma Aldrich that consists of an octapeptide tag that can be added to a protein to aid purification
F_o-F_c	Observed structure factor amplitudes -calculated structure factor amplitudes
Fum8/Fum8p	Fumonisin 8
FTY720	Fingolimod – Novartis Drug (Trade name – Gilenya)
GDC	Glutamate decarboxylase
HPLC	High Performance Liquid Chromatography
HSAN1	Hereditary sensory and autonomic neuropathy type I
IC_{50}	The concentration required to cause 50% inhibition of the desired activity.
ICR	Ion Cyclotron Resonance
IPTG	Isopropyl β-D-1-thiogalactopyranoside
IUPAC	The International Union of Pure and Applied Chemistry
LC-ESI	Liquid Chromatography followed by Electrospray Ionisation

LC-FT-ICR	Liquid Chromatography Fourier Transform Ion Cyclotron Resonannance Mass Spectrometry
JqsA	Janthionbacterium JAI-1 synthase
KBL	2-amino-3-ketobutyrate-CoA ligase
K_d	Dissociation constant
KDa	kilodalton
KDS	3-ketodihydrosphingosine
KDSR	3-ketodihydrosphingosine reductase
K_m	The Michaelis constant – the substrate concentration at half maximal velocity
KPhos	Potassium Phosphate buffer
LB	Lysogeny broth
LCB	Long chain base
lcb1	Gene responsible for lcb1 protein
LCB1	non-PLP binding subunit of SPT
lcb2	Gene responsible for lcb2 protein
LCB2	PLP binding subunit of SPT
LqsA	Legionella LAI-1 synthase
M	Mega ($x10^6$)
ms	Milliseconds
MS	Mass spectrometry
MW	Molecular weight
NIH	National Institutes of Health
NMR	Nuclear magnetic resonance
NTA	Nitrilotriacetic acid
OASU	O-actylserine sulfhyrylase
Orf34	5-aminolevulinate synthase
ORM	Orosomucoid
ORMDL	Orosomucoid like
PCR	Polymerase chain reaction
PDB	Protein Data Bank
pdx	Pyridoxine biosynthesis
PigH	Seryltransferase from Prodigiosin biosynthesis
PLP	Pyridoxal 5´-phosphate
PMP	Pyridoxamine 5´-phosphate
ppm	parts per million
PS-DVB	Polystyrene-divinylbenzene
RedN	Amino transferase from 2-undecylpyrrole biosynthesis
RF	Radio frequency
RMSD	Root-mean-square deviation
S1P	Sphingosine-1-phosphate
S1PL	Sphingosine-1-phosphate lyase
SAC1	Phosphatidylinositide phosphatase
SAR	Structure activity relationship

SD	Serine dehyratase
SDM	Site directed mutagenesis
SDS-PAGE	Sodium dodecyl sulfate-polyacrylamide gel electrophoresis
SerT	Seryltransferase
SHMT	Serine hydroxymethyltransferase
SK1	Sphingosine kinase
SOC	Super optimal broth with catabolite repression
SOR1	Singlet oxygen resistance gene from *Cercospora nicotianae*
SPOTS complex	**s**erine **p**almitoyltransferase, **O**rm 1/2, **T**sc3, **S**ac1complex
spSPT	C-terminally tagged *Sphingomonas paucimobilis* SPT
SPT	Serine palmitoyltransferase
SR	Serine racemase
ssSPT	small subunit of SPT
SxtA	Saxitoxin A
TAE	Tris-acetate-EDTA buffer
TamD	Tambjamine D
TEV	Tobacco Etch Virus
TLC	Thic Layer Chromatography
Tsc3	Gene coding for Tsc3p protein
Tsc3p	Small protein capable of up regulating the activity the yeast SPT complex
WT	Wild-type

Chapter 1: Introduction

1 Introduction

1.1 Pyridoxal 5′-phosphate

Although pyridoxal 5′-phosphate (PLP) (Figure 1-1) is one of the less complex organic cofactors it has been shown to catalyse a large and varied range of reactions. PLP is known to play a role in over 160 enzymatic reactions with almost 1.5% of all genes in prokaryotes encoding for a PLP dependent enzyme.[1] In contrast, the percentage of enzymes predicted to be PLP dependent in eukaryotes is decidedly smaller; probably due to two reasons – (i) PLP plays a more important role in basic metabolic pathways; and (ii) sequence variation making identification of PLP dependent enzymes difficult. Therefore the exact number of PLP-dependent enzymes in eukaryotes is unknown with new PLP dependent enzymes still being discovered.[2-3]

PLP is part of the vitamin B6 group which consists of 6 vitamers, pyridoxal, pyridoxine and pyridoxamine and their phosphorylated forms (Figure 1-1).

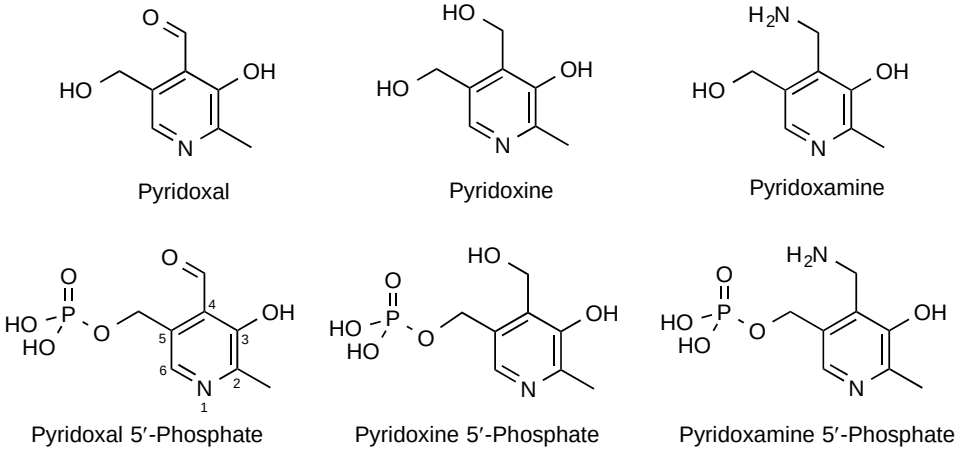

Figure 1-1 The six chemical forms of vitamin B6

PLP is only synthesised in bacteria, plants and fungi but not by humans where it is acquired exogenously from their diets and enzymatic salvage pathways.[4] Two *de novo* biochemical pathways are responsible for PLP synthesis; the *pdx* family and *SOR1*.[5] Neither of these are known to occur in the same organism making them truly divergent. *Pdx* is an abbreviation for pyridoxine and is used to denote the genes and enzymes present in this PLP biosynthetic pathway. The *pdx* pathway consists of 6 genes in total, four of which are unique to PLP biosynthesis and although best

characterised in *E. coli*. this family also exists in the plants and fungi.[6] *SOR1* was originally discovered by its ability to provide resistance to singlet oxygen species and was therefore denoted SOR for singlet oxygen resistance. However its ubiquitous nature and highly conserved sequence homology later led to the knowledge that it is also involved in PLP biosynthesis.[5] Until recently it was believed an unusual precursor (1-deoxyxylulose 5-phosphate, dxp) was required for vitamin B6 synthesis by the *pdx* family of enzymes but it has now been elegantly shown that the precursors are readily available from glycolysis (glyceraldehyde 3-phosphate) and the pentose phosphate (ribose 5-phosphate or ribulose 5-phosphate) pathways.[7-8] Interestingly Pdx1 not only catalyses the majority of PLP formation but has also been shown to isomerise both the precursor pentose and triose to their most utilisable forms.[9] A second enzyme (Pdx2) is required to generate ammonia from glutamine and facilitates its safe transport to the active site of Pdx1. A typical PLP biosynthetic route is summarised in Figure 1-2.

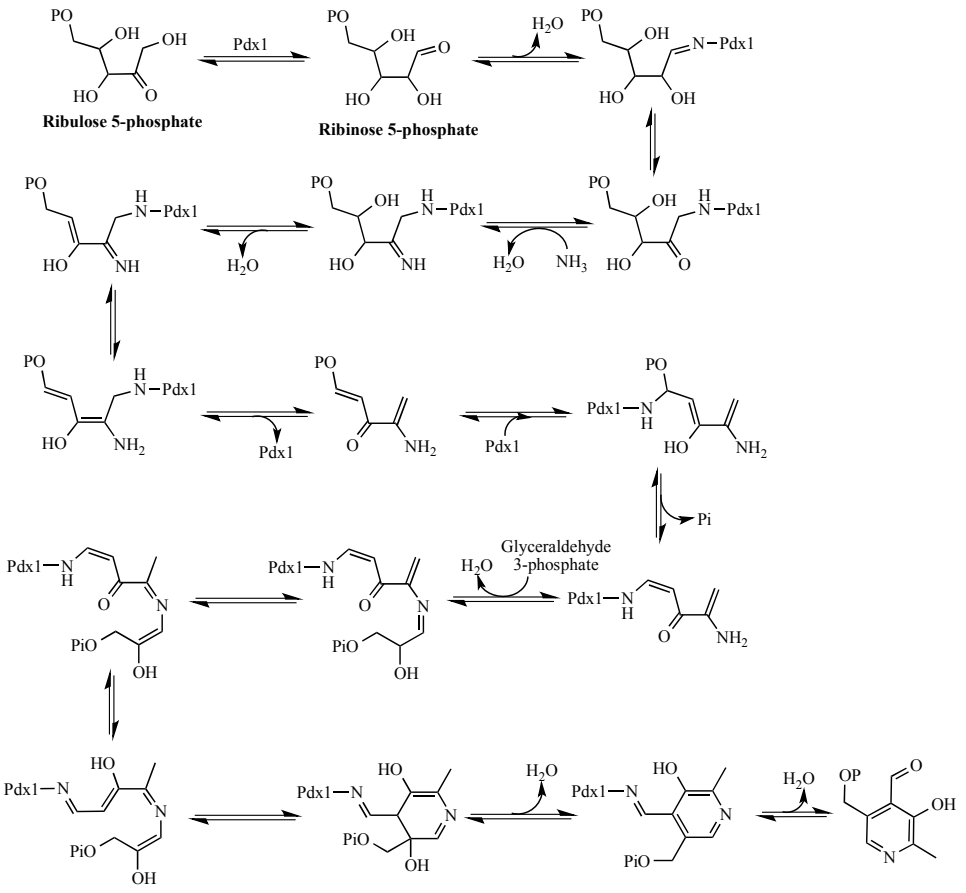

Figure 1-2 Suggested Pdx1 dependent biosynthesis of PLP[8]

There are more than 160 chemical reactions catalysed by PLP which span a large range of chemistries including racemisation, decarboxylation, α-elimination and substitution, transamination, β-substitution and replacement and γ-elimination and substitution examples of each are given in Table 1-1.

Reaction	Example	Chemistry
Racemisation	Serine racemase[10] (SR)	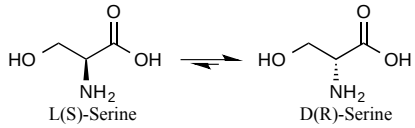 L(S)-Serine D(R)-Serine
Decarboxylation	Glutamate decarboxylase[11] (GDC)	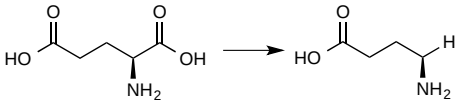 L(S)-Glutamic acid γ-aminobutyric acid
α-elimination	Serine hydroxymethyltransferase[12] (SHMT)	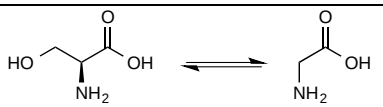 L(S)-Serine Glycine
α-substitution	Aspartate aminotransferase[13] (AAT)	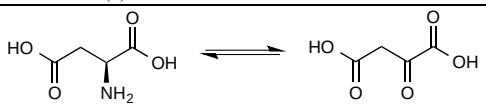 L(S)-Aspartic acid Oxaloacetic acid
β-elimination	Serine dehydratase[14] (SD)	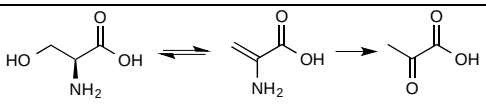 L(S)-Serine Pyruvate
β-substitution	O-acetylserine sulfhydrylase[15] (OASU)	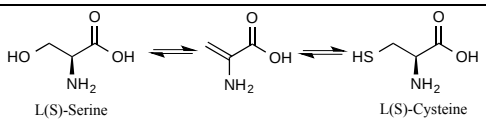 L(S)-Serine L(S)-Cysteine
γ-elimination	Cystathionine γ□lyase[16] (CγL)	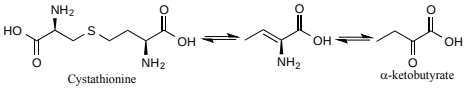 Cystathionine α-ketobutyrate
γ-substitution	Cystathionine γ□□□□□□□□□[17] (Cγ□)	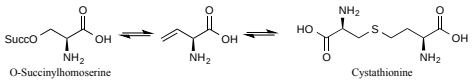 O-Succinylhomoserine Cystathionine

Table 1-1 Summary of PLP chemistries

Despite the array of chemistry catalysed by the cofactor, PLP, the general catalytic mechanism remains consistent throughout. PLP is initially held in the active site via an imine bond with an active site lysine residue in what is commonly referred to as the covalent "internal aldimine". The well established nomenclature also dictates that the PLP-free form of the enzyme is known as the "apo-form" while the PLP-bound

form is referred to as the "holo-form". Several other active site interactions have also been shown to be important for PLP binding including π-stacking with aromatic residues above the PLP ring and hydrogen bonds to the pyrimidine nitrogen.[18-19] Upon substrate binding the internal aldimine is replaced by an imine formed between the amine of the substrate and PLP to produce the "external aldimine". Additionally both the internal and external aldimines can exist in two tautomeric forms, a ketoenamine and an enolimine, which gives rise to the characteristic double maxima UV-vis spectrum (Figure 1-3).

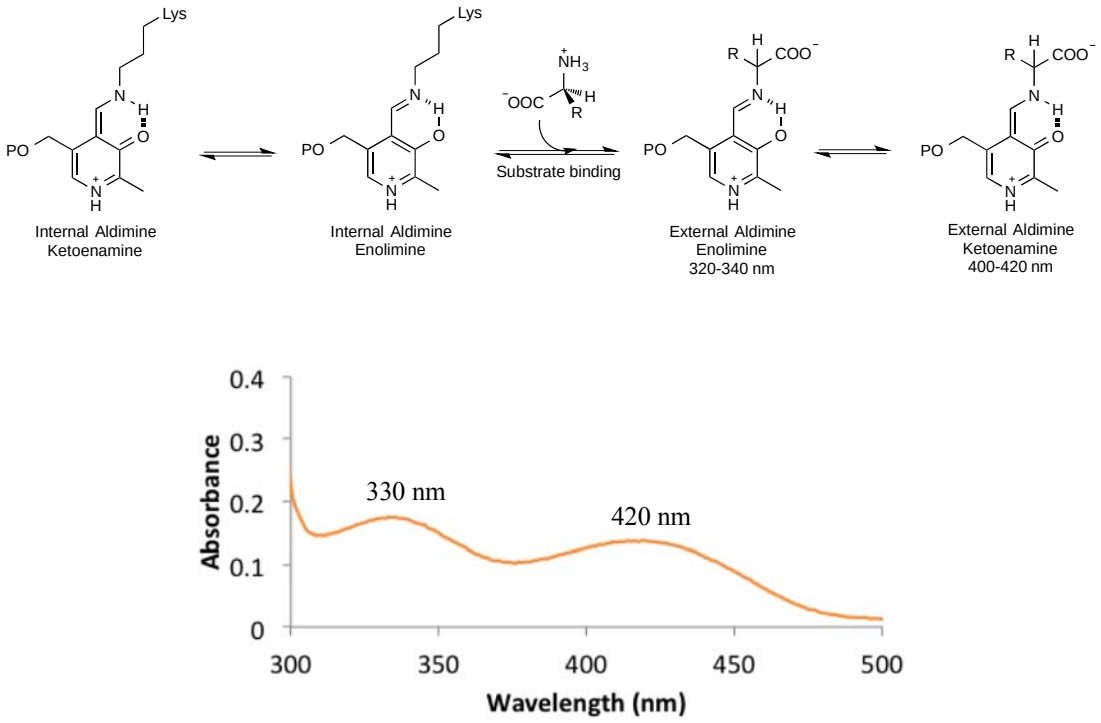

Figure 1-3 PLP binding in *S. paucimobilis* SPT
Top – Chemistry of PLP binding to both enzyme and substrate. Internal aldimine and external aldimine in both tautomeric forms. **Bottom –** UV-vis spectrum of 40 μM *S.paucimobilis* SPT Enolimine and ketoenamine absorb at 330 and 420 nm respectively.

The chemistry catalysed by PLP extends impressively far from the known electron sink capabilities of the pyridine ring. The γ-elimination and substitution reactions are made possible by double proton extraction allowing conjugation to continue out to the γ-carbon. This extension of the conjugated system coupled with the formation of a reactive enamine at the γ-carbon allows reactions to proceed. All the above examples require PLP to be "captured" inside an enzyme with the chemistry being

promoted by surrounding amino acids but PLP is also capable of catalysing reactions with no enzymatic assistance.

The initial discovery of the non-enzymatic dependent activity by pyridoxal was made by Metzler and Snell in 1952.[20-22] It was found that pyridoxal could transaminate amino acids to produce pyridoxamine and a keto-acid with the mechanism being completely elucidated through the extensive use of UV-vis spectroscopy.[23] Although non-enzymatic, these reactions all required a metal ion to chelate to the 3-hydroxy and the imine nitrogen. Pyridoxal is also capable of decarboxylating the α-carbon without the need of an enzyme, albeit slowly. This process follows a similar mechanism to transamination, where a chelated metal ion holds the system planar and aids the movement of the electrons into the pyridine ring.[24] Controversially, Toney *et. al* have since shown that the metal ion is not required for catalytic activity and only aids Schiff base formation when experiments are performed in non-saturating conditions.[25] More recently organic chemists have adapted pyridoxal and have now produced a pyridoxal based system capable of racemising amino acid derivatives which could be coupled with another enzyme in a dynamic kinetic resolution method.[26]

As previously mentioned, the chemical versatility of PLP is derived from its structure, which has been extensively studied. The vast array of information available now provides greater understanding of PLP chemistry and allows for accurate predictions of new reactivity based upon robust chemical understanding. PLP structure and its relation to function can be split into two categories. Firstly the stereoelectronic aspect, based largely around a hypothesis forwarded by Dunathan, and secondly the chemical structure, i.e. functional group incorporation and location.

Dunathan first proposed his stereoelectronic rationale for PLP activity in 1966.[27] His hypothesis was based upon hyperconjugation and can be used to predict which bond is to be broken in any specific reaction, if the three-dimensional arrangement of the substituents is known. The basic premise of Dunathan's work is that the chemistry PLP will perform is determined initially by the breaking of whatever α-carbon bond

is perpendicular to the PLP ring (Figure 1-4). The perpendicular sigma bond is weaker due to hyperconjugation and the transition state is also lower in energy due to the developing p-orbital being in optimal position for conjugation into the π-system. To date, the Dunathan hypothesis has held true - with all published structures so far confirming the theory.

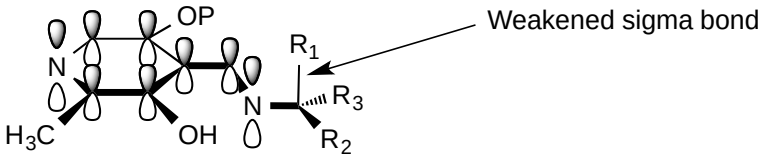

Figure 1-4 Dunathan Intermediate
PLP is drawn perpendicular to the plane of the page with thick bold bonds pointing towards the reader and thin bonds pointing away. P orbitals have been added to show the possible overlap and hyperconjugation. The weakened α-carbon bond has been highlighted.

To date, the 2-methyl group of PLP is the only functional group, of the five (methyl, pyridine nitrogen, aldehyde, hydroxyl and phosphate), not to have been extensively investigated and its importance shown. Nevertheless until its role is systematically analysed its importance can only be hypothesised. The methyl group has the potential to both change the electronics of PLP, by donating electrons inductively onto the ring. As well as the obvious steric affects such as the ability to subtly change conformation and thus influence enzyme selectivity. Most recently the role of the phosphate in PLP was analysed in our research group by Beattie *et al.*, showing for the first time that the phosphate of PLP can be used to orientate the α-carbon substituents.[28] In the structure of the *S. paucimobolis* serine palmitoyltransferase (SPT) PLP:L-serine external aldimine, the phosphate group of PLP was shown to hydrogen bond to the hydroxyl group of L-serine, limiting rotation around the nitrogen-α-carbon bond.[29] This nuance of PLP chemistry came from the close examination of PLP crystal structures and partially explains the amino acid specificity of SPT.[29]

The aldehyde moiety of PLP is universally accepted as essential; ever since the initial understanding of PLP mechanisms and the requirement for imine formation in both the internal and external aldimine was known, therefore its importance cannot be questioned.[30] Indeed the significance of the carbonyl functionality, due to its ability

to form Schiff bases, has prompted the use of acetone and other ketones in comparison studies with PLP.[31-33]

The role of the hydroxyl group in PLP has not been probed with most of the discussion focussing on whether the oxygen remains protonated and what affect this has on the electronics of the ring.[31] In the early days of PLP chemistry, the C3 hydroxyl group was shown to be catalytically essential in non-enzymatic reactions.[24] The use of several C3 derivatives produced no active compounds and was the basis for the hypothesis that the hydroxyl group hydrogen bonded to the imine nitrogen. Indeed a hydrogen bond between the C3 hydroxyl and the imine nitrogen has been confirmed by recent enzyme crystal structures.[29] The pyridine ring was always thought to provide the basis for PLP chemistry due to the belief that it formed an electron sink. Pyridine was believed to be the ideal electron sink as it is more electron deficient than benzene, due to the electronegative nitrogen. The electron withdrawing capacity could be increased further by protonation of the nitrogen thus producing an even more electron deficient ring. Not long after the discovery of the catalytic capability of PLP it was widely understood that the pyridine nitrogen needed to be protonated to allow Cα deprotonation, this hypothesis has now been shown not to be correct for all PLP-dependent enzymes.[34] Toney *et al.* demonstrated that the protonated nitrogen and the extra electrophilic capacity that follows is only required in PLP reactions where a 1,3-prototropic shift is required (Figure 1-5).

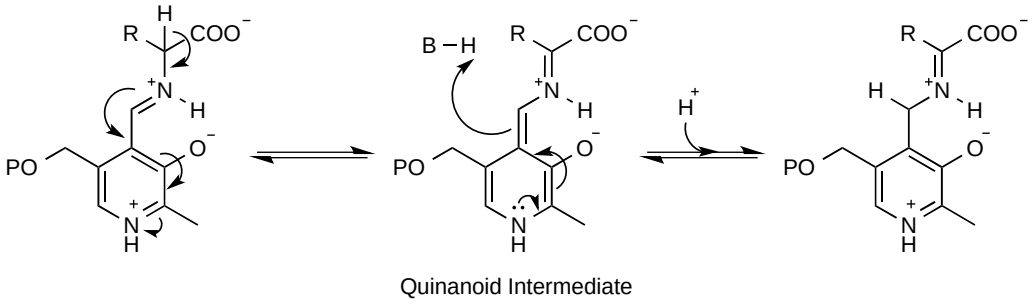

Figure 1-5 Example of a 1,3-prototropic shift
Movement of a proton from the α-carbon to the β-carbon of PLP. The shift occurs via a quinanoid intermediate and is catalysed by a near-by base allowing nucleophilic attack onto the α-carbon and subsequent seperation of the substrate forming a pyridoxal amine derivative.

Toney suggests that for PLP reactions not requiring this shift the carbanion stabilisation offered through the Schiff base/imine is sufficient. An example of a reaction that requires a 1,3-prototropic shift is a transamination whilst racemisations and eliminations do not require such a rearrangement.

As further proof of the effect variation in electrophilicity has upon reaction outcome Toney *et al.* used 1-deazapyridoxal-5′-phosphate (deazaPLP, Figure 1-6); a PLP derivative where the pyridine nitrogen has been replaced with a carbon.[34]

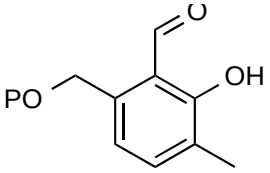

Figure 1-6 The structure of 1-deazapyridoxal-5′-phosphate (deazaPLP)

Substitution of PLP for deazaPLP decreased the catalytic activity for all the enzymes used in this study but crucially only the reactions that required a protonated pryridine nitrogen e.g. reactions that required 1,3-prototropic shift demonstrated a compete lack of function. These findings imply that the "electron sink" capabilities of PLP can be partially fulfilled by any aromatic system with only a few PLP catalysed reactions requiring the "full" electrophillicity offered by the pyridine ring.

1.2 PLP dependent enzymes

PLP-dependent enzymes are classified by their tertiary structure and are split into 5 categories, or fold-types (type I, II, III, IV and V) (Figure 1-7). It was initially hypothesised that the enzymes function was related to its fold-type but over time and with the publication of more structures this has since been shown not to be true.[35-36]

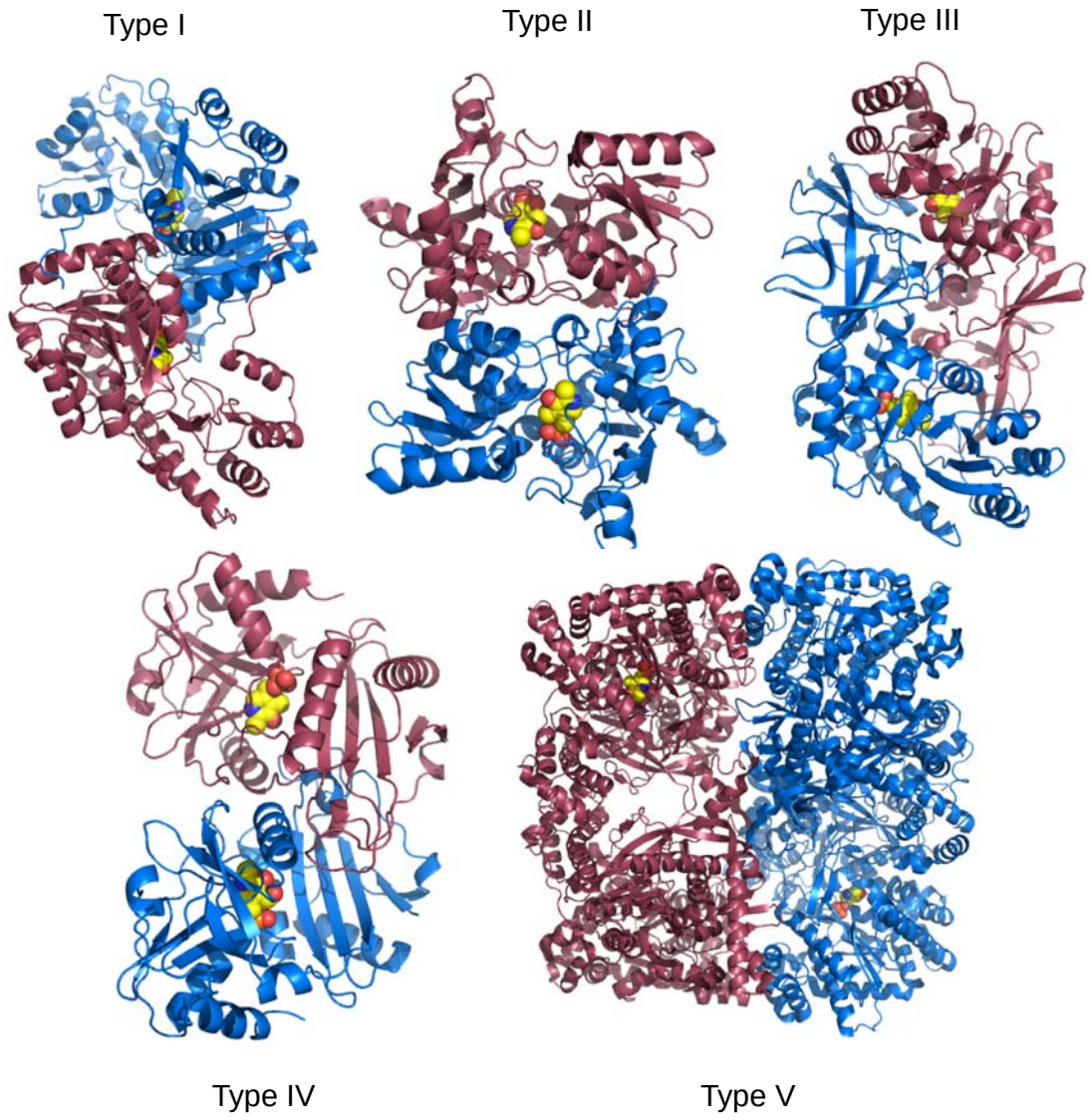

Figure 1-7 Representations of the five different fold types of PLP enzymes
Each monomer is coloured differently and PLP is shown in spacefill with carbons in yellow. **Top Left.** Fold Type I - *E. coli* aspartate aminotransferase; PDB code: 1ASN. **Top Middle.** Fold Type II - *Salmonella typhimurium* O-acetylserine sulfhydrylase; PDB code: 1OAS. **Top Right.** Fold Type III - *Bacillus stearothermophilus* alanine racemase; PDB code: 1SFT **Bottom Left.** Fold Type IV - *Thermophilic Bacillus sp*. D-amino acid aminotransferase; PDB code: 1DAA. **Bottom Right.** Fold Type V – *Rabbit* glycogen phosphorylase; PDB code: 1GPA

Fold type I is the largest sub class of PLP dependent enzymes and also the most diverse class.[37] Within this large sub class exists the α-oxoamine synthase (AOS) family or CoA-dependent acyltransferases which constitutes a small but still growing family of enzymes many of which play important biological roles as summarised in Table 1-2. This thesis will concentrate on one member of the AOS, SPT.

Enzyme	Amino acid	Thioester	Product	Pathway	PDB Code
Serine Palmitoyltransferase (SPT)	L-serine	Palmitoyl CoA	3-ketodihydrosphingosine (KDS)	Sphingolipid	*SP* apo: **2JGT** *SP* holo: **2JG2** *SP* L-serine:PLP: **2W8J** *SW* holo: **2X8U** *SM* L-serine:PLP: **3A2B**
2-amino-3-ketobutyrate-CoA ligase (KBL)	Glycine	Acetyl-CoA	2-amino-3-ketobutyrate (AKB)	Threonine degradation	*EC* holo: **IFC4** *CB* holo: **3TQX**
5-aminolevulinate acid synthase (ALAS)	Glycine	Succinyl-CoA	5-aminolevuliante (ALA)	Tetrapyrrole	*RC* holo: **2BWN** *RC* glycine:PLP: **2BWP** *RC* succinyl-CoA:PLP: **2BWO**
8- amino-7-oxononanoate synthase (AONS)	L-alanine	Pimeloyl-CoA	8-amino-7-oxononanoate (AON)	Biotin	*EC* apo: **1BSO** *EC* holo: **1DJE** *EC* AON:PLP: **1DJ9**
Cholerae CAI-1 Synthase (CqsA)	L-threonine or , L-2-aminobutyric acid or (S)-adenosylmethionine	Decanoyl-CoA	Cholera autoinducer-1 (CAI-1)	Quorum sensing	*VC* apo: **2WK7** *VC* holo: **2WK8** *VC* L-threonine:PLP: **2WK9** *VC* Decanoyl-CoA:PLP: **2WKA**
Legionella LAI-1 Synthase (LqsA)	-	-	-	-	-
Janthionbacterium JAI-1 Synthase (JqsA)	-	-	-	-	-
Seryl transferase (SerT/PigH)	L-serine	Pyrrolyl-β-ketoacyl-S-ACP	4-hydroxy-2,2'-bipyrrole-5-methanol (HMB)	Prodigiosin	-
Fumonisin8 (Fum8)	L-alanine	Steroyl-ACP		Fumonisin	-
SaxitoxinA (SxtA)	Arginine	Proponoyl-CoA	Saxitoxin intermediate	Saxitoxin	-
5-aminolevulinate synthase (Orf34)	Glycine	Succinyl-CoA	5-aminolevulinate (ALA) (cyclase)	2-amino-3-hydroxycyclopent-2-enone polyketide (C5N)	-
TambjamineD (TamD)	L-serine	Malonyl-CoA	Tamjamine intermediate	Tamjamine	-
Amino transferase (RedN)	Glycine	Acyl-ACP	Pyrrole intermediate	2-undecylpyrrole biosynthesis.	

Table 1-2 Members of the AOS family

1.3 Sphingolipids

The discovery of sphingolipids is accredited to Johann Ludwig Wilhelm Thudichum, a German born medical doctor and biochemist, in 1884.[38] Upon discovery Thudichum noted the compounds were *"...of an alkaloidal nature, and to which, in commemoration of the many enigmas which it has presented to the inquirer, I have given the name of Sphingosin.*" The naming of the compounds after the puzzling Egyptian creature the sphinx has remained and upon elucidation of the structure of sphingosine in 1947 by Carter *et al.* it was decided to name " *... those lipids derived from sphingosine as sphingolipids.*"[39-40] This definitively non-systematic/IUPAC nomenclature has led to some confusion in the literature; however a sphingolipid is generally recognisable from the amino diol (or sometimes triol) head group connected to a long alkyl chain (Figure 1-8). More specifically the configuration of the sphingoid base of which sphingosine, dihydrosphingosine or phytosphingosine (Figure 1-8) are three examples can be used to help identify the host organism e.g. dihydrosphingosine is the major base in mammalian cells while phytosphingosine is the principal base in plants, yeast and fungi, but some crossover does exist.[41]

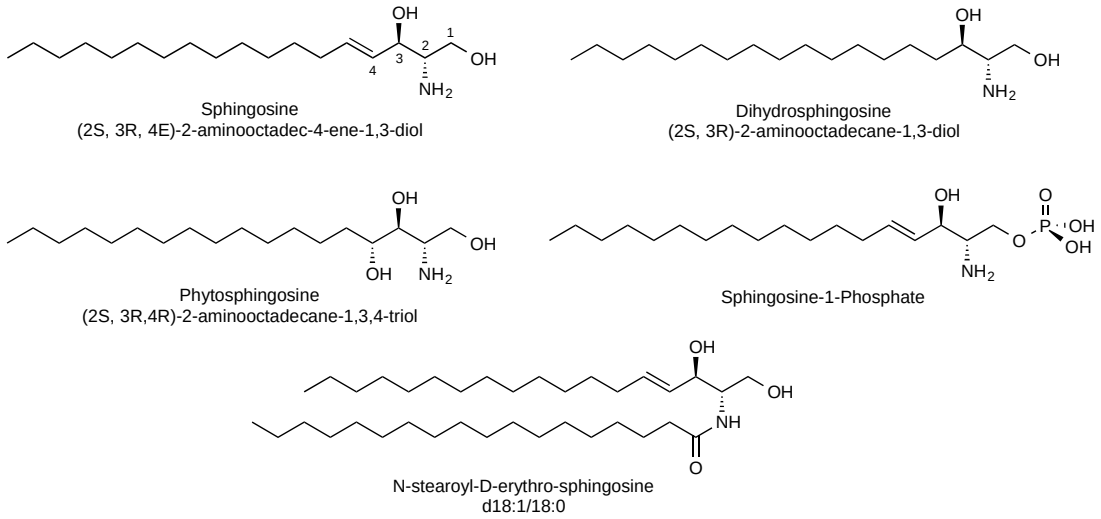

Figure 1-8 Structure of the three sphingoid bases along with the most widely known sphingolipid (sphingosine-1-phosphate) and a simple example of a ceramide

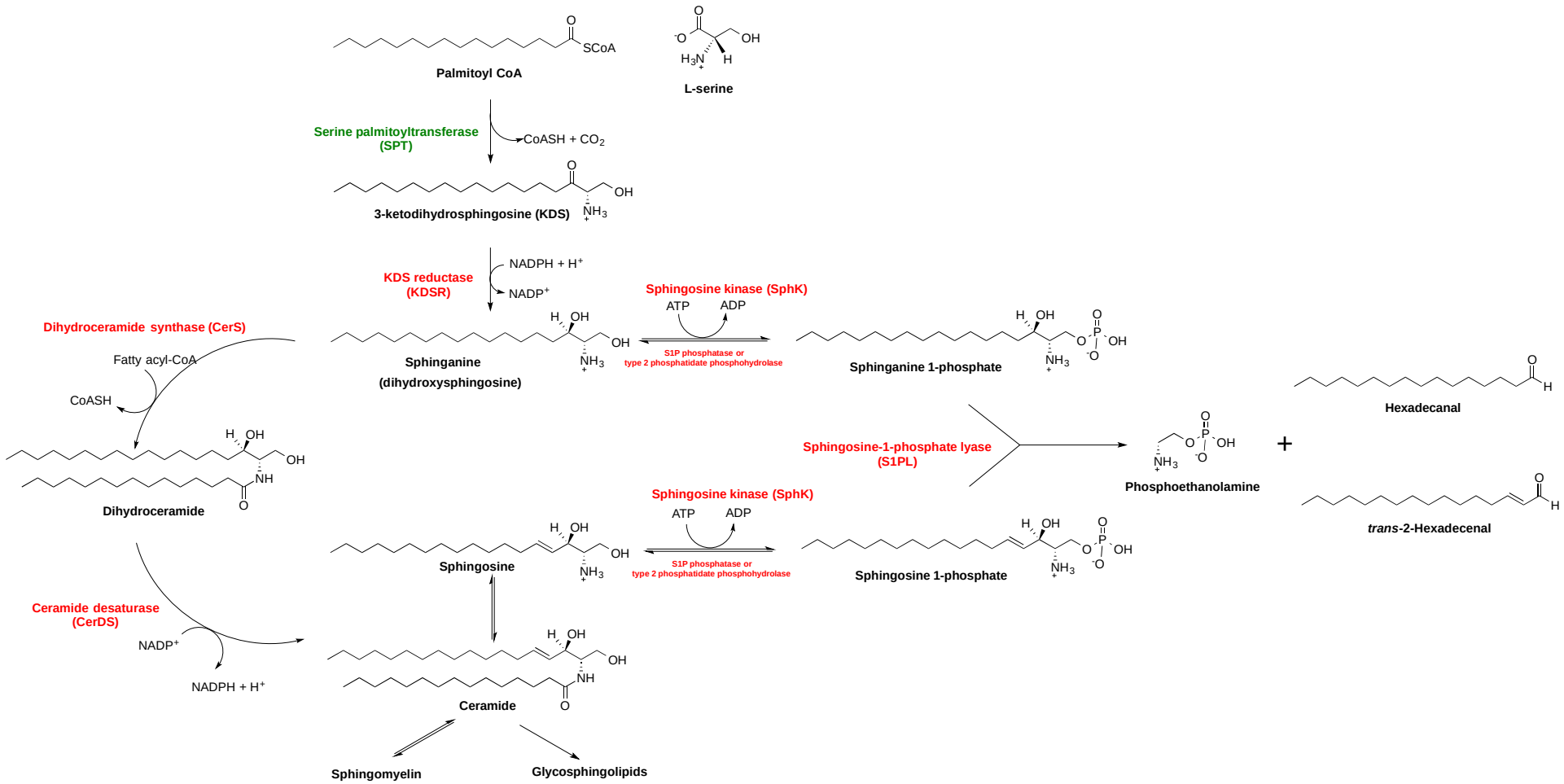

Figure 1-9 Abbreviated mammalian sphingolipid biosynthetic pathway[42]

The series of enzymatic steps that constitutes the sphingolipid *de novo* biosynthesis in mammals. Serine palmitoyltransferase (highlighted in green) catalyses the first and rate limiting step in the pathway. The other enzymes involved in the pathway are shown in red.

The first and rate limiting step of sphingolipid biosynthesis (Figure 1-9), in all organisms studied to date, is the condensation of L-serine with palmitoyl coenzyme A, which is catalysed by the enzyme SPT. SPT is the rate limiting step in *de novo* sphingolipid biosynthesis and is also a key sphingolipid regulator as excess sphingosine inhibits SPT activity.[43] There are a few variations in SPT specificity with the most common being the variation in acyl-Coenzyme A chain length.[44-45] It is thought that the product of the SPT-catalysed reaction, 3-ketodihydrosphinganine (KDS), never accumulates to appreciable levels in cells as the rate of KDS reductase (KDSR) is substantially faster than that of SPT.[46] However, there is potential for this reduction step to be slowed under oxidative stress.[47] Independent of whether sphingosine is sequestered into the ceramide synthase pathway or phosphorylated by sphingosine kinase, the only exit point from the sphingolipid pathway is by cleavage of sphingosine-1-phosphate (S1P). The enzyme S1P lyase (S1PL) breaks the C2-C3 bond to form phosphoethanolamine and hexadecenal in what is now known to be an irreversible manner.[48-49] S1PL is a PLP-dependent enzyme in the fold type 1 sub family and thus displays the characteristic UV-Vis absorbances and well understood chemistry of similar PLP enzymes. This has aided the elucidation of the enzyme's structure and mechanism and it is now known that S1P is broken down via a retro-aldol type reaction, but the identity of the base required for deprotonation is as yet unknown.[50-52] Upon exiting the sphingolipid pathway there seems some ambiguity as to the role of hexadecenal and phosphethanolamine. Hexadecenal can be metabolised to palmitate then palmitoyl-Coenzyme A, which could be recycled into sphingolipid biosynthesis.[53] The recycling of the sixteen-carbon alkyl chain back into the sphingolipid pathway is believed to explain the increase in ceramide levels upon over expression of S1PL.[54] The role of phosphethanolamine is even more complex again as this product goes on to be incorporated into the phospholipid pathway thus linking the sphingolipid and phospholipid biosynthetic pathways.[55]

Through the work of the NIH-funded Lipid Maps consortium a repository has been created for newly discovered lipids and now has in the region of 4300 documented sphingolipids.[56] Free sphingoid bases themselves are rarely found in nature, with

most sphingolipids consisting of a sphingoid base linked to a fatty acid via an amide bond to form ceramides (Figure 1-8 and Figure 1-9), which themselves can be glycosylated into increasing larger and more complex molecules (Figure 1-10).[57]

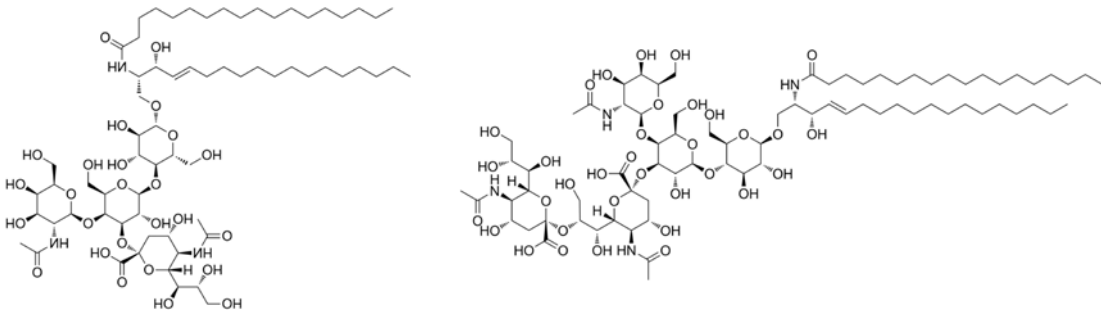

GM2 Ganglioside GD2 Ganglioside

Figure 1-10 Examples of more complex sphingolipids

GM2 levels are raised in melanomas and has been investigated as a possible target for new chemotherapies.[58] GD2 has been linked to Tay-Sachs disease, a disease of the nervous system that is caused by build-up of excess GM2/GD2 in the brain.[59]

It was initially thought that sphingolipids played only structural roles, along with other lipids, in membranes but it is now known that they are involved in a much wider plethora of cellular functions. Even within membranes the role of sphingolipids is not simple. Due to their predominantly saturated alkyl tails, sphingolipids pack more effectively with cholesterol forming lipid rafts, more rigid cholesterol and sphingolipid enriched regions of the membrane.[60] As research continues sphingolipids have now been shown to be involved in all major disease areas, including cancer, diabetes, Alzheimer's and asthma. S1P, probably the most widely known sphingolipid (Figure 1-11), is a known regulator of cell growth and delays programmed cell death.[61] There are 5 characterised human S1P nuclear receptors and all are members of the large, medicinally important G-protein coupled receptor (GPCR) family. Leading on from these discoveries, S1P has been investigated extensively as a possible oncology target and has led to one isoform of sphingosine kinase (SK1) being denoted an "oncogene" as it is overexpressed in multiple cancers.[62] The importance of the kinase is compounded by sphingosine promoting cell death whereas S1P promotes cell survival and has prompted more than thirteen distinct new therapeutics developments specifically targeting the S1P pathway, with the most famous of these being FTY720 (Fingolimod; trade name Gilenya, Novartis) (Figure 1-11).[62] This drug is now being used clinically as the first

oral, disease-modifying agent approved by the Food and Drug Administration (FDA) to reduce relapses and delay disability progression in patients with relapsing forms of multiple sclerosis.

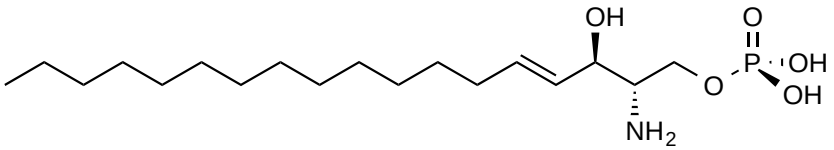

Sphingosine-1-Phosphate

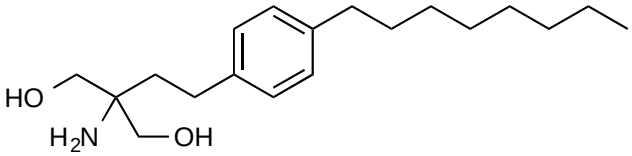

FTY720

Figure 1-11 The structure of sphingosine-1-phosphate (S1P) and FTY720, a synthetic pharmaceutical derived from myriocin but found to block S1P receptors

The observation that obese individuals are more likely to develop diabetes was proven long before the biochemical explanation was elucidated. However it is now believed that an increase in free fatty acids drives sphingolipid biosynthesis (Figure 1-9) producing an excess of ceramide.[63] Ceramide is capable of blocking several of the key steps in glucose uptake, which insulin is supposed to activate, including inhibiting the phosphorylation of the Insulin Receptor Substrate-1.[64]

It seems pertinent that, as sphingolipids were first discovered in the brain 130 years ago, they have recently been linked to Alzheimer's disease. In the brain the first step of sphingolipid biosynthesis varies slightly, with both palmitoyl and stearoyl-CoA being condensed to increase the variety in the sphingolipid pool. The proportion of sphingolipids containing the additional two carbons increases with cell age and varies depending upon sphingolipid type.[65] The molecular understanding of the roles sphingolipids play in disease is relatively limited due to their variation and multiple modes of action with confusion being compounded by the changing quantity and structure of sphingolipids with age.[66-67] Three such sphingolipid anomalies found in the brain of Alzheimer patients include: (i) a decrease in more complex ganglosides;[68] (ii) an increase in 18-carbon alkyl chains in proportion to the more common 16-carbon[69] and (iii) the presence of a sphingolipid binding domain on the disease related amyloid β-protein.[70-71] Similarly, sphingolipids have also been

conclusively linked to asthma, through both small molecules[72] and genetically.[73] A large scale genome comparison aimed at elucidating the origin of childhood asthma compared DNA from asthmatics and non-asthmatics and successfully mapped single base pair mutations only present in asthma suffers. These mutations clustered on chromosome 17 at q21 and resulted in up regulation of ORMDL3.[74] ORM proteins are now known to negatively regulate the activity of SPT.[73] When the ORM protein is phosphorylated there is low SPT activity but this rate can also be conversely increased by dephosphorylation of the ORM, see Figure 1-12.

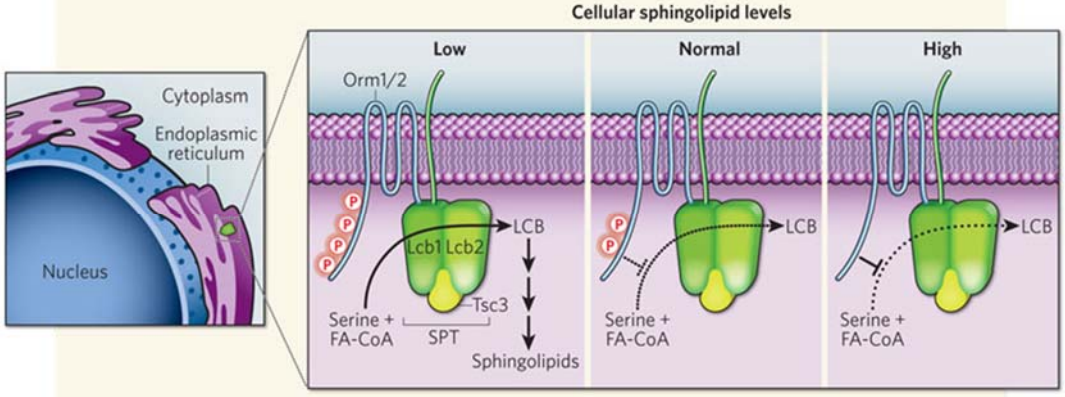

Figure 1-12 Regulation of yeast SPT activity by ORM proteins[75]
SPT subunits Lcb1, Lcb2 and Tsc3 form a complex with the proteins Orm1and Orm2. When cellular sphingolipid levels are plentiful, Orm proteins act as negative regulators of LCB synthesis. But when sphingolipids are in short supply, multi-site phosphorylation of Orm proteins gradually relieves their inhibitory activity, thereby restoring sphingolipid homeostasis.

The importance of sphingolipids cannot be overstated and although they play many important roles, as is demonstrated in the four diseases above, there are still no commercially available sphingolipid modulating therapies, with the only breakthrough occurring with multiple sclerosis and FTY720. This is mainly due to the complexity of both sphingolipid biosynthesis and metabolism but also the variety of reactions that involve sphingolipids requiring any potential sphingolipid inhibitor to be highly specific.

1.4 Serine palmitoyltransferase

1.4.1 Discovery of SPT

SPT is the first enzyme in the *de novo* sphingolipid biosynthetic pathway. SPT was first isolated from yeast in the laboratories of Snell and Stoffel in 1970.[76-77] Initially SPT had several names including 3-keto-dihydrosphingosine synthetase and 3-keto-dihydrosphinganine synthetase before SPT was adopted in line with the IUPAC nomenclature.[78] Snell also progressed the development of a new SPT assay based on monitoring CO_2 production from carbon-14 labelled L-serine.[76] Interestingly, this is in contrast to nearly all the other published assays, which monitor activity by the use of radioactive labelled substrates and TLC. Initial studies by Snell and Stoffel demonstrated SPT activity in yeast and later that year Braun and Kanfer found the first SPT activity in mammals through microsomal preparations of mouse and rat brains.[79-80] Characterisation of SPT was initially attempted from microsomal preparation with kinetic analysis, substrate scope and pH dependence all being investigated.[78-79] However, working with impure enzyme in unknown concentrations was not reliable.

The genes responsible for SPT activity were initially found in yeast through the use of auxotrophic mutants and were denoted lcb1 (long chain base 1) and then lcb2 corresponding to their order of discovery.[46, 81] Until this point the structure of SPT was completely unknown and the discovery of two genes needed for SPT activity complicated the initial work. The similarity of LCB1 and LCB2, the proteins coded by the lcb genes, was 21% with both showing some similarity to 5-aminolevulinic acid synthase (ALAS) and to 2-amino-3-ketobutyrate coenzyme A ligase (KBL).[82-83] Interestingly, only lcb2 contained the conserved lysine residue required to bind PLP. However, as expression of both proteins together led to a 2.5 fold increase in activity the existence of a heterodimeric complex was correctly hypothesised. Building upon the work of Lester *et al.,* Stoffel managed to cloned and successfully overexpressed both mouse and human LCB1 and LCB2 proteins.[84] The cloning and overexpression of the two SPT subunits marked a major step forward in the detailed understanding of how SPT functioned, with the relatively low concentrations of SPT protein thus far hampering detailed mechanistic studies. Through this work the location of SPT in the endoplasmic reticulum (ER) was confirmed and the PLP binding lysine was also confirmed to exist only in LCB2, by mutagenesis studies. The function of LCB1 and

its relationship to LCB2 was complicated by the reported increase in SPT activity only being dependent on LCB2 expression. The uncertainty over the role of LCB1 in the SPT complex was solved the following year by Hanada *et al.*[85] Hanada showed the heterodimeric nature of mammalian SPT for the first time by observing that both LCB1 and LCB2 co-purified from Chinese hamster ovary (CHO) cells when using only affinity-tagged LCB1. The result was then confirmed by antibodies for LCB2 immunoprecipitating both proteins.

The purification of eukaryotic SPT remained elusive even after the discovery of the responsible genes due to the added complexity of a multi-enzyme system; which requires dual expression and purification, as well as each subunit containing at least one hydrophobic membrane spanning domain.[41, 86] One attempted purification of note involved the use of an immobilised SPT inhibitor, myriocin, on a solid phase support pulling out both LCB1 and LCB2 from the lysate of murine cytotoxic T lymphocyte cells (CTLL-2). Unfortunately, the quantities of enzyme purified where very small due to the expense and technical difficulty of producing a myriocin resin and unfortunately the purified enzyme was inactive. However, as the main impetus of this work was to conclusively determine the *in vivo* target of myriocin, the ingenious approach by Schreiber and colleagues must be applauded.[87] In 2000 Hanada *et al.* doubly labelled lcb1 with both a hexa-his and a FLAG® tag and, for the first time, managed to isolate 1.2 μg of twice purified, active lcb1/lcb2 complex.[88] The use of FLAG® affinity chromatography and sucrose monolaurate as a detergent appear to be two of the critical elements in this purification. Indeed FLAG® affinity chromatography is still used today to purify the mammalian SPT complex.[89] The addition of two tags onto a protein could have affected the enzymatic efficiency; however, comparison of pH studies and substrate scope analysis are all in line with earlier results published from microsomal SPT studies. Hanada has undertaken a comprehensive acyl-CoA substrate specificity study of mammalian SPT from CHO cells that shows the substrate specificity for palmitoyl-CoA is reasonably tight; however a one carbon change is tolerated relatively successfully (Table 1-3)

Acyl-CoA	% KDS formed
Myristoyl (14 carbons)	13.0 ± 1.4
Pentadecanoyl (15 carbons)	73.1 ± 1.1
Palmitoyl (16 carbons)	100 ± 4
Heptadecanoyl (17 carbons)	61.9 ± 5.4
Stearoyl (18 carbons)	11.1 ± 0.8
Arachidoyl (20 carbons)	<2

Table 1-3 Acyl CoA specificity of purified mammalian SPT from CHO cells[88]

The biosynthesis of sphingolipids has continued to bring new challenges as it was found that the activity of the yeast SPT heterodimer is increased by the presence of a small protein, Tsc3p.[90] This 80 amino acid protein was discovered by Dunn *et al.* and found to increase SPT activity up to 30 fold. Unfortunately it was unclear exactly how much the rate was enhanced by the addition of Tsc3p as some of the difference in activity was attributable to the known substrate inhibition caused by palmitoyl-CoA.[91] Nevertheless Tsc3p undoubtedly increases the rate of KDS production significantly; and mutant Tsc3p-deficient yeast cells are unable to grow at elevated temperatures, thus demonstrating their inability to make sufficient KDS to sustain life. Following the discovery of a small activating subunit of SPT in yeast, similar proteins were sought in mammals, specifically humans, but sequence analysis yielded no results. Through the transfection of yeast LCB1/LCB2 deficient mutants with their human homologs, hLCB1 and hLCB2, Dunn and colleagues used a similar thermo-sensitive screening technique to test a human DNA expression library. This work led to the successful isolation of two small proteins that promote SPT activity in humans.[44] The two small subunits, ssSPTa and ssSPTb, were 71 and 76 amino acids long respectively. Although similar to each other (45% identity) they shared no similarity with Tsc3p, both ssSPTa and ssSPTb contain two proposed membrane spanning domains. More interestingly the catalytic enhancement of the human lcb1/lcb2 complex by either small subunit is over 100 fold. Surprisingly, however the addition of either of these small subunits to the SPT complex can also alter the chain length specificity of SPT. Dunn and co-workers showed that various combinations of lcb1 with the different isoforms of lcb2 and either of the small subunits produced various proportions of product each with a different acyl chain length (Figure 1-13).

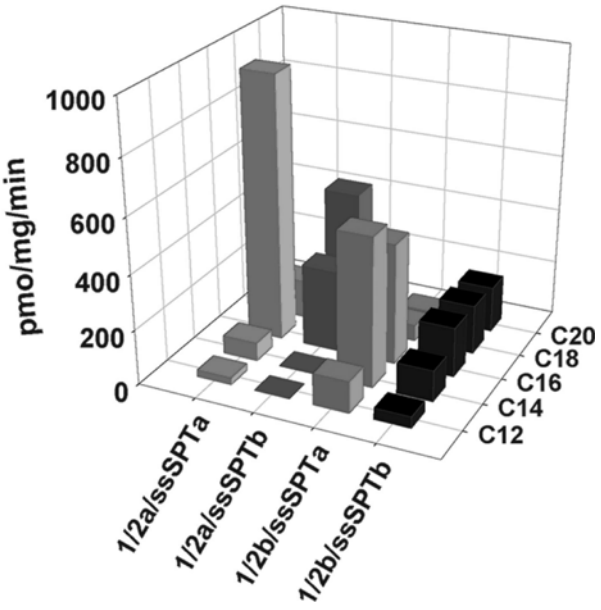

Figure 1-13 Varying SPT activity from different combinations of lcb1, lcb2 and small subunit
Activity was measured in microsomes prepared from yeast expressing each of the 4 isozymes using [3H]serine and acyl-CoAs of the indicated (C12–C20) chain lengths.[44]

Again progression in the understanding of eukaryotic KDS production was led by a discovery in yeast; independently, the groups of Weissman[73, 89] and Chang[92] discovered that Orm1 and Orm2 (orm stands for orosomucoid) bind to the SPT complex and negatively regulate SPT activity. The proposed model of regulation involves the Orm proteins binding to SPT and inhibiting activity, this inhibition is then stopped by phosphorylation of the Orms in response to low sphingolipids levels (Figure 1-12). The role of Orm proteins in SPT regulation was initially discovered through epistatic mini-array profiles, which involves the comprehensive mapping of phenotypes to known mutations, which allowed catastrophic mutations in Orm1 and Orm2 to be linked to lcb1 and lcb2 knockouts.[93] The link between SPT and the Orm proteins was confirmed after purification of either Orm 1 or 2 with the aid of a FLAG®- affinity tag led to the co-purification of lcb1, lcb2 and Tsc3p (Figure 1-14).

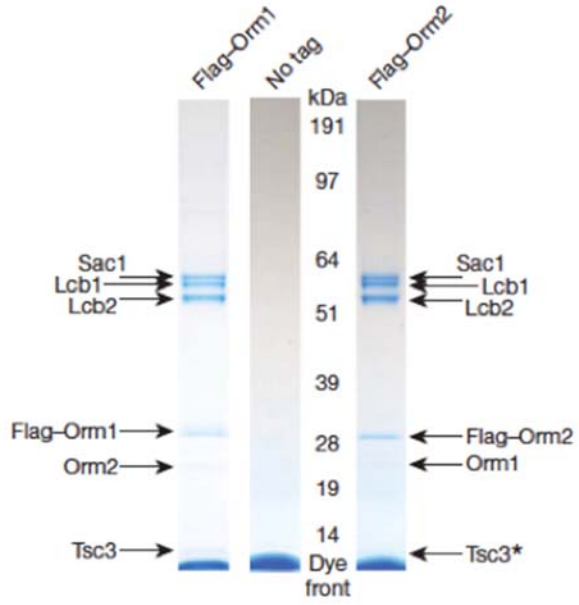

Figure 1-14 Orm proteins form a complex with serine palmitoyltransferase
Colloidal-comassie stained gels are shown for yeast proteins eluted after affinity purifications from strains expressing FLAG®–Orm1 or FLAG®–Orm2.[93]

The presence of Sac1, a phosphatase, along with the other four proteins gave rise to the terms SPOTS complex, **s**erine **p**almitoyltransferase, **O**rm 1/2, **T**sc3, **S**ac1. The discovery of the SPOTS complex in yeast was thought to predict the existence of a similar arrangement in higher eukaryotes. Indeed it was already know that the human equivalent to the Orm proteins, ORMDLs, bind to human SPT.[73] Lack of ORMDL expression leads to an increase in sphingolipids but direct evidence of their regulatory role is not available. [94-95]

In contrast to eukaryotes, sphingolipids are only found in a select group of bacteria, most of which are anaerobic.[96] Some of the earliest investigations of bacterial sphingolipid production was also undertaken by Stoffel *et al.* using the knowledge gained through study of the eukaryotic system.[97] The first attempt at purification of bacterial SPT was made from *Bacteroides melaninogenicus* by Lev *et al.* in 1981.[98] This was only partially successful, but the isolated SPT was subjected to kinetic analysis and the K_m for L-serine was determined to be 1.13 mM, which very closely matches recent published results. In 2001 Ikushiro and colleagues chose to investigate the known sphingolipid-containing organism *Sphingomonas paucimobilis* and isolated the wild type SPT from soluble bacterial extracts. They succeeded in isolation of sufficient quantities of pure SPT which was then subjected to protein mass fingerprinting and N-terminal sequencing. Based on this data, they carried out a

reverse genetic analysis and generated degenerate DNA primers. This allowed them to clone the *S. paucimobilis* gene and prepare recombinant SPT in *E. coli*. This bacterial SPT showed high sequence homology to eukaryotic lcb1 and lcb2 as well as other members of the AOS family.[99] In contrast to the eukaryotic enzyme, bacterial SPT is encoded by a single gene and is a soluble homodimer. The 48% similarity of bacterial SPT and lcb2 coupled with good solubility and the homodimeric nature made bacterial SPT the ideal model for the more complex eukaryotic system. The ability to readily express and purify active SPT led to the promise of a high resolution x-ray crystal structure,[99] which finally arrived from Campopiano *et al*. in 2007 in collaboration with Jim Naismith in St. Andrews (Figure 1-15).[100] The first evidence based visualisation of SPT elegantly showed the homodimeric nature of SPT, the location of the active site at the dimer interface, the location of the conserved PLP binding residues, confirmation of the presence of magnesium and highlighted the structural similarity between SPT and other AOS family members.

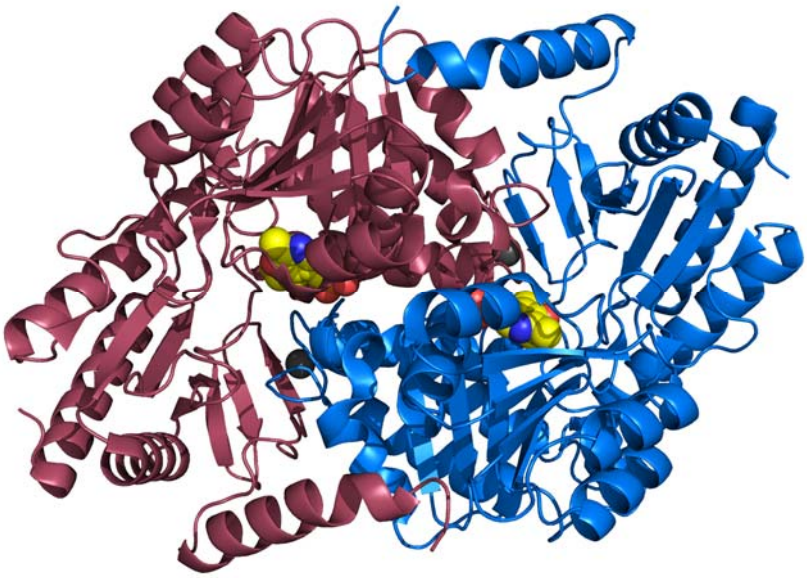

Figure 1-15 The first crystal structure of *S.paucimobilis* SPT in its natural homodimeric form
One monomer is coloured red and the other blue. The PLP in each monomer is shown in spacefill with the carbons in yellow, the two magnesium ions are shown in gray. PDB Code 2JG2.

The positions of the Cα atoms in the protein backbone of SPT were compared to 8-amino-7-oxononanoate synthase (AONS, PDB code 1DJE),[101] 2-amino-3-ketobutyrate CoA ligase (KBL, PDB code 1FC4)[102] and 5-Aminolevulinate Synthase, (ALAS, PDB code 2BWN).[103] The root-mean-squared deviation (RMSD) between SPT and AONS was 1.6 Å, 1.4 Å between STP and KBL and 1.5 Å between

SPT and ALAS. The majority of structural diversity between the four enzymes is in the remote N-terminal regions.

Following the publication of the x-ray structure, mutagenesis,[29, 104] inhibition[105-106] and further mechanistic studies[29] all quickly followed. Although the important residues for PLP binding can be observed via the lack of evolutionary variability through sequence alignments with other PLP binding enzymes, their proximity and location in SPT can now be confirmed. The widely reported group of PLP binding residues can be seen in Figure 1-16 and the individual functions of PLP binding for each residue can now be assigned – residues are numbered based on the *S. paucimobilis* SPT sequence. His 159 sits above the PLP ring and adds a π-stacking interaction, Asp 231 is in the correct position to stabilise the protonated nitrogen of the PLP ring, as discussed earlier. His 234 is within H-bonding distance of the hydroxyl group on carbon-3 of the PLP ring.[107] It has been clearly demonstrated through both crystal structures (PDB code 2JG2) and through mutation studies that lysine 265 binds PLP. From comparison of the internal aldimine structure of SPT (PDB code 2JG2) with the external aldimine structure (PDB code 2W8J) lysine 265 is obviously very flexible, having moved more than 4 Å from PLP. (Figure 1-16)

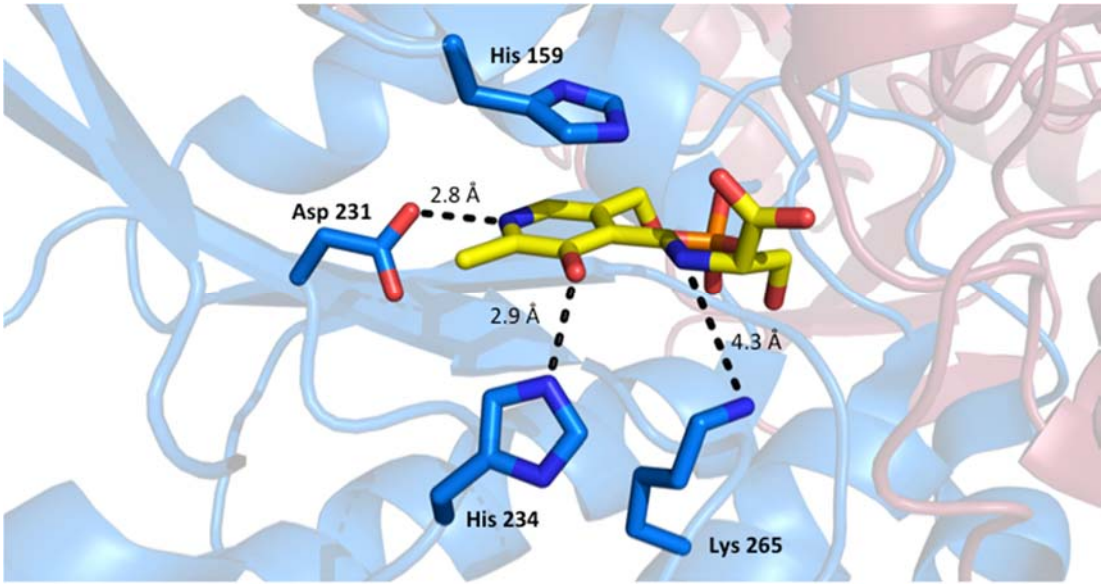

Figure 1-16 Active Site of SPT and the bound PLP:L-Serine external aldimine complex
Showing the four key residues involved in PLP binding. PLP is captured as the external aldimine form with L-serine. Monomers are coloured blue and red. Important side chains are highlighted as sticks with carbon atoms coloured blue, nitrogen darker blue, oygen red and phosphorus orange. The PLP-L-serine aldimine carbons are yellow but all other atoms are the same colours as the side chains. (PDB Code: 2W8J)

Viruses were not known to contain sphingolipids until the successful sequencing of the Coccolithovirus genome in 2005 showed putative sphingolipid producing enzymes.[108] Interestingly, the virus contains a single gene encoding for an 870 amino acid SPT with the C-terminal region showing similarity to the eukaryotic lcb1 and the N-terminal region showing similarity to lcb2.[109] This natural fusion shows a unique preference for myristoyl-CoA (14 carbons) and produces the corresponding shorter (C16) sphingolipids in larger quantities. The catalytic ability also seems to have diminished through fusing both subunits together with the viral enzymes only showing a tenth of the activity of the wild-type yeast SPT proteins. Nevertheless, the existence of a natural fusion gave rise to the concept of man-made SPT fusions with the hope that the expression and purification of a single SPT would be more achievable. To date recombinant forms of both yeast and human lcb2-lcb1 head-to-tail fusions have been successfully produced in microsomal preparations but only exhibit roughly a third of the activity of the natural enzymes.[109]

1.4.2 **SPT Mechanism**

Following the publication of the structure of sphingosine[40] hypotheses were proposed as to its biosynthesis, with the first insight coming in 1953.[110] Zabin *et al.* used carbon-14 labelled acetate to inoculate rats before extracting sphingolipids from their brain and analysing the carbon-14 content in a chemically astute, but now relatively crude, experiment. Zabin discovered that only carbons 3-18 of sphingosine were derived from acetate but acetate was shown four years later only to be the precursor of palmitoyl-Coenzyme A.[111] Further experiments by Sprinson *et al.* used carbon-14 in partnership with deuterium and nitrogen-15 labelling to determine that the head group carbons came from L-serine. (Figure 1-17).[112]

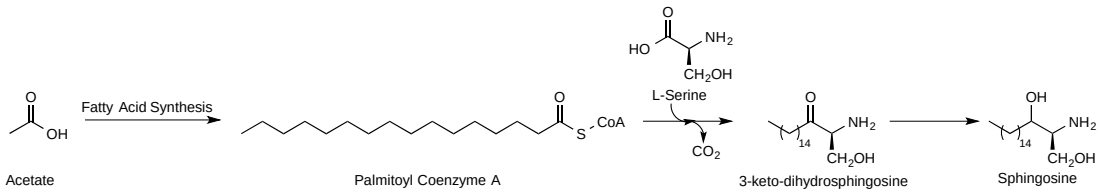

Figure 1-17 Proposed synthesis of sphingosine and the preceding ketone
Acetate-CoA and malonyl-CoA are the substrates for fatty acid synthase to produce Plamitoyl-CoA which condenses with L-serine to produce a ketone intermediate. The ketone intermediate is then reduced to form sphingosine.

Following determination of serine as the second substrate Sprinson also deduced the formation of a ketone intermediate before reduction to the target molecule, sphingosine (Figure 1-17). The existence of a long chain keto intermediate between L-serine/palmitoyl-CoA and sphingosine was further expected from what was known of PLP chemistry;[91, 113] however, the identification of the reductase responsible was not made until 1968.[47]

Once the substrates for sphingosine biosynthesis had been elucidated the molecular details of the enzymatic reaction were investigated. PLP was identified as a cofactor, shortly after in 1958[111] and was confirmed by the production of sphingolipids being inhibited by cysteine, a well-known PLP inhibitor.[91] Incorporating the well characterised chemistries of PLP with the known starting materials and product, the following Schiff base, decarboxylation and/or deprotonation mechanism shown in Figure 1-18 could be suggested.[24]

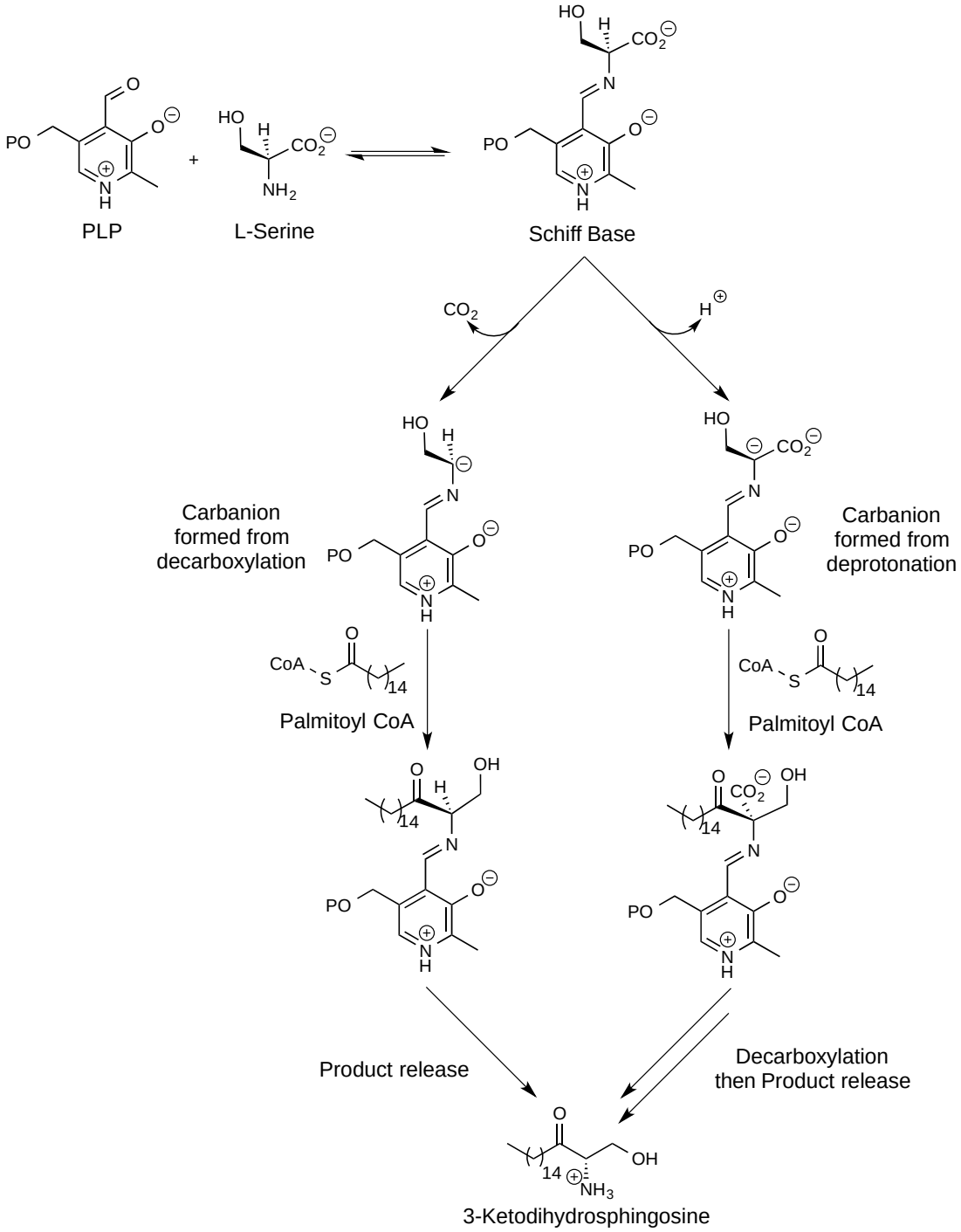

Figure 1-18 Initial proposed mechanisms for sphingosine biosynthesis

Both of the above proposed mechanisms involved decarboxylation at some stage; therefore in order to determine which was correct, the ability to monitor the α-proton of L-serine throughout the course of the reaction was required. Replacement of the α-proton of L-serine with tritium provided a window into the active-site; and studies initially suggested the α-hydrogen was retained during sphingosine synthesis.[113] The retention of the α-hydrogen on L-serine necessitates the loss of carbon dioxide as the

only plausible mechanism for the formation of the proposed carbanion. Although in his paper Weiss leaves open the possibility that another mechanism might be responsible, but does not suggest what that may entail. Eventually Krisnangkura *et al.*[114] repeated the labeling experiments with L-serine and, through a combination of better techniques, concluded that the α-proton of L-serine was lost and then replaced. The strongest evidence to support the order of deprotonation to generate the carbanion, condensation with the acyl-thioester then decarboxylation of the β-keto acid intermediate was provided by Ikushiro *et al.* in 2008. Using elegant NMR experiments Ikushiro and colleagues managed to monitor the α-carbon of L-serine during the course of a reaction. This allowed them to conclude that deprotonation did precede decarboxylation but deprotonation was controlled by binding of the second substrate, palmitoyl-CoA.[115] Interestingly palmitoyl-CoA has repeatedly been shown to exhibit substrate inhibition at high concentrations.[42, 91] Upon addition of the second substrate palmitoyl-CoA the reaction preceded so rapidly that monitoring was impossible on the NMR timescale. Therefore a special thioether palmitoyl-CoA analogue (S-(2-oxoheptadecyl)-CoA, Figure 1-26) was designed that contained an extra methylene bridge between the carbonyl and the sulfur thus breaking the thioester linkage and making loss of free CoA unlikely at physiological conditions. Using the palmitoyl CoA analogue allowed the rate of hydrogen-deuterium exchange at the α-carbon to be monitored after both substrates were bound and showed a 100 fold increase in exchange compared to before the addition of palmitoyl-CoA, thus demonstrating the increased stability of the resulting carbanion. The rationale for the rate enhancement observed upon palmitoyl-CoA binding remains only theoretical, as the fast turn-over of substrates has prevented any L-serine:palmitoyl-CoA:SPT co-crystals being obtained. The use of the same palmitoyl-CoA mimic (Figure 1-26), as used in the NMR experiments above, made obtaining a L-serine:palmitoyl-CoA:SPT crystal structure a possibility; though, to date, no crystal structure of this tertiary complex is available. However, a model of S-(2-oxoheptadecyl)-CoA in the active site suggests the binding causes conformational change that pushes the α-proton of the L-Serine:PLP aldimine perpendicular to the ring and therefore favourable for deprotonation. Combining more than 50 years of mechanistic studies has produced a widely accepted and detailed reaction mechanism for SPT (Figure 1-19).

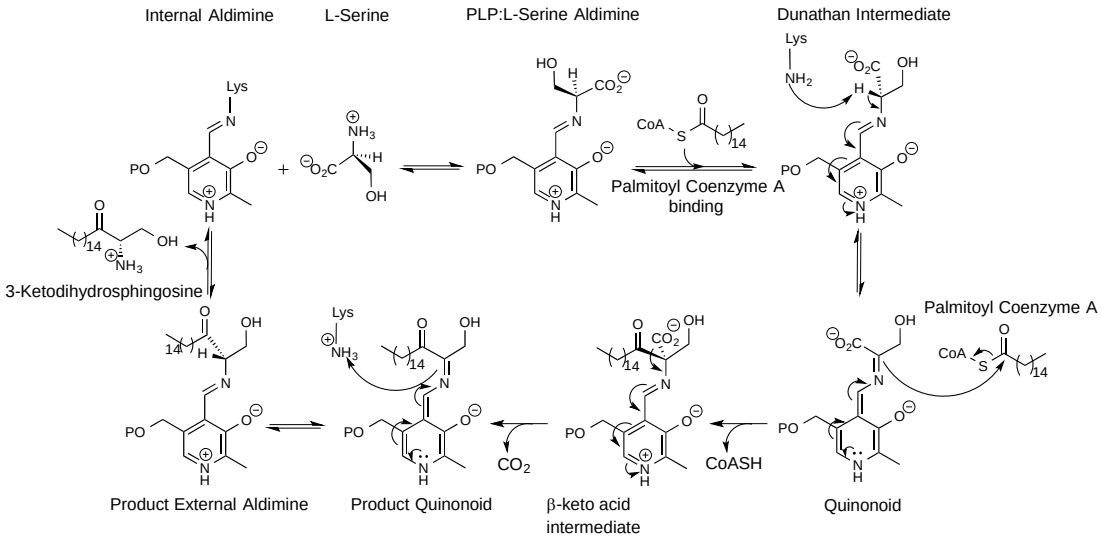

Figure 1-19 Accepted SPT mechanism
Proposed PLP-dependant catalytic mechanism of SPT. The internal aldimine (holo-SPT) is displaced by L-serine to form the external aldimine. Binding of the second substrate, palmitoyl-CoA, causes conformational change to give the Dunathan intermediate. This conformation allows deprotonation of Cα hydrogen by Lys265, forming the quinonoid. This is followed by nucleophilic attack from the Cα on to the palmitoyl-CoA thioester, releasing CoASH and forming the β-keto acid intermediate. This intermediate undergoes decarboxylation, before release of the product 3-ketodihydrosphingosine (KDS) and regeneration of the internal aldimine.

For the correct sphingolipids to be produced in any organism, the serine based polar head group must be introduced in this first step and so SPT must be exquisitely specific for L-serine as a substrate. Interestingly several mutations have been discovered in human SPT that further broaden the reaction specificity allowing L-alanine and glycine to replace L-serine thereby producing deoxysphingolipids (doxSAs). It is thought that these aberrant products build up in the body due to a lack of metabolic pathways for their degradation.[116] This is due to deoxysphingolipids being unable to be phosphorylated by any kinase and therefore cannot be degraded by the S1P lyase. Several genetic mutations in the human SPT gene have been catalogued which display this phenotype and are associated with the extremely rare human neuropathy Hereditary Sensory and Autonomic Neuropathy type 1 (HSAN1).[104]

1.4.3 SPT Inhibitors

Sphingolipids have been implicated in the progression of several disease states and inhibition of the sphingolipid pathway has been proposed as a novel therapeutic strategy for treatment of several diseases. As SPT catalyses the first and rate limiting step in sphingolipid biosynthesis, SPT is a particularly attractive target for inhibition. Initially inhibition studies of SPT utilised well known PLP inhibitors such as cysteine.[76, 78] More recently, SPT specific natural product inhibitors have been used to probe the role of sphingolipids *in vivo* as well as a biochemical tool *in vitro* to allow the sphingolipid pathway to be paused while investigations are undertaken.[73, 92, 117] The newfound relationship between SPT and the human ORMDL proteins has produced another potential therapeutic interest in SPT inhibitors.[68] The negative regulation of SPT by the ORMDL proteins, which themselves have been mapped to asthma suffers,[118] gives rise to the hypothesis that mutations in ORMDL may cause a loss of function. Any loss of function would lead to disregulation of SPT and a build-up of downstream sphingolipids; which could be responsible for the increased prevalence of asthma.

A more definite link has been made between sphingolipid production and both hepatitis B and C. Both hepatitis B and C are class 3 pathogens (on a scale of 1-4) but preliminary studies suggest they can be treated with myriocin, an SPT specific inhibitor (Figure 1-20).[119-120]

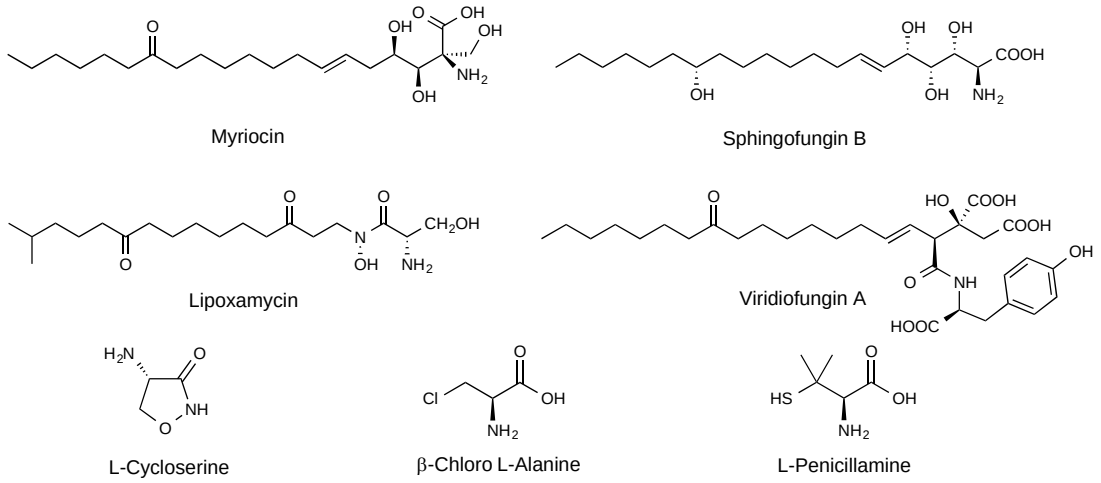

Figure 1-20 Structures of SPT inhibitors

Interestingly the therapeutic effect of myriocin is now thought not to derive from the inhibition of SPT but its sphingolipid like structure. Comparative studies with FTY720, a myriocin derived drug that does not inhibit SPT but mimics sphingosine gave the same therapeutic effect.[121] Still more promisingly, SPT inhibition has been convincingly linked to improvements in cancer treatments. From the discovery that sphingolipid levels were raised in several cancersmyriocin has been tested as a known specific SPT inhibitor.[122-123] These studies have shown myriocin can cause tumour regression through lower sphingolipid levels and increased p53 activity even in the most aggressive forms of cancer.[122-124] It has also been shown that ceramides, down stream products of sphingolipid biosynthesis, have direct effects on insulin signalling components which has linked sphingolipids and SPT to diabetes.[125] Again through the use of myriocin preliminary evidence shows SPT inhibition can prevent defects in glucose metabolism and improved glucose tolerance in obese mice.[126-127] Finally but by no means exhaustively, sphingolipids have been connected to Alzheimer's due to their high concentration in neuronal membranes but as yet this work has yet to progress to using specific sphingolipid inhibitors to further probe their role in this disease.[67, 128]

SPT is without doubt a target for the pharmaceutical industry, with Lilly, Pfizer and Bayer as well as smaller BioTech companies openly declaring interest in this area through the publication of research papers and patents.[129-132] However, as yet, no company has managed to progress any synthetic compounds into the clinic; therefore most of the work on inhibition of SPT has been driven by natural product discoveries (Figure 1-20**Error! Reference source not found.**). Sphingofungin B, myriocin, lipoxamycin and, to some extent, viridofungin A, all share the same general structural core as sphingosine. The slight modifications on the aliphatic tail seem to play an important role in gaining increased inhibitory activity, but the stereochemistry at carbon-14 does not seem to be crucial.[133] Hanada *et al.* also made several analogues of sphingofungin B, systematically inverting the stereocentres at the head group and proved the crucial importance of all the chiral centres.[133] Sphingofungins were initially identified from *Aspergillus fumigatus* as broad spectrum antifungal agents that were noted for their lack of antibacterial activity.[134] The lack of antibacterial activity exhibited by sphingofungins led to the hypothesis that sphingofungin B was an inhibitor of sphingolipid biosynthesis as most bacteria do not produce sphingolipids. The identification of sphingofungin B as a specific

SPT inhibitor was achieved by adding back different sphingolipid intermediates to see when cellular viability was rescued, along with radio labelled substrates and specific SPT assays which gave sphingofungin B an IC_{50} of 20 nM.[135]

Viridiofungin A (Figure 1-20**Error! Reference source not found.**) was isolated from *Trichoderma viride* as a very minor product and although initially wrongly classed as a squalene synthases inhibitor; it was later discovered to selectively inhibit sphingolipid biosynthesis.[136] The Viridiofungin family is a very small group of compounds with their relatively small structural diversity arising from variations of the amide side chain, resulting in several of the family inhibiting SPT. Both tritium labelled palmitate and L-serine were used in SPT activity assays with viridiofungin A; which was found to have an IC_{50} of 22 nM in the correct strain of yeast cells. Wide variation in inhibition across different strains of yeast was noted and in *Saccharomyces cerevisiae* viridiofungin A inhibits several pathways at the micromolar level. Structure activity relationship (SAR) studies demonstrated that the length and saturation of the alkyl chain had only a modest effect on potency while substitution of the unusual extra acid group at C1 led to a 30 fold decrease in activity.

Lipoxamycin (Figure 1-20**Error! Reference source not found.**) is the least spingosine-like natural product inhibitor of SPT but still exhibits remarkable potency with an IC_{50} of 21 nM in the correct strain of yeast.[137] Unfortunately, the different structural features of lipoxamycin have not been investigated through any sort of SAR studies.

Myriocin (Figure 1-20**Error! Reference source not found.**) is undoubtedly the best-known SPT inhibitor; it has been well characterised and is widely utilised in studies of sphingolipid biosynthesis. Myriocin was first discovered in 1972 from two different thermophilic fungi by both Kluepfel *et al.* and Aragozzini *et al.*[138-139] Whilst working with *Myriococcum albomyces,* Kluepfel isolated, purified and determined the structure of a previously unknown antimicrobial agent which was named myriocin. In this early study the lack of antibacterial activity was noted along with potential solubility problems that arose during the first *in vivo* analysis of myriocin. In the same year Aragozzini published details of the same compound which was isolated from *Mycelia sterilia* and called Thermozymocidin. The stereochemical configuration of myriocin was published a year later following complex

derivatisation to aid NMR assignment of the chiral centres.[140] A small molecule crystal structure was attempted with myriocin but the project only managed to crystallise the N-acetyl-lactone derivative (Figure 1-21).[141]

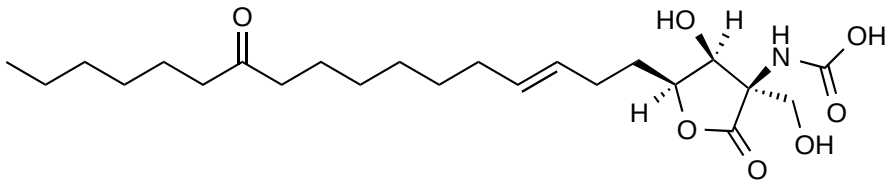

Figure 1-21 Crystallisable N-acetyl-γ-lactone myriocin derivative

Myriocin is now commercially available (from Sigma-Aldrich) having been fermented from the parent fungus. As well as the natural product, two total synthesis methods have been published with the first method utilising the similar stereochemistry of D-fructose as a starting material.[142-143] Over 20 years after its initial isolation myriocin was re-isolated in 1994 under the name ISP-1 form *Isaria sinclairii* due to its potent immunosuppresent activity.[144] Kawasaki and colleagues determined an IC_{50} value of 15 nM, using CTLL-2 cells as a model for myriocin dependent inhibition of cell growth and elimination of ceramide production.[145] Since growth was restored by the addition of sphingosine, it suggested that SPT was the primary target of myriocin. In 1999 Schreiber and colleagues used a myriocin-like affinity resin to confirm the two subunits of murine SPT (lcb1 and lcb2) as the primary targets of the natural product myriocin.[87] The known immunosuppressant activity of myriocin is unlikely to stem from its inhibition of SPT, otherwise all SPT inhibitors would show some immunosuppressant characteristics. Nevertheless, comparison of myriocin to other known immunosuppressants such as cyclosporine A and tacrolimus have shown it to exhibit remarkably high activity, despite its comparatively simple structure. Myriocin is consistently more active than cyclosporine A and inhibits the production of T-cell dependent antibodies at least ten fold more successfully.[144] The differences in activity were rationalised by the suggestion that myriocin and cyclosporin A acted upon different pathways. Cyclosporin A was a known inhibitor of the production of the signalling molecule, interleukin 2, whereas myriocin did not inhibit interleukin 2 production.

Structure activity studies on myriocin have shown that the unusual carbonyl group at carbon-14 on the alkyl tail of myriocin is not required for activity.[146] While $NaBH_4$ reduction of the ketone to the corresponding alcohol produced no change in activity but the Clemmensen reduction to produce the corresponding methylene produced a 10 fold increase in activity. Conversely reduction of the double bond decreased the immunosuppressant activity by an order of magnitude.

The efficacy of myriocin as an immunosuppressor or indeed for the treatment of any condition is severely limited by its low solubility, which led Fujita and colleagues to try and find more pharmaceutically suitable alternatives. In 1995 FTY720 (Figure 1-22) was published utilising the information that the myriocin C14 carbonyl moiety was unnecessary along with extensive simplification via the removal of the three chiral centres and partially locking the movement of the alkyl chain by the introduction of an aromatic ring.[147-148]

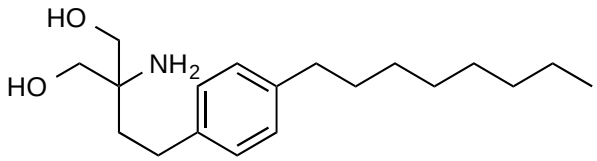

Figure 1-22 FTY720 (Fingolimod)

FTY720 remains almost equipotent in the same immunosuppresant assays but the chemical modifications made to myriocin on route to FTY720 have removed all SPT inhibition activity. The lack of SPT inhibition along with the persistence of immunosuppressant activity is further evidence for SPT inhibition not being the cause of the immunosuppressant activity displayed by myriocin. The mode of action of FTY720 has now been traced to its structural similarity to sphingosine. This similarity allows it to be phosphorylated and then act as an agonist for the four G-protein coupled sphingosine-1-phosphate receptors thus pushing FTY720 into the pro-drug category as it must be activated *in vivo* before it is effective.[149]

Intriguingly, the mode of action of myriocin upon SPT remains largely unknown. It has been assumed that myriocin forms an external aldimine with PLP due to the presence of a primary amine group (Figure 1-23).[41]

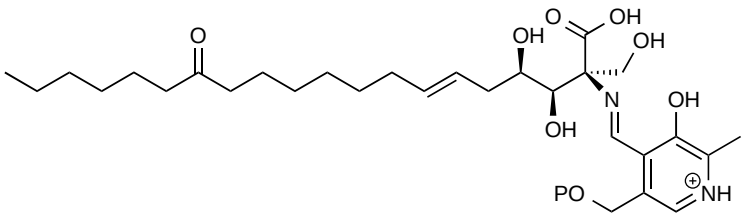

Figure 1-23 Proposed myriocin-PLP intermediate

Some excellent mechanistic work has also been carried out on the mode of action of L and D-cycloserine (Figure 1-20**Error! Reference source not found.**) as an SPT inhibitor, aided by SAR data obtained from a crystal structure.[106] From this data Lowther *et al.* showed that SPT effected a ring-opening, then decarboxylation of cycloserine to generate PLP and an amino aldehyde adduct (Figure 1-24). This is in contrast to other PLP dependent enzymes where an isoxazole-PMP derivative is formed from the initial PLP-cycloserine aldimine via deprotonation at C-α.

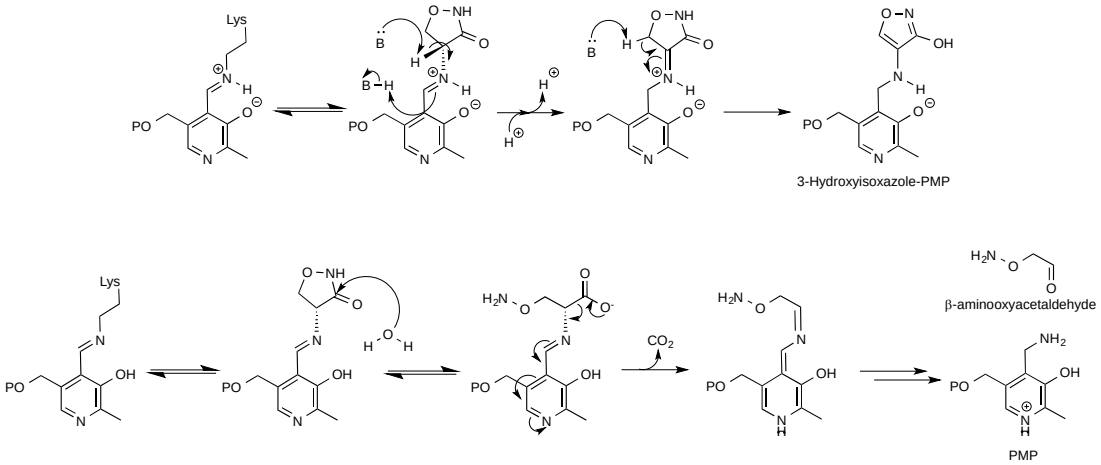

Figure 1-24 Cycloserine inhibition
Top – Cycloserine interacting with PLP bound to alanine racemase and forming the expected inactive 3-hydroxyisoxazole PMP derivative. **Bottom –** Cycloserine interacting with PLP bound in SPT, catalysisng the conversion of PLP to inactive PMP.

Again through the detailed understanding of PLP chemistry Beattie *et al.* elucidated the mechanism of SPT inhibition by L-penicillamine.[105] Coupling previous knowledge gained from crystal structures along with historical PLP literature which details in-depth UV-vis analysis of PLP and its intermediates, Lowther elucidated that L-penicillamine inhibits SPT by rendering PLP inactive by the formation of a thiazolidine-PLP adduct (Figure 1-25).

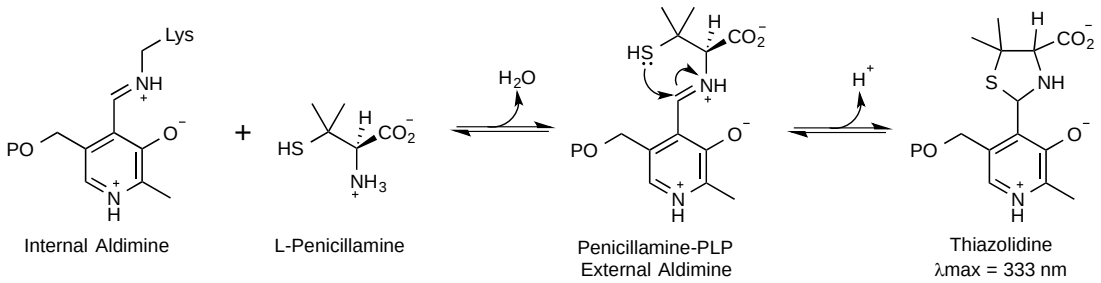

Figure 1-25 L-Penicillamine inhibition of SPT

The production of the thiazolidine-PLP adduct was confirmed by elegant native mass spectrometry analysis which showed the adduct either present in one or both of the active sites. Both the studies with cycloserine and L-penicillamine show how in-depth understanding of PLP coupled with the use of an array of complex techniques is required to understand the versatile catalytic activity of SPT. β-chloro-alanine (Figure 1-20**Error! Reference source not found.**) is another example of a broad spectrum PLP inhibitor, but at the correct concentrations, can also act as a selective SPT inhibitor.[150] Studies by Medlock show that inhibition of SPT is achieved with a much lower concentration of β-chloro-alanine than was required for inhibition of other PLP-dependent enzymes.[151] Inhibition of SPT can be achieved with 5 mM, while no inhibition of aspartate or alanine aminotransferases was seen at that level. Studies with excess L-serine have shown that L-serine and β-chloro-alanine, unsurprisingly, compete for the same site. This hypothesis is further substantiated by the highly enantioselective binding of β-chloro-alanine, with the L conformation exhibiting 20 times more potency than β-chloro-D-alanine. Binding at the PLP binding site of the enzyme would also explain the broad spectrum of PLP inhibition. The utility of β-chloro-alanine is limited even with the most potent conformation, as even β-chloro-L-alanine only has an IC_{50} of 1 mM, which is far too high for use *in vivo*.

The only published man-made SPT inhibitor is a modification of the palmitoyl-CoA substrate (Figure 1-26), which was first synthesised by Ikushiro *et al.* as a tool for probing the SPT reaction mechanism.[115]

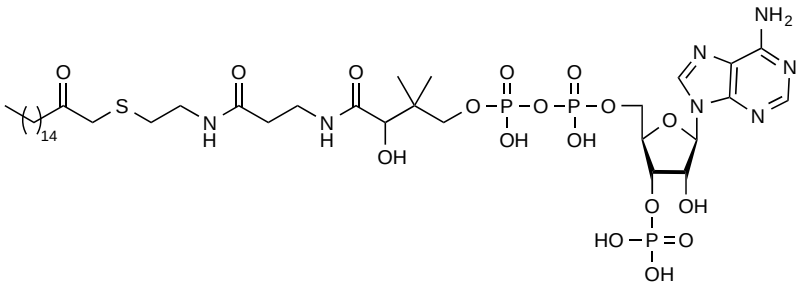

Figure 1-26 S-(2-Oxoheptadecyl)-CoA (Palmitoyl CoA Analogue)

The only difference between the 2-oxoheptadecyl-CoA analogue and palmitoyl-CoA is the addition of a methylene linker between the sulfur and the end carbonyl. This important addition halts the mechanism after deprotonation, just before nucleophilic attack of the Cα onto the palmitoyl-CoA substrate (Figure 1-19). The extra carbon results in the leaving group having a carbanion, not the more stable sulfur anion. The instability of the leaving group means the reaction no longer proceeds and stops at the quinonoid intermediate.

Chapter 2: Aims

2 Aims

Having introduced the field of sphingolipid chemistry and biology and reviewed the key role that the first enzyme, SPT, plays in the pathway this thesis has the following aims:

1. To understand the molecular details of how myriocin interacts with and inhibits SPT. Initially the myriocin-SPT relationship was probed through examination of inhibition kinetics but the ultimate goal was to produce a myriocin-SPT co-crystal structure, which could then be used to guide future drug development.

2. To probe the role of the N-terminus in SPT.

3. To continue the work on development of fusion SPT proteins.

Chapter 3:
Material and Methods

3 Materials and Methods

3.1 Materials and Reagents

Unless otherwise stated all reagents and chemicals were purchased from Sigma-Aldrich or Fisher Scientific. Palmitoyl Coenzyme A was purchased from Avanti Polar lipids. All primers were purchased from Sigma-Aldrich. Competent cells were purchased from either Novagen, Invitrogen or New England Biolabs (Table 3-1). All chromatography columns and equipment were purchased from GE Healthcare or Qiagen.

Myriocin is a poorly soluble compound even in 100% DMSO, with the highest possible concentration being only 5 mM and is only acheivable when the sample is heated to 80ºC to aid solvation. Upon cooling to less than 5 ºC myriocin would precipitate from DMSO and required further heating to re-dissolve. Therefore myriocin solution cannot be stored conveniently at either 4 ºC or -20 ºC until use. When adding myriocin stock solution to assays care must be taken not to add myriocin directly to cold buffers as this can also cause precipitation thus introducing inaccuracies into assays as well as problematic background absorbance in UV-vis experiments.

The pET28a-N-terminalHis-spSPT plasmid had already been constructed in house by Beverley Yard and Dominic Campopiano.[100]

3.1.1.1 Competent *E. coli* Cell Lines

Species	Cell Line	Application	Volume
E. coli	BL21 DE3 (Novagen)	Transformation and protein expression	10 µL
E. coli	DH5$_\alpha$ (Invitrogen)	Transformation and plasmid storage	25 µL
E. coli	HMS 174 DE3 (Novagen)	Transformation and protein expression	25 µL
E. coli	C2987 (NEB)	Transformation of ligations and mutagenesis products	15 µL

Table 3-1 Competent Cells

3.1.1.2 Cell Stocks

DNA was transformed into the appropriate cell line (depending upon end usage) and plated onto LB agar and grown overnight at 37 ºC. One colony was used to inoculate LB (5 mL). The culture was grown overnight at 37 ºC with agitation. Glycerol (20 % v/v) was added and cells were frozen at -80 ºC until required.

3.1.1.3 Sterile Conditions

All media, agar, pipette tips, eppendorfs and flasks were sterilised prior to use. Sterilisation was performed in a LTE® touchclave lab autoclave at 120 ºC, 1 atm for 20 minutes. All manipulations of cultured cells were performed in close vicinity to a lit Bunsen burner to help create a sterile environment.

3.1.1.4 Growth Media

All media was dissolved in water that had been deionised, 0.22 µm filtered and UV treated before the final pH was adjusted to 7.5 using either hydrochloric acid (conc) or sodium hydroxide (5 M). The media was then autoclaved and either used that day or stored at 4 ºC for a maximum of 4 days.

Formulations

2YT	tryptone (16 g L^{-1}), yeast extract (10g L^{-1}) and sodium chloride (5 g L^{-1})
LB (Lysogeny broth)	tryptone (10 g L^{-1}), yeast extract (5 g L^{-1}) and sodium chloride (10 g L^{-1})
SOC (Super Optimal broth with Catabolite repression)	tryptone (20 g L^{-1}), yeast extract (5 g L^{-1}), sodium chloride (0.58 g L^{-1}), potassium chloride (1 M, 2.5 mL), magnesium chloride (1 M, 10 mL), magnesium sulfate (1 M, 10 mL) and glucose (1 M, 20 mL)
Terrific	tryptone (12 g L^{-1}), yeast extract (24 g L^{-1}), glycerol (4 mL), potassium phosphate (2.31 g L^{-1}) and di-potassium phosphate (12.54 g L^{-1})

Table 3-2 Media Formulations

3.1.1.5 Agar

LB-Agar was purchased from Sigma-Aldrich and dissolved in purified water before being autoclaved. The appropriate antibiotic was added only when the agar had

cooled to less than 50 ºC. Plates were poured and allowed to set before being stored at 4 ºC for up to 1 week before use.

3.1.1.6 Antibiotic Solutions

Antibiotic stock solutions were made with deionsied, 0.22 µm filtered and UV treated water. Kanamycin 30 mg/mL stock solution was made and stored at 4 ºC until needed. The required volume was added to media to give a final concentration of 30 µg/mL.

3.1.1.7 Buffers

All buffers were made by dissolving the appropriate reagents in deionised, 0.22 µm filitered and UV treated water and adjusted, if required, to the correct pH using either conc HCl or 5 M NaOH. Buffers used for chromatography were 0.22 µm filtered again, and degassed before use. Buffers were stored for up to 2 weeks at 4 ºC.

Abbreviation	**Components**
Stock Buffer	0.2 M potassium phosphate (KPhos), pH 7.5 (3.84 g L^{-1} potassium phosphate , 45.07 g L^{-1} di-potassium phosphate
Buffer A	20 mM KPhos, pH 7.5, 150 mM NaCl, 25 µM PLP, 10 mM imidazole
Buffer B	20 mM KPhos, pH 7.5, 150 mM NaCl, 25 µM PLP, 50 mM imidazole
Buffer C	20 mM KPhos, pH 7.5, 150 mM NaCl, 25 µM PLP, 100 mM imidazole
Buffer D	20 mM KPhos, pH 7.5, 150 mM NaCl, 25 µM PLP, 150 mM imidazole
Buffer E	20 mM KPhos, pH 7.5, 150 mM NaCl, 25 µM PLP, 300 mM imidazole
Buffer F	20 mM Tris pH 7.5, 150 mM NaCl and 25 µM PLP
Buffer G	20 mM KPhos pH 7.5, 150 mM NaCl and 25 µM PLP

Table 3-3 Buffers

3.2 Methods

3.2.1 DNA Manipulation

3.2.1.1 Primers

Name	5'-3' Sequence
spSPT H159C Forward	ACAGCTGTGCGTCGATCTATGAC
spSPT H159C Reverse	ACGCACAGCTGTCGGCG
spSPT Nco1 Forward	ATATACCATGGCCGAAGCCG
spSPT Nco1 Reverse	TTCGGCCATGGTATATCTCCTT
spSPT HIS TEV STOP Forward	ATGGGCTGAGAGCACCACCAC
spSPT HIS TEV STOP Reverse	GTGCTCTCAGCCGATGACG
spSPT HIS TEV PLASMID STOP Forward	ACTCGAGTGACACCACCACCACC
spSPT HIS TEV PLASMID STOP Reverse	TGGTGGTGTCACTCGAGTGC
AmSPT K286A Forward	GTCGGCACTTTCTCTGCGTCTGTTGGAACT GTTGGC
AmSPT K286A Reverse	ACCCGCCAACAGTTCCAACAGACGCAGAG AAAGTGCCGAC
AmSPT 19AA Truncation Forward	CCCGACATCGCCATGGCACGCGACGTGCTC
AmSPT 19AA Truncation Reverse (pET Reverse)	CTAGTTATTGCTCAGCGGT

Table 3-4 Primers

SDM primers were designed using the Liu method,[152] which uses primers incorporating 3′ overhangs resulting in amplified DNA that is not nicked thus allowing newly synthesised DNA to be used as a template in subsequent rounds of

amplification. This simple alteration to existing SDM protocols results in SDM reactions becoming chain reactions which ultimately leads to less template DNA being required and thus making complete Dpn1 digestion easier.

3.2.1.2 Transformation of competent *E. coli*

Cells were removed from the -80 ºC freezer and allowed to thaw. Once thawed, plasmid DNA (2 µL) was added to the aliquot and allowed to incubate for 20 minutes. Cells were then heat-shocked for 40 seconds at 42 ºC before cooling on ice. SOC media (80 µL) was immediately added and the cells were left shaking at 37 ºC. After at least 1 hour, the cells were spread onto an LB kanamycin (30 µg mL^{-1}) plate and left to grow overnight at 37 ºC.

3.2.1.3 Polymerase Chain Reaction (PCR): Site directed mutagenesis

Each reaction contained forward primer (125 ng), reverse primer (125 ng), reaction buffer (5 µL, x 10 buffer), deoxynucleotide triphosphates (100 µM), template DNA (100 ng), Pfu Turbo DNA polymerase (2.5 U, 1 µL) with the reaction volume being adjusted to 50 µL with sterile water.

The PCR reaction consisted of one initial 1 minute denaturation at 95 ºC, followed by 18 cycles of 95 ºC for 30 seconds, annealing at 57 ºC for 1 minute and extension at 68 ºC for 12.5 minutes. The reaction finished with one final 10 minutes 68 ºC extension and then the sample was held at 4 ºC and used within 24 hours.

The PCR reaction mixture was then cut with the restriction enzyme DPN1 (10 U, 1 µL) to remove any methylated template DNA. The restriction digest was carried out at 37 ºC for greater than 1 hour. The product was used to transform C2987 cells as mentioned in Table 3-1.

3.2.1.4 PCR: Taq Polymerase Beads (GE Healthcare)

To each Taq bead forward primer (125 ng), reverse primer (125 ng), DNA template (50 ng) and enough sterile water to make the volume up to 25 µL were added.

The PCR reaction consisted of 30 cycles each containing a 95 ºC denaturation for 1 minute, a 55 ºC annealing for 1 minute and a 72 ºC extension for 2 minutes. An

additional 72 ºC extension for 10 minutes was also added at the end. PCR products were stored at 4 ºC and used within 24 hours.

The PCR reaction mixture was then cut with the restriction enzyme DPN1 (10 U, 1 µL) to remove any methylated template DNA. The restriction digest was carried out at 37 ºC for greater than 1 hour. The product was then analysed by gel electrophoresis.

3.2.1.5 Ligation into an Expression Vector

Restricted plasmid (50 ng), insert DNA (3 times the number of moles of plasmid), buffer (5 µL 2x buffer), T4 ligase (3 U, 1 µL) and sterile water to make the volume of the reaction mixture up to 10 µL. Ligation reactions were left overnight at 4 ºC.

The product was used to transform C2987 cells as mentioned in Table 3-1.

3.2.1.6 Digestion by Restriction Endonuclease

A typical double restriction digest contained template DNA (40 µL), restriction buffer (4 µL, 10x buffer from New England Biolabs) and restriction enzymes (2 µL). The mixture was incubated at 37 ºC for more than 1 hour before being separated by electrophoresis.

3.2.2 DNA Purification

3.2.2.1 Purification of DNA from cells: Qiagen Spin Miniprep Kit

An overnight culture (5 mL) was centrifuged to give a cell pellet (1100 g for 10 minutes). The supernatant broth was then discarded and DNA extracted following the manufacturer's instructions. The cell pellet was resuspended in 250 µL buffer P1 (50 mM Tris-HCl, pH 8.0, 10 mM EDTA and 100 µg mL^{-1} RNAse A) and transferred to an eppendorf tube. The cells were lysed by alkaline lysis by the addition of 250 µL buffer P2 (200 mM NaOH and 1% SDS). The tube inverted several times, before the addition of 350 µL of neutralisation buffer N3 (4.2 M GuHCl, 0.9 M KOAc, pH 4.8), which was immediately followed by vigorous mixing. The resulting suspension was centrifuged (11000 g for 10 minutes) following which the supernatant was transferred to a QIAprep™ spin column and centrifuged (11000 g for 1 minute). The flow through was discarded, and the column washed with 750 µL of buffer PE (10 mM Tris, pH 7.5, 80% ethanol) and centrifuged (11000 g for 1 minute). The supernatant was discarded and the column was centrifuged (11000 g for 1 minute) again to remove any residual buffer. The DNA was then eluted with sterile water (70 µL) into a sterile eppendorf tube and stored at -20 ^{o}C until required.

3.2.2.2 Extraction of DNA from Agarose gel: Qiagen Gel Extraction Kit

DNA in agarose gel (1%) was visualised using UV light (254 nm) and the appropriate portion of the gel was removed and DNA extracted following the manufacturer's instructions. Agarose containing DNA was covered with the minimal volume of buffer QG (usually about 300 µL, 20 mM Tris HCl pH 6.6 and 5.5 M guanidine thiocyanate) and incubated at 50 ^{o}C until all the agarose gel had dissolved. The solution was transferred to a spin column, and centrifuged (11000 g for 1 minute). The flow through was discarded, and the column was washed with more buffer QG (500 µL) and centrifuged (11000 g for 1 minute). The flow through was again discarded, and the column washed with 750 µL of buffer PE (10 mM Tris, pH 7.5, 80% ethanol) and centrifuged (11000 g for 1 minute). The flow through was again discarded, and the column centrifuged (11000 g for 1 minute) to remove any residual buffer. The DNA was eluted into an eppendorf tube with sterile water, (15 µL) and stored at -20 ^{o}C until required.

3.2.3 DNA Analysis

3.2.3.1 Digestion by Restriction Endonuclease

A typical single restriction digest contained template DNA (8 μL), restriction buffer (1 μL, 10x buffer from New England Biolabs) and restriction enzyme (1 μL). The mixture was incubated at 37 ºC for more than 1 hour before being analysed by electrophoresis.

3.2.3.2 Horizontal Electrophoresis

Agarose (1 g) was added to TAE buffer (100 mL, Qiagen) and heated until all the agarose was in solution. Once the solution had cooled to less than 50 ºC, either ethidium bromide (10 μL, 10 mg mL^{-1}) or GelRed™(10 μL, Biotium) where added. After mixing the solution was poured in the casting mould and allowed to set at room temperature. DNA loading dye (5 × buffer, Bioline) was added to each sample. The gel was submerged in TAE buffer, samples loaded and the gel was run at a constant voltage (100 V) until good separation was achieved between all bands.

3.2.3.3 Sequencing PCR

To the DNA sample (3 μL) that required sequencing, sequencing buffer (2 μL, 5 x, Applied Biosceince), Big Dye™ version 3.1 (2 μL) and either forward or reverse sequencing primer (1 μL, 10 μM stock). All primers were purchased from Sigma-Aldrich. The sequencing programme consisted of 25 cycles of 95 ºC for 30 seconds, 50 ºC for 30 seconds and 60 ºC for 4 minutes.

Primer Name	5'-3' Sequence
pET Forward	TTAATACGACTCACTATAGGG
pET Reverse	CTAGTTATTGCTCAGCGGT
pGem Forward	TAATACGACTCACTATAGGG
pGem Reverse	ATTTAGGTGACACTATAGAA

Table 3-5 Sequencing Primers

3.2.4 Protein Purification and Isolation

3.2.4.1 Large Scale Over-Expression in *E. coli*

One colony was used to inoculate LB broth (500 mL) containing kanamycin (30 µg mL^{-1}) and was allowed to grow overnight at 37 ºC with shaking (250 rpm). The inoculant was divided into LB broth (9 x 500 mL) containing kanamycin (30 µg mL^{-1}) and grown to an OD_{600} of 0.6 at 37 ºC before protein expression was induced with IPTG (0.1 mM). Protein was expressed for 5 hours at 30 ºC. Cells were harvested by centrifugation (7277 g, 10 minutes). Cells were stored at -20 ºC until required.

3.2.4.2 Cell Lysis – Sonication

All manipulations of cells were performed on ice. The cell pellet was resuspended in buffer A (6:1 v/w ratio, also containing protease inhibitor cocktail (Roche)) and sonicated for 10 cycles (30 seconds on, 30 seconds off) using a Soniprep 150. Sample was kept on ice during the sonication process to counteract heat generated by sonication. Cell debris was separated by centrifugation (47000 g, 30 minutes at 4 ºC). Supernatant, cell free extract (CFE) was retained for purification.

3.2.5 Protein Purification

3.2.5.1 Purification of *S. paucimobilis* SPT

Ni-NTA Agarose Affinity Chromatography

The CFE was filtered (0.22 µm) and incubated with Ni-NTA agarose resin (2 mL, Qiagen) at 4 ºC for 1 hour. Nickel resin was centrifuged (11000 g, 1 minute) prior to use to remove excess ethanol. After incubation the slurry was poured into an empty polypropylene column (5 mL) and allowed to pack under gravity. The column was washed with buffer A (40 mL) and protein eluted with buffer B, C, D and E (20 mL of each).

Qiagen resin regeneration

Previously used resin was washed and stored in 20% ethanol until it was recycled following the "quick protocol" outlined by Qiagen. This involved a 30 minute wash with 0.5 M NaOH, thorough rinsing with water to remove any excess NaOH and storage in 20 % ethanol at 4 ºC for up to two months. If cleaned correctly and stored in the fridge in 20% ethanol regenerated resin could be used for 4 times before poor protein binding was observed.

Size Exclusion Chromatography

A HiPrep™ 16/60 Superdex™ S-200 High Resolution size exclusion column was equilibrated with 1 column volume of buffer F (120 mL). The protein sample was concentrated (5 mL) and loaded on to the column. The protein was eluted with 1 column volume of buffer F which was collected in 5 mL fractions. The molecular weight of the eluted protein was calculated using Equation 3-1.

$$K_{av} = \frac{\textit{Elution}\ \text{Volume - Void Volume}}{\textit{Total}\ \text{Volume - Void Volume}} \qquad \text{MW} = \left(\frac{K_{av} - 1.827}{-0.129} \right)$$

Equation 3-1 Equations required to convert elution volume to predicted molecular weight
Kav = proportion of pores available to the protein. MW is plotted against Kav and the equation of the line of best-fit is rearranged to give the MW formula above.

3.2.6 Protein Analysis

3.2.6.1 Sodium Dodecyl Sulfate-Polyacrylamide Gel Electrophoresis (SDS-PAGE)

A typical gel (6 mL) consisted of a 4 mL 15 % running gel (2.185 mL H_2O, 5 mL acrylamide (30 %), 2.5 mL TRIS 1.5 M pH 8.8, 100 µL 10 % w/v SDS, 200 µL ammonium peroxodisulfide 50 mg mL^{-1} and 15 µL TEMED) and 2 mL 4 % stacking gel (5.8 mL H_2O, 1.35 mL acrylamide (30 %), 2.5 mL TRIS 0.5 M pH 6.8, 100 µL 10 % w/v SDS, 200 µL ammonium peroxodisulfide 50 mg mL^{-1}, 15 µL TEMED). All protein samples were denatured by the addition of SDS loading buffer (3 mL Tris 1.5 M pH 8.8, 5 % v/v glycerol, 10 % w/v SDS, 0.4 mL β-mercaptoethanol and 0.05 % w/v bromophenol blue) and boiled for 10 minutes. The mixture was centrifuged (11000 g, 1 minute) before sample was loaded on to the gel. Molecular weight marker (10 µL, Low Molecular Weight Marker, GE Healthcare) was also loaded. The gel was run for 50 minutes at a constant voltage of 200 volts. The protein was visualised by staining with Coomassie stain (H_2O, 0.1 % w/v Coomassie brilliant blue R250, 40 % v/v methanol and 10 % v/v acetic acid) and incubated for 20 minutes at 37 ºC. The gel was destained (H_2O, 40 % v/v methanol and 10 % v/v acetic acid) until excess blue was removed.

3.2.6.2 Bicinchoninic acid (BCA) Protein Assay

This assay relies on reduction of Cu^{2+} to Cu^{+} by peptide bonds in the protein in an alkaline environment (Figure 3-1).[153]

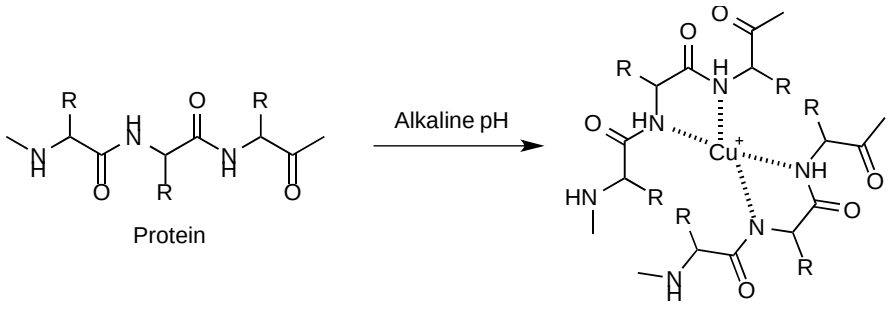

Figure 3-1 Reduction of cupric by the peptide bonds present in protein

The Cu^{+} is then detected by the bicinchoninic acid (Figure 3-2) in a 2:1 ratio. The binding of Cu^{+} causes a colour change from green to purple and can be detected by a change in absorbance at 562 nm. The assay was developed and produced by Pierce.

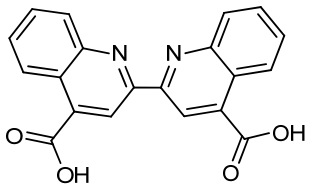

Figure 3-2 Bicinchonic Acid

The protein sample (50 µL) was added to the working solution (1 mL, 50:1 solution A:solution B) and incubated for 30 minutes at 37 ºC. A standard curve was produced from serial dilutions (2. 1.5, 1, 0.75, 0.5, 0.25, 0.125, 0.025 and 0 mg mL^{-1}) of a known stock of BSA. The absorbance of the sample was then taken and the concentration calculated from the standards.

3.2.7 Protein Chemistry

3.2.7.1 Spectroscopic Measurements

All UV-vis spectra were recorded on a Varians Cary 50 UV-Vis spectrophotometer and analysed using Cary WinUV software (Varian). To ensure SPT was in the holo form the enzyme was dialysed overnight at 4 ºC against buffer G. Excess PLP was removed by passing the protein through a PD-10 desalting column (Sephadex^{TM} G-25 medium, GE Healthcare) before any spectrophotometry was under taken. The spectrophotometer was blanked with 20 mM KPhos (pH 7.5) containing 150 mM NaCl.

3.2.7.2 5,5'-dithiobis-2-nitrobenzoic acid (DTNB) Assay

SPT activity was measured using a continuous spectrophotometric assay by monitoring the release of CoASH from palmitoyl-CoA. The principle of the assay is that the free thiol on the CoA will react with 5,5'-dithiobis-2-nitrobenzoic acid breaking the disulfide bond and making the coloured TNB^- anion ($\varepsilon = 14150\ M^{-1}\ cm^{-1}$) (Figure 3-3).

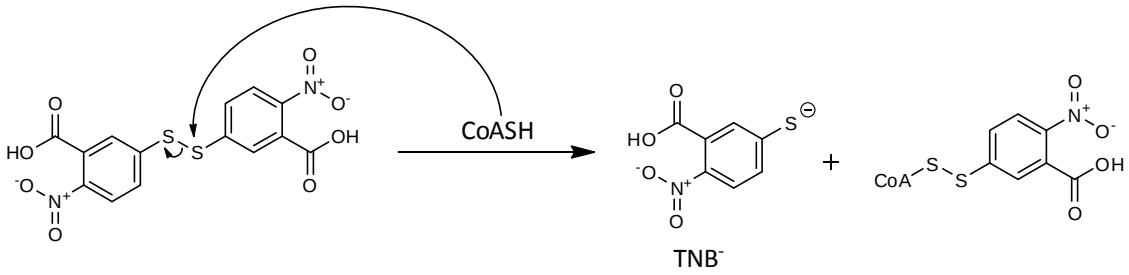

Figure 3-3 DTNB Assay

The production of TNB^- can be monitored by an increase in the absorbance at 412 nm. A typical experiment was carried out in a 0.5 mL plastic cuvette and contained SPT (50 µL, 2 µM), L-Serine (50 µL, 200 mM), DTNB (250 µL, 0.4 mM in 5 mM sodium acetate and 100 mM HEPES pH 8) and H_2O (100 µL). The absorbance at 412 nm was monitored for 1 minute to check for any background absorbance before the addition of palmitoyl-CoA (50 µL, 2.5 mM). Absorbance was monitored for another 14 minutes. L-Serine concentrations were varied from 0.1 mM – 40 mM. Kinetic constants (k_{cat} and K_m) were calculated from Michaelis-Menten plots using Sigma Plot.

3.2.7.3 Determination of dissociation constants for substrates and product quinonoid

Binding assays typically contained 20 µM enzyme in 20 mM KPhos (pH 7.5). Varying amounts of L-serine (0-40 mM) were added and after addition of the substrate, the reaction mixture was allowed to equilibrate for 15 min at 25 °C. The K_d values were calculated from plots of Δ_{425} versus L-serine concentrations by fitting to a hyperbolic saturation curve using Sigma Plot software (Equation. 3-2).

$$\Delta A_{obs} = = \frac{\Delta A_{max}\,[\text{serine}]}{K_d + [\text{serine}]}$$

Equation 3-2 Equation for calculating K_d
ΔA_{obs} represents the observed change in absorbance at 425 nm, ΔAmax is the maximal absorbance change, [serine] represents L-serine concentration, and the K_d is the dissociation constant.

To form the substrate quinonoid, 40 mM L-serine and 1.5 mM S-(2-oxoheptadecyl)-CoA were added to the enzyme. After addition, the reactants were mixed and allowed to equilibrate for 15 min at 25 °C. To form the product quinonoid, 25 µM KDS was added to the enzyme and allowed to equilibrate for 15 min at 25 °C.

3.2.7.4 Hexadecanal Assay

Activity was quantified by monitoring the reaction of the co-product CoASH with DTNB. The reaction was performed on a 250 µL scale, SPT (200 nM) was incubated with L-serine (20 mM) in the presence of varying hexadecanal concentrations (20, 40, 80, 125, 250, 500 and 1000 µM). The reaction was started by the addition of the second substrate palmitoyl-CoA (250 µM). A typical experiment contained 200 nM SPT, 20 mM L-serine, 250 µM palmitoyl-CoA, hexadecanal and 0.2 mM DTNB in 100 mM Hepes, pH 8.0. An IC_{50} value of 144 ± 17 µM was calculated using GraphPad Prisim 6 software.

3.2.7.5 Mass Spectrometry

Liquid Chromatography Fourier Transform Ion Cylotron Resonance Mass Spectrometry (LC-FT-ICR)

On-line liquid chromatography was performed using an Ultimate 3000 HPLC system (Dionex) equipped with a monolithic PS-DVB (500 μm × 50 mm) reverse-phase analytical column (Dionex) coupled to electrospray ionisation (nESI). Protein digests (5 pmoles) were loaded onto the column (maintained at 60°C) followed by a 30 min linear gradient from 2 to 70% acetonitrile (flow rate 20 μl/min). All mass spectra were recorded on SolariX FT-ICR mass spectrometer equipped with a 12 Tesla superconducting magnet (Bruker Daltonics). Transient data size was set to 1 M word for each acquisition.

Native mass spectrometry

Data was acquired on a SolariX FT-ICR mass spectrometer, as described above. Samples, typically 2 μM, were treated with 0.5% para-nitrobenzoic acid prior to analysis; and ESI ionisation was employed using a syringe pump operating at a flow of 500 μl h^{-1}. RF frequencies used in all ion-transmission regions were the lowest available value: multipole 1 (2 MHz), quadrupole (1.4 MHz) and transfer line (1 MHz). Ion-funnel and skimmer voltages were 200 V (funnel 1), 130 V (skimmer 1), 8 V (funnel 2) and 3V (skimmer 2). The collision voltage for the collision cell was varied between 10 and 20 V, to produce optimal signal. Ions were accumulated for 400 ms in the RF-hexapole ion trap before being transmitted to the infinity ICR trap and detected between m/z 1000 and 5000 to yield a broadband 1 M time-domain transient. Typically, each spectrum was the sum of 100 mass analyses. Mass spectra were externally calibrated using ES tuning mix (Agilent). The resulting spectra were analysed using DataAnalysis software (Bruker Daltonics); spectra were smoothed using the Gaussian algorithm and a smooth width of 0.15 m/z, before maximum entropy deconvolution was performed.

Online Tandem Mass Spectrometry

Online tandem mass spectrometry (MS) was performed on the SolariX FT-ICR Instrument. After the initial LC-MS run specific peptides of interest were selected for fragmentation. The protein digest was separated using an identical gradient to the above. However, the mass resolving quadrupole was set to select for a specific m/z throughout the LC-MS run and MS/MS was performed using collision-induced dissociation (CID). All spectra were externally calibrated using ES tuning mix (Agilent Technologies) and analyzed using DataAnalysis software (Bruker Daltonics), as above. For analysis of the tryptic digest, the SNAP 2.0 algorithm was used for automated peak picking in order to create a list of peptide masses. For CID experiments, fragment lists were created (using SNAP 2.0) and the resulting mass lists were searched against the relevant primary sequences using Prosight PTM software. Error tolerances were set to 10ppm. Isotope distributions of specific charge states were predicted from theoretical empirical formulae. These were overlaid upon the recorded experimental data as scatter plots.

3.2.7.6 Structural Biology

Proteins were screened for suitable crystallisation conditions in St Andrews in collaboration with Dr Stephen McMahon in the laboratory of Professor Jim Naismith. All proteins underwent both Ni affinity and size-exclusion chromatography (column eluted with 10 mM Tris, 150 mM NaCl and 25 μL PLP to avoid KPhos which readily crystallises). Protein was then concentrated to 20 mg mL^{-1} and the screens built on a Hamilton Microstar liquid handling robot controlled by the Rhombix system software (Thermo). Crystallisation trials were set up as a 1+1 (150 nL Protein and 150 nL well solution) and 2+1 (300 nL Protein and 150 nL well solution) sitting drops. Plates were immediately sealed and left for up to 2 weeks at room temperature for crystals to form.

K265A SPT:PLP-myriocin external aldimine inhibitor complex – PDB code 4BMK

Protein for crystallisation was concentrated to 20 mg mL^{-1} and incubated with 5 equivalents of myriocin immediately prior to crystallisation trials. Crystals of K265A SPT were grown by vapour drop diffusion at 20 °C over the course of 2 weeks and are readily reproducible. The optimum growth conditions are 32% PEG MME 2000, 0.1 M HEPES pH 7.5, and a protein:precipitant ratio of 1:1. Prior to data collection the crystals were cryo-cooled in mother liquor doped with 20% glycerol. Data were collected at Beamline I04-1 at the Diamond Synchrotron Light Source, Oxfordshire, England, and processed in an automated manner using Xia2.[154] The structure was solved by molecular replacement using PHASER[155] and PDB code 2JG2 as a model. The myriocin dictionary was created using PRODRG.[156] The model was refined using REFMAC5[157] with TLS. COOT[158] was used for manual manipulation of the structure and model quality was assessed throughout with MOLPROBITY.[159] Data collection and refinement statistics can be found in Table 4-.

.

Chapter 4:
Results and Discussion

4 Results and Discussion

4.1 SPT Variants

The first identification, isolation and cloning of *Sphingomonas paucimobilis* SPT was accomplished by Ikushiro *et al*. in 2001[99] (DNA and protein sequences are shown in Appendix 1). This cloning by Ikushiro allowed the Campopiano lab to generate recombinant spSPT from genomic *Sphingomonas paucimobilis DNA* in 2006[100] (see also Yard B.A. PhD Thesis). The resulting DNA sequence was cloned into a pET-28a vector and named pET-28a SPT. Subsequent lab members later re-cloned pET-28a SPT to encode for a C-terminal histidine tag in preference over the original N-terminal tag, for purification purposes, henceforth that protein is referred to as spSPT (DNA and protein sequences are shown in Appendix 1). This recombinant spSPT form matches the published sequences exactly but also contains an extra eight amino acids; leucine, glutamic acid and six histidines at the C-terminus.

4.1.1 Purification, characterisation and activity of spSPT

Plasmid pET 28a spSPT was used to transform BL21 (DE3) cells which were in turn used to express spSPT in LB with 0.1 mM IPTG for 5 hours at 30 ^{o}C. The protein was isolated from the CFE by gravity flow nickel affinity chromatography using nickel resin (Ni-NTA Agarose – Qiagen) followed by a stepwise imidazole gradient performed on the bench at room temperature (Figure 4-1 Left).

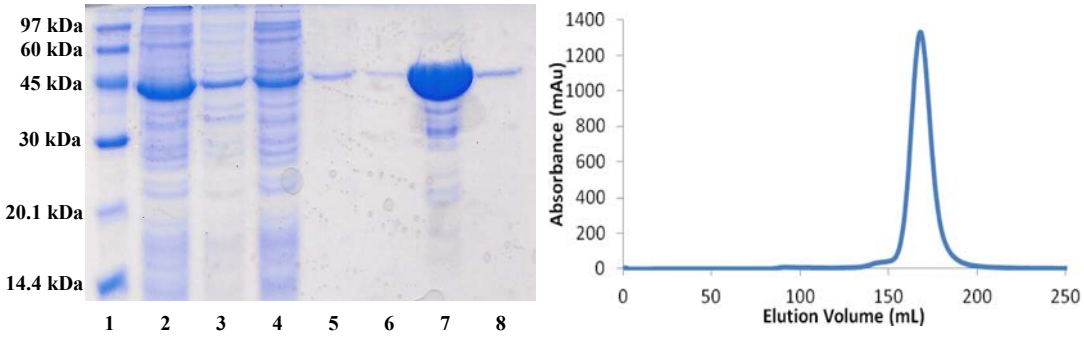

Figure 4-1 Optimised purification of spSPT
Left - Lane 1: Low molecular weight marker, Lane 2: Supernatant, Lane 3: Pellet, Lane 4: Flow through, Lane 5: Wash 1 - 30 mM Imidazole wash, Lane 6: Wash 2 - 30 mM Imidazole, Lane 7: Elution 1 - 300 mM Imidazole, Lane 8: Elution 2 – 300 mM Imidazole. **Right** - Elution profile from 26/60 S200 size exclusion column, blue line showing absorbance at 280 nm.

Size exclusion chromatography revealed that spSPT behaved as a single species in solution with a mass of roughly 92 kDa, corresponding to the formation of a homodimer (Figure 4-1 Right).

Purified protein was routinely analysed by LC-ESI MS to confirm purity and assure reproducibility. The predicted mass of apo spSPT is 46104 Da and would also be the expected observable species under LC-MS conditions. The labile nature of the imine bond between the active site lysine and PLP in the internal aldimine conformation, results in the loss of PLP in normal mass spectrometry conditions. The experimentally observed mass was 45975 Da, demonstrating spSPT had lost its N-terminal methionine after translation (Figure 4-2). A relatively common post-translational modification in recombinant proteins expressed in *E. coli*.

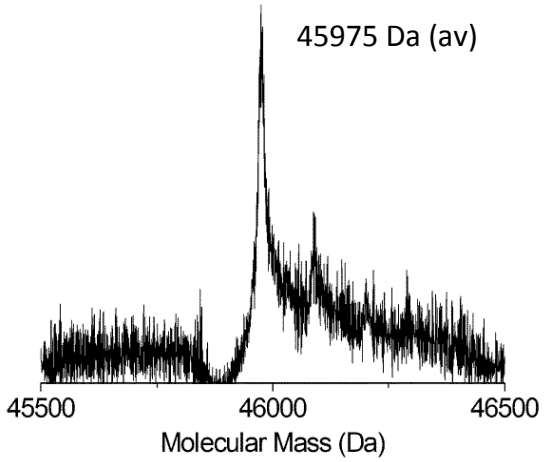

Figure 4-2 Intact protein mass spectrometry of spSPT
Deconvoluted intact protein mass spectrum of spSPT (40 μM) with an average neutral mass of 45975 Da.

Following purification the protein could then be stored for long periods of time frozen at -80 ^{o}C, once mixed with 20% glycerol the protein was rapidly cooled in liquid nitrogen before being transferred to the freezer. When required the protein was removed from the freezer, thawed on ice and dialysed against a fresh PLP buffer (buffer G in Table 3-3). Both mass spectrometry and enzymatic assays showed no deterioration in the protein following up to 6 months in the freezer.

At all points throughout the purification the presence of PLP can be observed due to its distinct yellow colour which is faintly visible in the *E. coli* cell pellet, more

distinctly in the supernatant and unmistakable in the affinity column elution fraction (which is bright yellow) (Figure 4-3).

Figure 4-3 Characteristic colour of PLP containing solutions
Left – 750 µL aliquot of the supernatant generated after lysis of spSPT producing *E. coli* cells. **Right** – 750 µL aliquot of the elution fraction generated from the Nickle affinity purification step of spSPT.

Before all UV-vis experiments excess PLP was removed by passing the sample through a PD-10 desalting column (Sephadex G-25M, GE Healthcare). UV-vis spectroscopy showed that PLP was bound to the enzyme and existed in the expected two tautomeric forms (Figure 4-4 Top and Bottom Left).

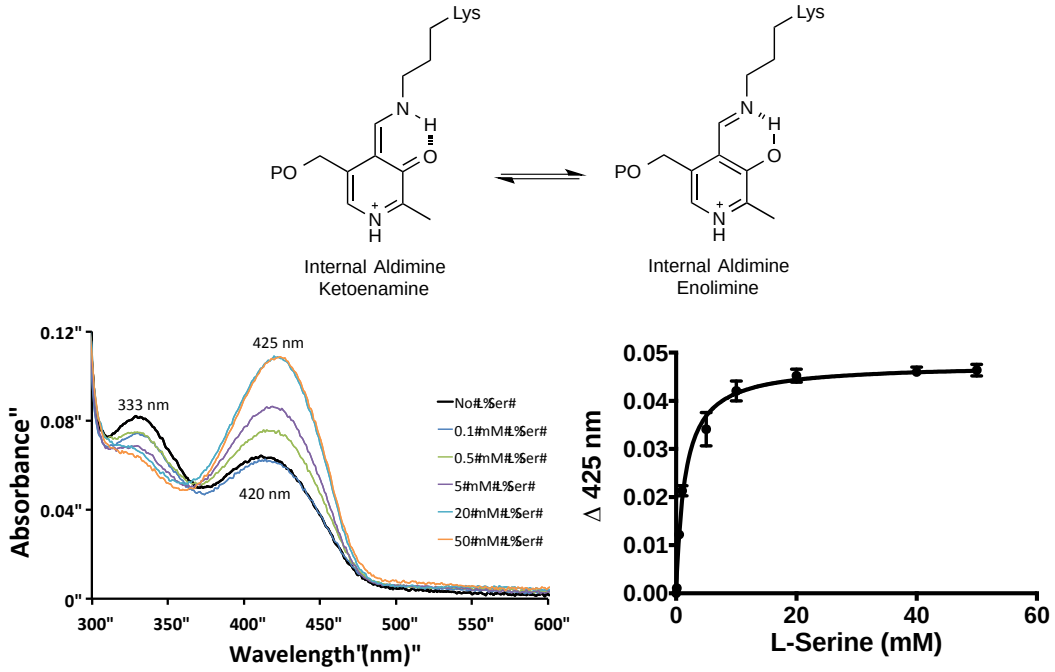

Figure 4-4 UV-vis spectrum and kinetic analysis of spSPT
Top – The two visible, tautomeric, forms of PLP when it is bound to SPT in the internal aldimine conformation. **Bottom left** - The black line shows the holo-form of the enzyme (40 µM SPT, 20 mM KPhos buffer (pH 7.5), 150 mM NaCl, 25 °C). Increasing concentrations of L-serine were added (0.1, 0.5, 5, 20, and 50 mM) coloured lines. **Bottom right** - Analysis of L-serine binding to generate a K_d.

Addition of L-serine to the enzyme altered the PLP equilibrium as expected, producing more of the ketoenamine form of PLP.[29] The titration of increasing amounts of L-serine (0.1, 0.5, 1, 5, 20, 40 and 50 mM) to the enzyme produces a successively larger 425 nm absorbance which can be used to calculate the dissociation constant (K_d) for L-serine, 1.4 ± 0.1 mM (Figure 4-4 Bottom Right). Alternatively substrate concentrations can be varied in rate assays, with the resulting changes in rate plotted in the typical Michaelis-Menten manner to produce a Michaelis constant (K_m) for L-serine of 1.5 ± 0.1 mM (Figure 4-5).

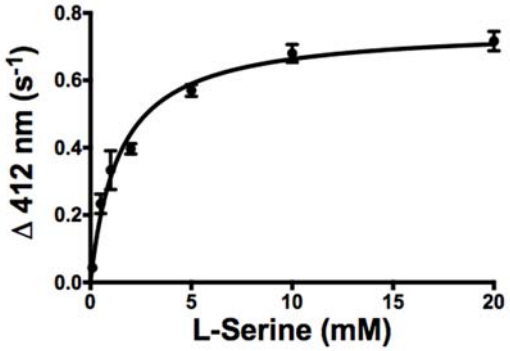

Figure 4-5 The effect of changing L-serine on initial reaction rate
Kinetic analysis of spSPT using the DTNB assay. Initial rates of CoASH release measured spectrophotometrically at 412 nm and at several final concentrations of L-serine (0.1, 0.5, 1, 5, 10 and 20 mM) Each assay contained 700 nM enzyme, 250 μM palmitoyl-CoA, 0.2 mM DTNB and the appropriate L-serine standard.

Although spSPT had previously been purified in our lab, improvements upon repetition were made. Purification was completed successfully at room temperature, rather than at 4 ºC for the first time with no deleterious effects upon enzyme activity or UV-vis spectroscopy, although the enzyme was always stored at 4 ºC if it was not required immediately. The optimal nickel affinity chromatography conditions were determined for Qiagen resin. Two 30 mL washes (30 mM imidazole) followed by a 5 mL elution (300 mM imidazole). Nickel affinity chromatography has been shown to work equally as well with both new and recycled resin.

4.1.2 Purification, characterisation and activity of AmSPT

Initial work focussed on re-establishing the ability to grow diffraction quality crystals of spSPT following the success of previous group members, especially Dr. Marine Raman.[29] Unfortunately this goal was never reached. Despite fastidious attention to detail and accurate replication of the published method no adequately-sized, good quality spSPT crystals could be grown. After several failed crystal trials it became apparent that the ability to produce SPT crystals had actually been lost approximately 9 months prior to me starting of my PhD. However initial trials started by trying to exactly replicate Dr. Raman's published method. The use of the same construct, preparation procedure, columns and crystal screens all failed to yield any results. In an attempt to circumvent this roadblock other SPT constructs were considered. Our collaborator Professor Teresa Dunn (Uniformed Services University, Bethesda, U.S.A.) provided the group with a new, unpublished spSPT isoform, denoted AmSPT due to its American origin. This synthetic AmSPT gene had been codon optimised for *Arabidopsis* expression for another project but expression in *E. coli* was attempted (DNA and protein sequences are shown in Appendix 1). Due to the difficulties experienced in purifying N-terminally tagged SPT and the mobile nature of the N-terminus in crystal structures AmSPT has been engineered with a 12 amino acid linker between the start of the sequence and the N-terminal histidine tag (Figure 4-6).

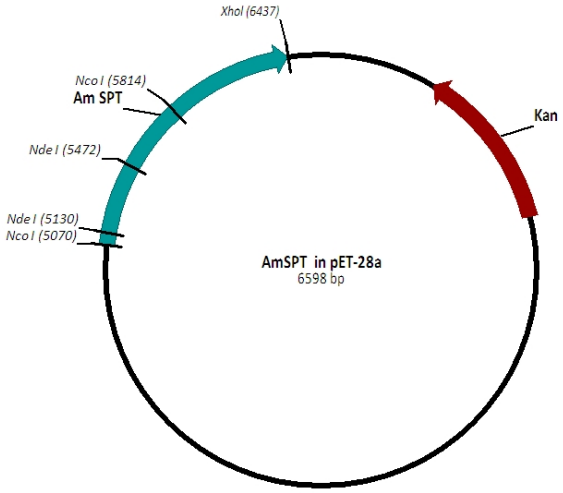

Figure 4-6 pET28a plasmid map of AmSPT

AmSPT was treated as a completely new protein and therefore underwent expression and purification screens before the optimal procedure was deduced. Protein

expression was initially attempted in both HMS174 (DE3) and BL21 (DE3) for various lengths of time under the control of numerous IPTG concentrations. Optimal expression was observed in BL21 (DE3) cells for 5 hours with only 0.1 mM IPTG required. Initial purification was undertaken at both room temperature and 4ºC but no difference in UV-vis characteristics or enzyme rates were observed therefore all subsequent purifications were carried out at room temperature. Nickel affinity chromatography (Figure 4-7 Left) followed by size exclusion chromatography (Figure 4-7 Right) generated pure AmSPT as expected. AmSPT eluted from the gel filtration column in the predicted homodimeric state with an elution volume roughly corresponding to 92 kDa, similar to what was obtained with spSPT.

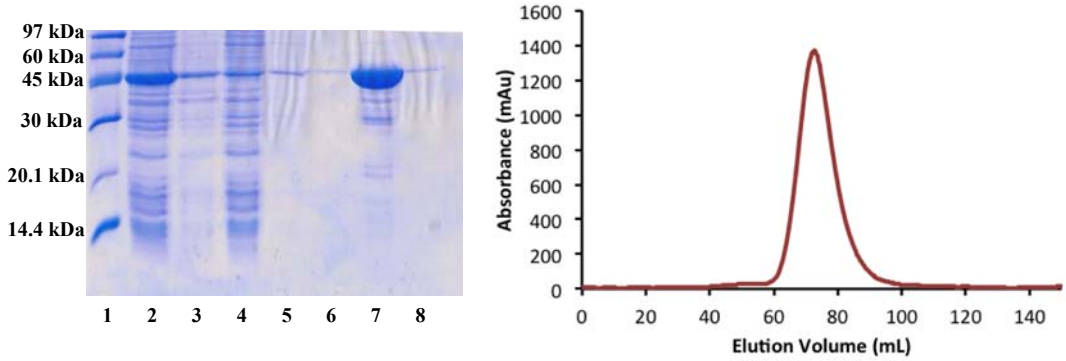

Figure 4-7 Optimised purification of AmSPT

Left - Lane 1: Low molecular weight marker, Lane 2: Supernatant, Lane 3: Pellet, Lane 4: Flow through, Lane 5: Wash 1 - 30 mM Imidazole wash, Lane 6: Wash 2 - 30 mM Imidazole, Lane 7: Elution 1 - 300 mM Imidazole, Lane 8: Elution 2 – 300 mM Imidazole. **Right** - Elution profile from Sephacryl16/60 S200 size exclusion column, red line showing absorbance at 280 nm.

AmSPT was routinely analysed by mass spectrometry to monitor the effectiveness of individual protein preparations. The measured AmSPT apo mass of 47231 Da (Figure 4-8) matches the predicted mass (47363 Da) minus the initial methionine (Δmass -131 Da).

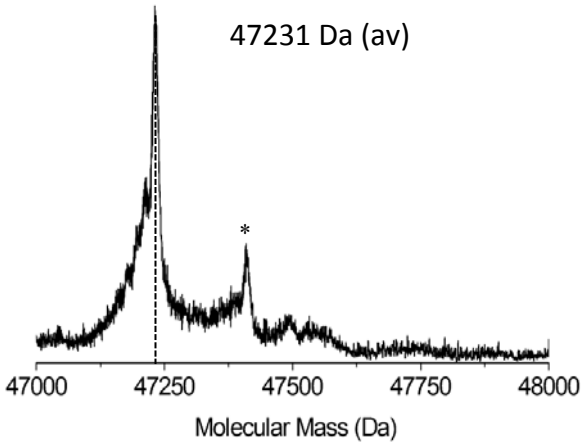

Figure 4-8 Intact protein mass spectrometry of AmSPT
Intact protein mass spectrometry of AmSPT (40 μM) with an average neutral mass of 47231 Da. α-N-6-gluconoylation is marked was an *.

Consistently throughout mass analysis a minor contaminant of larger mass can be observed (asterisks in Figure 4-8) which was eventually determined to be α-N-6-gluconoylation of the histidine tag (Figure 4-9).

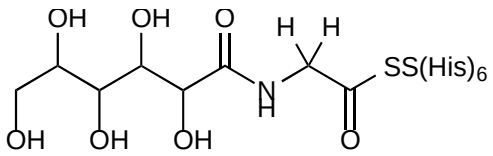

Figure 4-9 Structure of the α-N-6-gluconoylation product
Showing the adduct attached to the N-terminal glycine which is characteristically linked to two serines and then the histidine tag.

α-N-6-gluconoylation is a relatively new post-translational modification coinciding with the new era of highly overexpressed, affinity purified proteins from *E. coli* and corresponds to a 178 Da increase in mass from the addition of a gluconic acid derivative to the histidine tag.[160]

AmSPT exhibited the characteristic UV-vis spectrum expected from an SPT isoform, consisting of PLP in both the enolimine and ketoenamine forms with absorbance maxima at 333 and 420 nm respectively (Figure 4-10). Upon addition of L-serine the resultant PLP:L-serine aldimine demonstrated the same preference for the ketoenamine form as it does with spSPT. The difference in absorbance at 425 nm at a range of L-serine concentrations (0.1 – 250 mM) allows the estimation of the K_d for L-serine binding to be made, 13.8 ± 0.6 mM (Figure 4-10). The reason why L-serine binding is 10-fold weaker in AmSPT than in spSPT is unknown. As the only

structural change in AmSPT is the 20 amino acid N-terminal extension it must be concluded that this extension must cause a small conformational change that prevents optimum PLP:L-serine aldimine binding. Interestingly in the original crystal structure of spSPT the first 21 amino acids are not well defined in the electron density map and so the structure of the N-terminus is not known (see below).

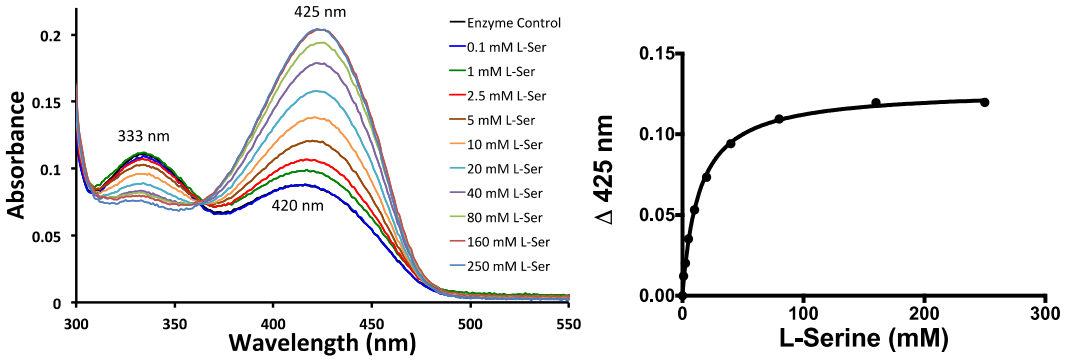

Figure 4-10 UV-vis spectrum and kinetic analysis of AmSPT
Left - The black line shows the holo-form of the enzyme (40 μM SPT, 20 mM Kphos buffer (pH 7.5), 150 mM NaCl, 25 °C). Increasing concentrations of L-serine were added (0.1, 1, 2.5, 5, 10, 20, 40, 80, 160 and 250 mM) coloured lines. **Right** - Analysis of L-serine binding to generate a K_d.

Utilisation of the DTNB assay at multiple substrate concentrations produced a K_m for both L-serine and palmitoyl CoA of 2.9 ± 0.2 mM and 95 ± 6 μM respectively (Figure 4-11). The kinetic parameters agree reasonably well with the determined values for spSPT, demonstrating that the addition of the N-terminal extension has had only a minor effect on the catalytic capability of AmSPT. The N-terminal extension was originally predicted to affect the palmitoyl-CoA binding due to the long alkyl chain of palmitate being predicted to occupy a hydrophobic channel pointing towards the disordered N-termini. To some extent this hypothesis could be correct as the K_m for palmitoyl-CoA has increased 3 fold in comparison to spSPT.

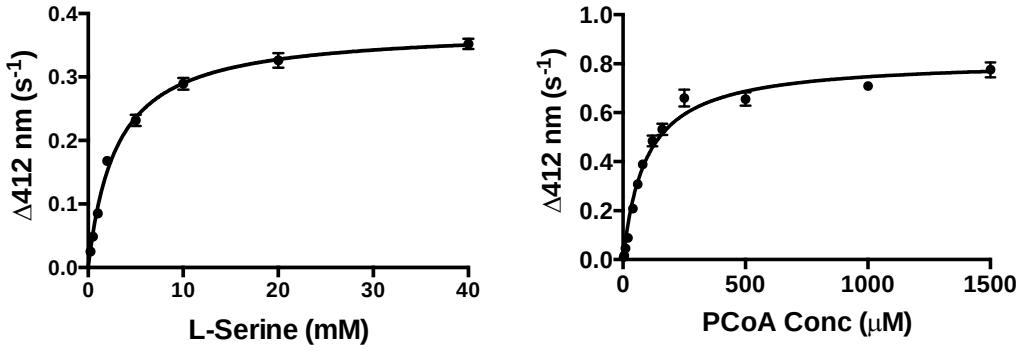

Figure 4-11 K_m determination for L-serine and palmitoyl-CoA with AmSPT
Kinetic analysis of AmSPT using the DTNB assay. Initial rates of CoASH release measured spectrophotometrically at 412 nm and at several final concentrations of L-serine (0.1, 0.5, 1, 5, 10, 20 and 40 mM) (Left) or palmitoyl-CoA (2, 5, 10, 20, 40, 60, 80, 120, 160, 250, 500, 1000 and 1500 μM) Each assay contained 700 nM enzyme, 250 μM palmitoyl-CoA or the appropriate standard, 0.2mM DTNB and 20 mM L-serine or the appropriate standard. All experiments were done in triplicate. Graphs are plotted as mean readings with ± 2SDs appearing as error bars, for points without error bars the range is covered within the circular mark.

The rates of reaction catalysed by spSPT and AmSPT were compared directly again by utilisation of the DTNB assay. Comparison of the turnover number (k_{cat}) showed AmSPT to be half the velocity of spSPT (Table 4-1). With both enzymes having the same amino acid sequence this was difficult to rationalise and must again be attributed to the long N-terminus of AmSPT undergoing conformational change during catalysis, perhaps slowing down product release. When the rate of AmSPT is compared to other isoforms from different bacterial strains the small variation with spSPT appears less significant. Both *S.wittichii* and *Bacteroides fragilis* SPT are more than 10 fold slower than spSPT but this variation should be expected due to the differences in amino acid sequences, *S.wittichii* and *Bacteroides fragilis* respectively have only 75% and 35% identity with spSPT. Interestingly myriocin does not inhibit all of the SPT isoforms equally (Tabel 4-1). Previously the inhibition of SPT by myriocin had been unquestioned but the comparison of natural bacterial isoforms of SPT shows a wide variation in myriocin potency.

	k_{cat} (s^{-1})	Rate proportional to spSPT	Activity with 2 eq. of Myriocin	Activity with 5 eq. of Myriocin
spSPT	1.27 ± 0.06	1	40%	31%
AmSPT	0.63 ± 0.05	0.49	29%	2.3%
Sphingomonas wittichii	0.068 ± 0.007	0.053	29%	17%
Bacteroides fragilis	0.005 ± 0.0006	0.004	100%	100%

Table 4-1 Rate and myriocin inhibition comparison of various SPT isoforms

Taken together with Ikushiro's work with SPTs from *Sphingobacterium multivorum, Sphingobacterium spiritivorum and Bacteriovorax stolpii* produces the most comprehensive kinetic comparison of bacterial SPTs to date (Table 4-2).

Bacteria	k_{cat} (s^{-1})
Sphingomonas paucimobilis	1.27 ± 0.06
Sphingomonas wittichii	0.068 ± 0.007
Bacteroides fragilis	0.005 ± 0.0006
Sphingobacterium multivorum	0.47 ± 0.10
Sphingobacterium spiritivorum	1.20 ± 0.03
Bacteriovorax stolpii	2.55 ± 0.12

Table 4-2 Comparison of turnover rates for bacterial SPTs[161]

It is assumed that the active sites of each SPT shares a high level of similarity in order to allow them all to bind the same L-serine and palmitoyl-CoA substrates but clearly nuances in natural variation decrease myriocin binding affinity. In Ikushiro's pioneering early work she also demonstrated that spSPT could also accept glycine, alanine and to a lesser extent threonine as substrates as well as tolerating 1-2 carbon extensions and truncations to the acyl chain of CoA reasonably well.[99] The data also raises the possibility that myriocin acts allosterically at a site of greater variation in the amino acid backbone. As the mode of myriocin inhibition or site of action was

unknown at this point the data were used to confirm AmSPT as the most suitable SPT isoform to attempt myriocin-SPT co-crystal trials with. While investigating the effect of myriocin upon various SPT isoforms the concentration of myriocin needed to gain maximal inhibition was also elucidated. The use of 5 equivalents of myriocin, 200 μM against 40 μM SPT provided almost 98% inhibition within 2 minutes of addition with no further inhibition seen with 10 equivalents (400 μM).

4.1.3 Δ21 spSPT truncation

To date all the published spSPT crystal structures have lacked definition at the N-terminus with the first 21 amino acids not appearing in any structure. The lack of the N-terminal region has been apportioned to flexibility within the first 21 amino acids allowing several possible configurations thus resulting in indistinct electron density upon diffraction. During the course of research within the group the ability to crystallise any form of SPT with any combination of ligands or inhibitors was lost (occurring between 2009-2010). Following the dogma that smaller molecules crystallise easier resulted in the hypothesis that truncation of the mobile N-terminus could aid crystallisation. Comparing spSPT to *Sphingomonas wittichii* SPT (Figure 4-12) highlights the non-essential nature of the first 20 amino acids and guided the decision to truncate spSPT.

```
Sphingomonas_paucimobilis_SPT      MTEAAAQPHALPADAPDIAPERDLLSKFDGLIAERQKLLDSGVTDPFAIV 50
Sphingomonas_wittichii_SPT         ----------------------MADLLSKFDPLIAEREALLATGVRDPYAIV 30
                                                          ******* *****: ** :** **:***

Sphingomonas_paucimobilis_SPT      MEQVKSPTEAVIRGKDTILLGTYNYMGMTFDPDVIAAGKEALEKFGSGTN 100
Sphingomonas_wittichii_SPT         MDKVLSPTEAMINGRKTILLGTYNYMGMTFDPDVIAAGKQALDEFGSGTT 80
                                   *::* *****:*.*:.**************************:**::*****.

Sphingomonas_paucimobilis_SPT      GSRMLNGTFHDHMEVEQALRDFYGTTGAIVFSTGYMANLGIISTLAGKGE 150
Sphingomonas_wittichii_SPT         GSRVLNGTYQGHKACEDALKEFYGTEHAIVFSTGYQANLGMISTLAGKGD 130
                                   ***:****::.*   *:**::****  ******** ****:********:

Sphingomonas_paucimobilis_SPT      YVILDADSHASIYDGCQQGNAEIVRFRHNSVEDLDKRLGRLPKEPAKLVV 200
Sphingomonas_wittichii_SPT         YIILDADSHASIYDGCWLGDAEIVRFRHNSVEDLDKRLGRLPAEAGKLVV 180
                                   *:**************  *:********************** *..****

Sphingomonas_paucimobilis_SPT      LEGVYSMLGDIAPLKEMVAVAKKHGAMVLVDEAHSMGFFGPNGRGVYEAQ 250
Sphingomonas_wittichii_SPT         LEGVYSMMGDIAPLQEMVAVSKKHGAMILVDEAHGMGFFGEHGRGVFEEA 230
                                   *******:******:*****:******:******.***** :****:*

Sphingomonas_paucimobilis_SPT      GLEGQIDFVVGTFSKSVGTVGGFVVSNHPKFEAVRLACRPYIFTASLPPS 300
Sphingomonas_wittichii_SPT         GVEADVDFVVGTFSKSVGTVGGFCVSNHPKFEVLRLVCRPYVFTASLPPS 280
                                   *:*.::***************** ********.:**.****:********

Sphingomonas_paucimobilis_SPT      VVATATTSIRKLMTAHEKRERLWSNARALHGGLKAMGFRLGTETCDSAIV 350
Sphingomonas_wittichii_SPT         VVATAATSIRKLMHAGDKRAHLWKNSRRLHQGLRDMGYKLGTETAQSAII 330
                                   *****:******* * :** :**.*:* ** **: **::*****.:****:

Sphingomonas_paucimobilis_SPT      AVMLEDQEQAAMMWQALLDGGLYVNMARPPATPAGTFLLRCSICAEHTPA 400
Sphingomonas_wittichii_SPT         AVILTDMAQAVALWQGLLEAGLYVNTARPPATPAGMFLLRCSLCAEHSDE 380
                                   **:* *  **. :**.**:.***** ********* ******:****:

Sphingomonas_paucimobilis_SPT      QIQTVLGMFQAAGRAVGVIG 420
Sphingomonas_wittichii_SPT         QVEQILGMFESAGRATGVIP 400
                                   *:: :****::****.***
```

Figure 4-12 Protein sequence alignment comparing *Sphingomonas paucimobilis* SPT and *Sphingomonas wittichii* SPT

Key - * (asterisk) indicates positions which have a fully conserved residues, : (colon) indicates conservation between groups of strongly similar properties and . (full stop) indicates conservation between groups of weakly similar properties, red = small, blue = acidic, magenta = basic and green = Hydroxyl, sulfhydryl, amine or glycine.

Primers (Table 3-4) were designed to introduce a start codon into spSPT as part of an Nco1 site (CCATGG), resulting in the new protein beginning with a methionine and an alanine (DNA and protein sequences are shown in Appendix 1). PCR using Taq polymerase, ligation into pGEM followed by sequencing revealed three single base mismatches as well as the desired start codon. The first base change was a deliberate deviation from the original DNA sequence in favour of a more common codon and was therefore a silent mutation. The second base change resulted in an L5V mutation and was due to poor primer design. The third change corresponded to a L335Q mutation and was the result of using Taq polymerase, a relatively low fidelity polymerase in comparison to Pfu and others. The double L5V, L335Q Δ21 spSPT mutant was carried forward into protein studies with the knowledge that a wild-type Δ21 spSPT would be required later if initial crystal trials were successful.

Test expression showed optimal L5V L335Q Δ21 spSPT production with 0.1 mM IPTG over 5 hours at 30 ºC. Normal purification yielded copious protein (Figure 4-13 Left) but size exclusion chromatography revealed larger molecular weight protein aggregates were forming, indicating that the removal of the N-terminus had affected the stability of the homodimer (Figure 4-13 Right).

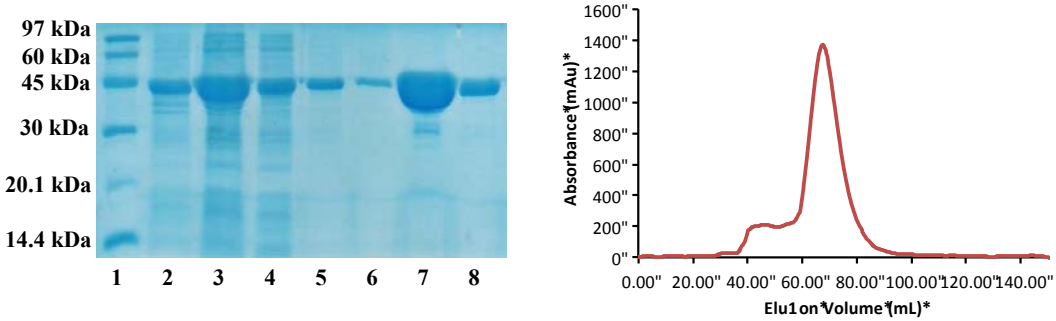

Figure 4-13 Optimised purification of Δ21 spSPT
Left - Lane 1: Low molecular weight marker, Lane 2: Pellet, Lane 3: Supernatant, Lane 4: Flow through, Lane 5: Wash 1 - 30 mM Imidazole wash, Lane 6: Wash 2 - 30 mM Imidazole, Lane 7: Elution 1 - 300 mM Imidazole, Lane 8: Elution 2 – 300 mM Imidazole. **Right** - Elution profile from Superdex 16/60 S200 size exclusion column, red line showing absorbance at 280 nm.

Preliminary UV-vis analysis showed normal PLP binding with two equal peaks at 325 nm and 415 nm when in a Tris buffer. Rate comparison of L5V L335Q Δ21 spSPT showed the truncation displayed decreased enzyme activity 5 fold compared with WT spSPT; the k_{cat} of L5V L335Q Δ21 spSPT was 0.21 s^{-1} in comparison to 1.27 sec^{-1} for spSPT. The role of the N-terminus is as yet unknown but should not be

under estimated as both extension of the N-terminus, in the case of AmSPT, and its truncation both influence the catalytic rate. The two amino acid substitutions listed above could also play a role in either the increase aggregation or the decrease in rate.

Crystal trials with L5V L335Q Δ21 spSPT yielded no crystals when either set-up natively or in combination with L-serine, myriocin or the palmitoyl-CoA analogue using either in-house or commercial screens. As the Δ21 spSPT was specifically developed to produce crystals upon failure to crystallise no further characterisation or attempts to rectify the two unwanted mutations were made.

4.1.4 **K286A AmSPT**

In an attempt to stall the catalytic mechanism after the addition of palmitoyl-CoA and trap the resulting tertiary complex before product formation a catalytically comprised mutant was engineered. This catalytically-inactive SPT isoform was designed to aid the elucidation of the palmitoyl-CoA binding site. Analysis of the SPT catalytic mechanism shows Lys265 to be crucial, not only for initial PLP binding, but also for deprotonation of the PLP:L-serine external aldimine. Therefore this residue was selected for mutagenesis. After the addition of the N-terminal linker and six histidine tag the amino acid numbering changes slightly with the key residue Lys265 corresponding to Lys286 in AmSPT. Employing the Liu *et al.*[152] method of site directed mutagenesis using over hanging primers (Table 3-4) yielded the correct mutation. Mutagenesis was checked by DNA sequencing and, after protein expression and purification, by mass spectrometry.

Test expression studies showed good expression in the same conditions as the wild type protein, 0.1 mM IPTG at 30 ºC for five hours. Purification by nickel affinity and size exclusion chromatography proceeded uneventfully and yielded pure protein (Figure 4-14).

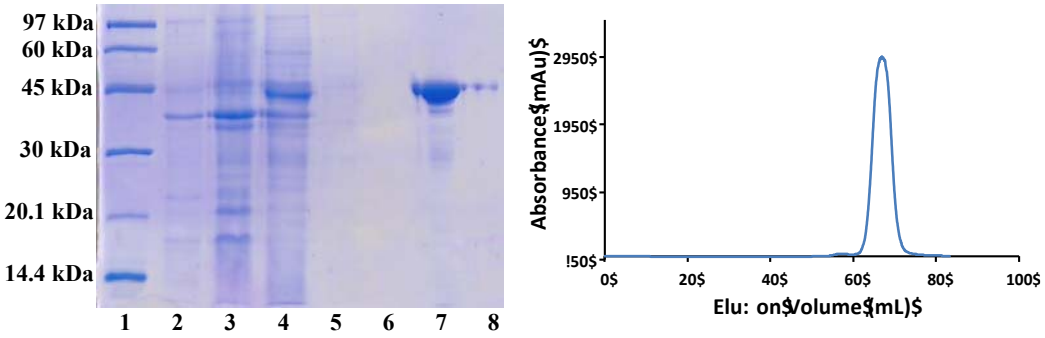

Figure 4-14 Optimised purification of K286A AmSPT
Left - Lane 1: Low molecular weight marker, Lane 2: Pellet, Lane 3: Flow through, Lane 4: Supernatant, Lane 5: Wash 1 - 30 mM Imidazole wash, Lane 6: Wash 2 - 30 mM Imidazole, Lane 7: Elution 1 - 300 mM Imidazole, Lane 8: Elution 2 – 300 mM Imidazole. **Right** - Elution profile from Superdex 26/60 S200 size exclusion column, blue line showing absorbance at 280 nm.

Following initial purification the integrity of the protein was confirmed by mass spectrometry, with the observed apo mass correlating exactly to the predicted mass of 47174 Da (Figure 4-15).

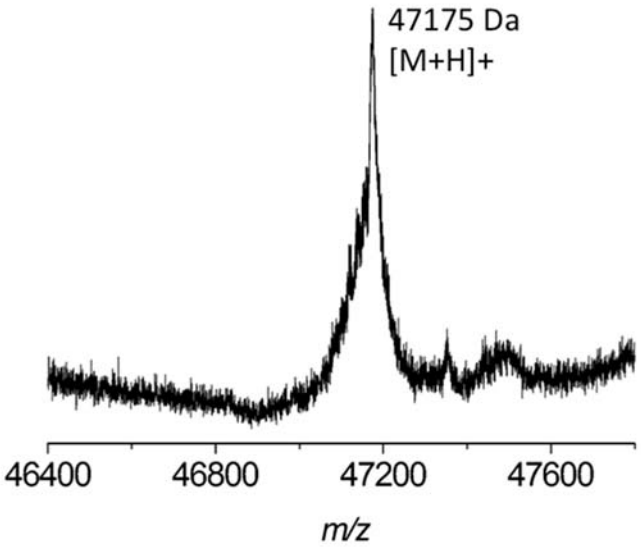

Figure 4-15 Intact protein mass spectrometry of K286A AmSPT
Intact protein mass spectrometry of K286A AmSPT (40 μM) with an average neutral mass of 47174

UV-vis analysis of the purified mutant protein showed one dominant peak at 400 nm and a much smaller peak at 323 nm, in contrast to the much more even distribution seen with WT AmSPT (Figure 4-16). This suggests that the non-covalently bound PLP preferred the ketoenamine form and that the K286A mutation had impacted upon PLP binding and shifted the equilibrium away from the usually dual PLP species. Upon addition of L-serine to this form of the protein no change in the UV-vis spectrum was observed suggesting that L-serine is not interacting with PLP presumably because the PLP cofactor is not bound in a favourable position. This result suggests that the internal aldimine (PLP:Lysine imine bond) is essential for the recognition of the amino acid substrate and subsequent formation of the external aldimine (PLP:Serine imine bond). Taken together these findings suggest that the removal of the active site lysine in AmSPT does not stop PLP binding but only limits it to a non-covalent interaction and at the same time precludes L-serine binding.

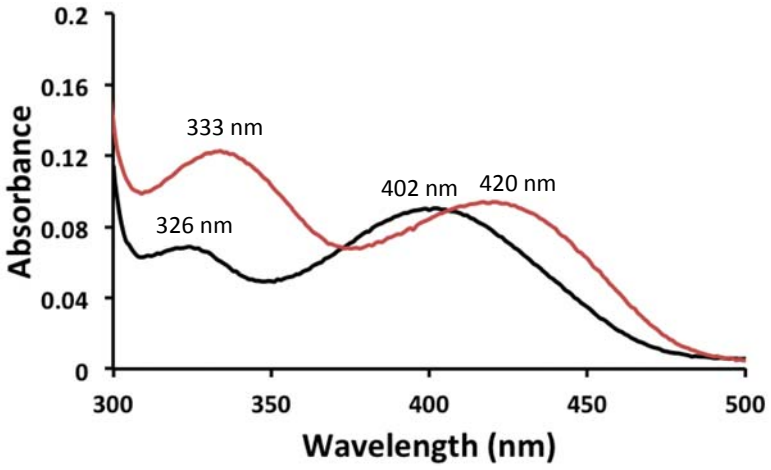

Figure 4-16 UV-Vis analysis of WT AmSPT and K286A AmSPT.
UV-vis spectrum of 40 μM AmSPT (red trace) and K286A AmSPT (black trace) after excess PLP has been removed.

The inability to bind PLP correctly, interact with L-serine or deprotonate the resulting aldimine all contribute to K286A AmSPT having no catalytic activity. Variation in DTNB assay conditions including a 10 fold increase in enzyme concentration coupled with the increases in substrate concentrations persisted in showing no enzyme turnover. The complete inactivity of AmSPT through a single amino acid change without causing protein mis-folding allows substrate and inhibitor binding studies to be undertaken without catalytic turnover, thus hopefully allowing capture of enzyme-bound substrates and inhibitors.

A note on AmSPT numbering

The emergence of the N-terminally tagged AmSPT has produced a nomenclature complication when comparing AmSPT to spSPT. The additional 21 N-terminal amino acids found in AmSPT increase all subsequent residue numbers, therefore making a functional comparison of the same residue between isoforms more cumbersome and confusing. The widely published, well-known tetrad of PLP binding residues in spSPT (H159, D231, H234 and K265) becomes (H180, D252, H255 and K286) in AmSPT. In an attempt to minimise confusion within the literature the N-terminal tag of AmSPT has not been included in the numbering of AmSPT therefore the active site residues remain recognisable by retaining their previous numbering. The K286A AmSPT mutant described above therefore becomes the K265A mutant. For clarity all subsequent references to amino acids in AmSPT will now follow the same numbering as spSPT.

4.2 Myriocin

Following its discovery as an SPT inhibitor the fungal natural product myriocin quickly became an important and widely used molecule in sphingolipid research. The widespread use of myriocin arose from both its high selectivity and relative ease of availability, in comparison to other natural product SPT inhibitors, as it is now commercially available from Sigma Aldrich. Historically, myriocin could be isolated in relatively high yields with only the requirement for very limited purification. From a 5 L fermentation roughly 650 mg of myriocin could be obtained.[144] Despite its extensive use, the mode of action of myriocin has remained unknown with the only published comment on the mode of inhibition being made by Hanada in 2003, who suggests that the amine group of myriocin could condense with the aldehyde of PLP to form an aldimine (Figure 4-17).[41]

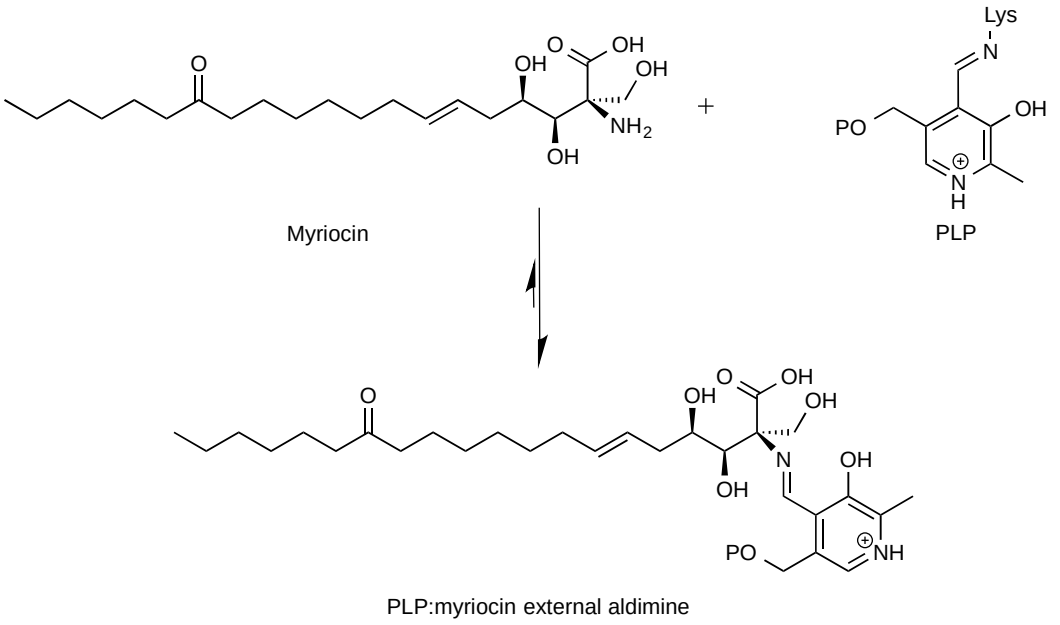

Figure 4-17 Possible formation of a PLP:myriocin external aldimine

Starting from this hypothesis the initial aim of the project was to find evidence for the existence of the PLP:myriocin aldimine. Utilisation of the characteristic UV-vis absorption pattern of PLP and its derivatives allowed the binding of myriocin by SPT to be monitored. After the dialysis of fresh PLP into the enzyme excess PLP was removed from the sample by passing through a PD-10 (Sephadex G-25M - GE Healthcare) desalting column before UV-vis analysis showed PLP to be present in its two tautomeric forms (Figure 4-18 solid line). Upon addition of 5 equivalents of myriocin an immediate change in absorbance was observed (Figure 4-18 dotted line),

this was also accompanied by a visible change in colour. The myriocin containing solution is a clear bright yellow in comparison to the much paler yellow enzyme control. The UV-vis spectrum indicates a change has taken place. The loss of the 333 nm peak indicates the disappearance of the original PLP:SPT aldimine. While the concomitant increase at 430 nm suggests the synthesis of a new species, potentially the formation of a PLP:myriocin aldimine complex.

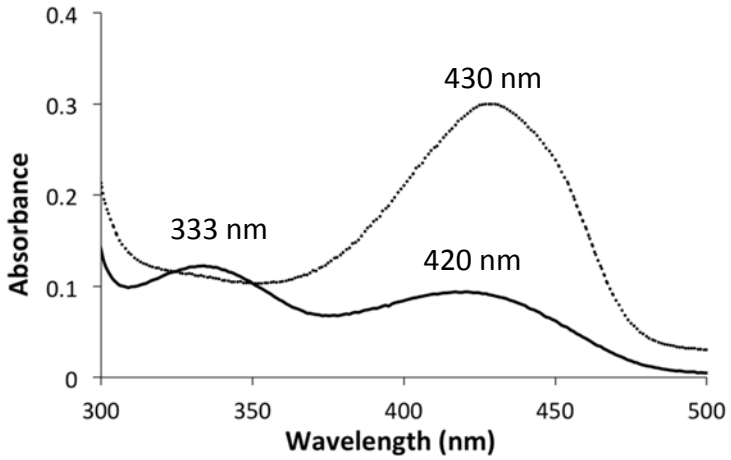

Figure 4-18 UV-vis spectrum of AmSPT before and after myriocin addition
40 μM AmSPT before (solid line) and after 200 μM myriocin addition (dotted line).

Following on from the work above (Section 4.1.2) five equivalents of myriocin was used throughout all inhibition studies as this produced the maximum enzyme inhibition and largest aldimine formation based on the 430 nm absorbance. Due to its low solubility, myriocin was solubilised in DMSO at a maximum concentration of 5 mM. Therefore myriocin concentrations were kept as low as possible to minimise any DMSO interference. Initial experiments assessed the enzyme activity in the presence of 1, 2.5, 5 and 10 equivalents of myriocin along with the appropriate DMSO controls. DMSO was shown to be tolerated up to 10% with only a very minor effect on enzyme rate. 98% inhibition of SPT was achieved when 5 equivalents of myriocin were added, with no greater inhibition observed with 10 equivalents. Throughout the UV-vis experiments precipitation was frequently observed if precautions were not taken. To minimise precipitation the inhibitor was only added when the enzyme solution had risen to room temperature. Although SPT was stored at 4 ^{o}C immediately prior to use the temperature of all UV-vis experiments was maintained at 25 ^{o}C throughout.

To prove the existence of the hypothetical PLP:myriocin external aldimine further evidence of the structure was gathered. Initial attempts at structure verification centred around reducing the labile PLP:myriocin imine bond followed by mass spectrometry. The labile nature of the imine bond formed between the aldehyde of PLP and any amine has been well utilised during mechanistic studies and indeed forms the basis of PLP chemistry. PLP is initially held in the active site of SPT via an imine interaction, this interaction is then broken and replaced by a second imine bond upon L-serine addition. The well established field of reduction/oxidation chemistry has been used to aid SPT chemistry since its discovery.[76] With the addition of the relatively strong reducing agent, sodium borohydride, directly to enzyme assays becoming a well established technique for trapping PLP-substrate intermediates.[29, 34]

In this work, SPT that was treated with myriocin and the increase in absorbance at 430 nm was confirmed before reduction by addition of 10 mM sodium borohydride. After reduction all protein was removed from the sample by passing through a 6 kDa molecular weight cut-off membrane before LC-MS analysis was attempted. The pre-analytical chromatography consisted of a simple C18 reverse phase column. Surprisingly, no ions corresponding to the existence of a PLP:myriocin aldimine could be observed. Extensive repetition and subtle modifications to the procedure produced no results. Considering possible sources of error the removal of the protein by molecular weight filter membranes was stopped to eliminate any possibility of the imine being lost at this step. Repetition of the experiment without protein removal but direct loading onto the LC-MS still did not produce any viable product ions. Ultimately neither a reduction or protein removal steps were used to detect the PLP:myriocin aldimine. The chromatography gradient was altered to remove the acid modifier from the mobile phase in an attempt to maintain the PLP-myriocin imine bond. This unorthodox approach led to the observation of a 631.30153 Da species which corresponds very well to the predicated PLP:myriocin external aldimine (Figure 4-17) mass of 631.29902 Da (Figure 4-19).

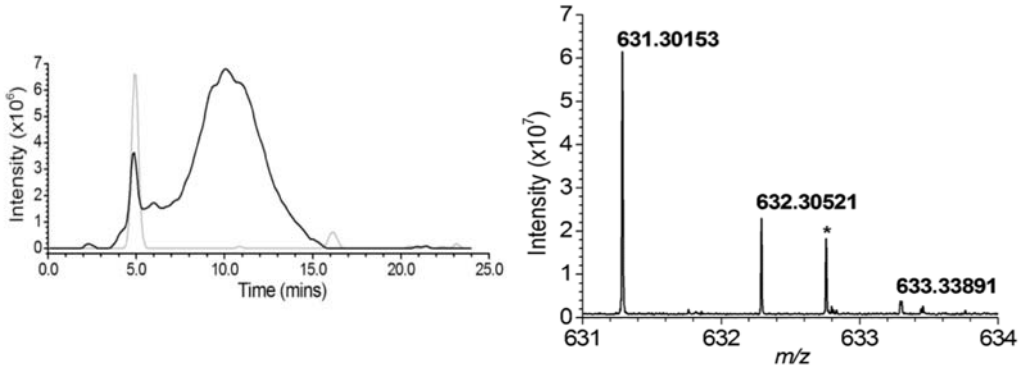

Figure 4-19 Detection of the PLP-myriocin aldimine by LC-MS
Left - Extracted ion chromatogram at m/z 631. Control enzyme shown in gray. Myriocin treated enzyme shown in black. The small peak at 5 minutes in the control reaction is of unknown origin and could relate to any small contaminant of mass 631 Da. **Right -** High-resolution mass spectrum of the PLP-myriocin aldimine, obtained by summing the spectra between t = 8−12 min. ([M + H]+ $C_{29}H_{48}N_2O_{11}P$; predicted m/z 631.29902; observed error 4.0 ppm). * denotes a contaminant.

Measuring the mass of this key aldimine, combined with the UV-vis data, is the first conclusive evidence that myriocin acts on SPT in the hypothesized manner, confirming for the first time that myriocin forms an aldimine with PLP. The changes in the UV-vis spectrum provide strong evidence that myriocin binds in or near the active site displacing the initial internal PLP aldimine.

Following confirmation of the correct inhibitory species fundamental inhibition studies were attempted. For the first time the effect of myriocin was analysed on purified SPT, with previous attempts to quantify myriocin inhibition having involved eukaryotic SPT expressed in whole cells and microsomal extracts.[73, 145] The only exception to this was Ikushiro,[162] who although unable to generate inhibition data for myriocin with purified bacterial SPT, managed to produce an apparent K_d for myriocin binding of 1.3 μM suggesting myriocin had a 1000 fold higher affinity for SPT that L-serine. The use of whole cell assays makes the calculation of robust kinetic parameters impossible due to uncertainties over cellular permeability and substrate concentrations. Thus, in order to characterise myriocin potency, inhibition studies to date have relied on IC_{50} determination. The most fundamental inhibition parameter, Ki, proved the most difficult to obtain due to the very high affinity of myriocin for SPT. A typical inhibition assay contained 200 nM SPT while myriocin concentrations were varied between 80 nm and 80 μM. In assays approaching the lower end of the myriocin concentration range the concentration of myriocin is less than the enzyme concentration. The high affinity of myriocin impacts directly on the

steady state approximation that is fundamental to Michaelis Menten kinetics. Therefore the observed change in rates must be analysed using an equation that incorporates the variation in inhibitor concentration. The Morrison equation (Equation 4-1) was developed especially for "tight binding" inhibitors that break the steady state approximation.[163]

$$v = v_o - v_o \left(\frac{\left(K_{i,app} + I + E\right) - \sqrt{\left(K_{i,app} + I + E\right)^2 - 4 \cdot I \cdot E}}{2 \cdot E} \right)$$

Equation 4-1 The Morrison Equation
ν = measured velocity, ν_o = velocity in the absence of inhibitor, $K_{i,app}$ = the apparent equilibrium inhibition constant, I = inhibitor concentration, E = enzyme concentration.

Running triplicate enzyme assays with saturating palmitoyl-CoA and L-serine concentrations, ten and twenty fold above their respective K_m values and increasing myriocin concentrations produced a K_i for myriocin of 967 ± 98 nM (Figure 4-20).

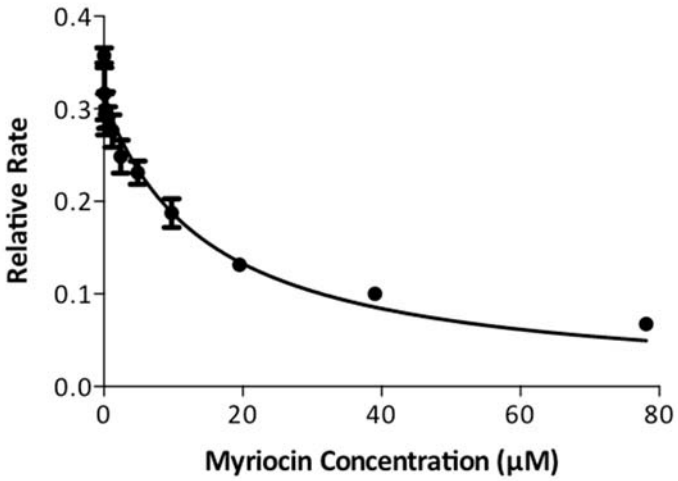

Figure 4-20 Inhibition of SPT by myriocin
Initial rates from the DTNB assay plotted against increasing myriocin concentration (0.075, 0.150, 0.312, 0.625, 1.25, 2.5, 5, 10, 20, 40, 80 μM). Each assay contained 200 nM enzyme, 250 μM palmitoyl-CoA, 20 mM L-serine, 0.2 mM DTNB and the appropriate myriocin standard. Data fitted using the Morrison equation. The K_i obtained for the PLP-myriocin aldimine is 967 ± 98 nM.

The mode of inhibition of SPT by myriocin has been disputed in the literature, with Miyake *et al.* initially declaring the inhibition non-competitive in 1995.[145] Almost ten

years later Ikushiro *et al.* suggested myriocin inhibition to be competitive.[162] To settle the disagreement about the mode of inhibition, competition studies were carried out between myriocin and both substrates, L-serine and palmitoyl CoA. Following the non-Michaelis Menten type kinetics observed during the calculation of the Ki the nature of inhibition by SPT was determined using the Cha method.[164] IC_{50} values for the inhibitor were determined at fixed enzyme concentrations while systematically varying each substrate concentration. The linear increase in IC_{50} values with varying L-serine and palmitoyl-CoA concentration, establishes myriocin as a competitive inhibitor for both L -serine and palmitoyl-CoA substrates (Figure 4-21).

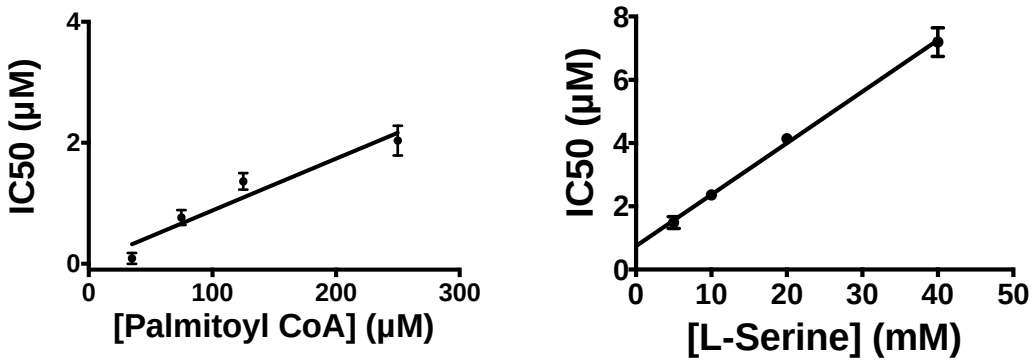

Figure 4-21 Determination of the mode of action between AmSPT by the inhibitor myriocin
A graphical method was employed to determine the mode of interaction between myriocin and SPT (in relation to the natural substrates L-serine and palmitoyl-CoA). Briefly, IC_{50} values were determined for myriocin at a fixed enzyme concentration (200 nM), whilst varying the concentration of a single substrate. Graphs were plotted of IC_{50} at varying concentrations of either L-serine, **(Right)** or palmitoyl-CoA, **(Left)**.

The differences in the concentration of L-serine required to inhibit 50% of the enzyme in comparison to palmitoyl-CoA can be seen on both the axis scales and the gradient of the line is a reflection upon the different binding efficiencies of the two substrates. The competitiveness for both substrates can be rationalised when viewed from a structural perspective. The PLP-myriocin aldimine shares structural features with both substrates, the long alkyl chain of myriocin mimics the alkyl chain of palmitoyl-CoA. While the carboxylic acid group and the hydroxymethyl at the head of the molecule mimic L-serine. Interestingly, the arrangement around carbon-2 of myriocin renders it in the D conformation but yet it still competes for L-serine. The lack of chiral specificity at the active site is not surprising after Ikushiro *et al.* showed that D-serine also interacts with bacterial SPT.[162] Presumably this would proceed via the formation of a hypothesised D-serine-PLP external aldimine but the

existence of such species is solely inferred from UV-vis changes upon D-serine addition. The apparent K_d for D-serine is 10 mM, an order of magnitude larger than L-serine (1.4 mM), showing SPT displays a clear preference for the L enantiomer. D-serine has also been shown to inhibit mammalian SPT with an IC_{50} of 0.3 mM in CHO cells with the inhibition thought to be caused by the inverse stereochemistry not allowing deprotonation at C-α.[41, 165]

A great step forward in the understanding of myriocin inhibition came rather unexpectedly through time dependent rate analysis coupled with extended UV-vis analysis. Assaying SPT activity over 16 hours in the presence of myriocin showed that SPT remained inhibited by myriocin for at least this length of time. Interestingly UV-vis analysis performed at 25 °C over the same time period showed a more complex and surprising picture. Combining SPT and myriocin immediately produces the predicted dominant 430 nm peak, but monitoring this reaction every 30 minutes by collecting a fresh UV-vis spectrum shows the 430 nm peak is only stable for 1.5 hours before it slowly diminishes. This reduction at 430 nm is followed by the concomitant increase in two new peaks at 331 and 400 nm, Figure 4-22.

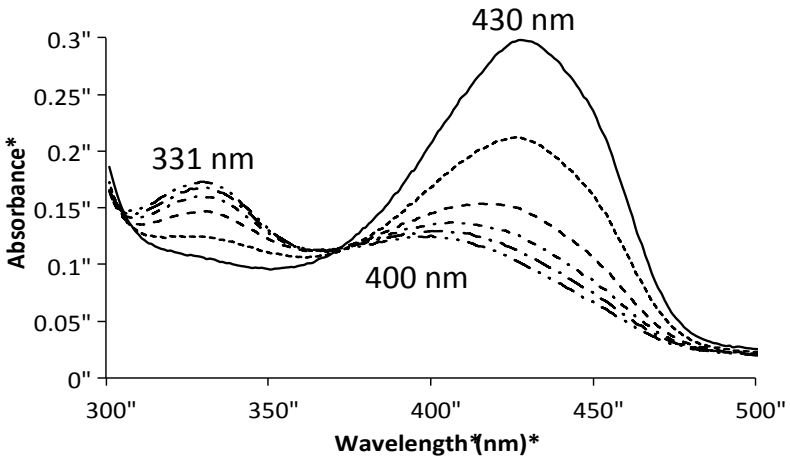

Figure 4-22 UV−vis analysis of the degradation of the myriocin-PLP aldimine in AmSPT
The PLP-myriocin external aldimine (solid line) is stable for 90 min, before a decrease at 430 nm is observed, which is accompanied by a concomitant increase at 331 and 400 nm over 16 h (dotted and dashed lines).

The change in the UV-vis spectrum suggests the PLP:myriocin aldimine is unstable and degrades to a previously unseen PLP derivative. Surprisingly, rate analysis over a long period of time shows SPT remains catalytically compromised for much

greater than 1.5 hours indicating that the new myriocin degradation product must also be inhibitory. During initial attempts to understand the changing UV-vis spectrum the incubation temperature was lowered to 4 °C. This resulted in the PLP:myriocin aldimine remaining stable for greater than 16 hours. (Figure 4-23)

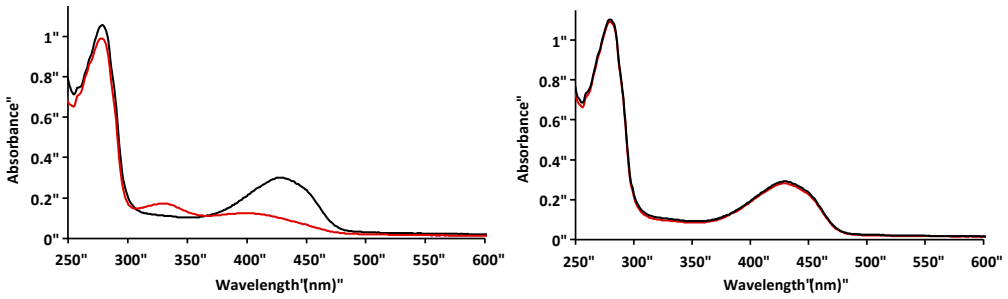

Figure 4-23 Effect of variation in temperature upon PLP-myriocin aldimine stability
AmSPT (40 μM) was treated with 200 μM myriocin, and incubated for 16 hours at either 25 °C (**Left**) or 4 °C (**Right**). UV-vis spectra after addition of myriocin at time 10 minutes (*black trace*) and 16 hours (*red trace*).

The temperature dependence of the degradation reaction facilitated the study of the PLP:myriocin aldimine as this allowed the lifetime of the species to be easily controlled. It was reasoned that degradation of the PLP:myriocin external aldimine could be hampering crystal formation and that the increase stability at 4 °C could be utilised to aid crystal trials. Therefore crystal plates were set up, incubated and monitored at 4 °C for four weeks but these attempts also failed to produce any appropriately sized crystals.

The absorbance maxima at 400 and 333 nm that arise following the disappearance of the myriocin-PLP aldimine, had not previously been observed in either spSPT or AmSPT, with the closest UV-vis spectrum arising from the K265A AmSPT mutant. The K265A AmSPT has no active site lysine and is therefore unable to bind PLP in the internal aldimine form but nevertheless, still purifies with PLP bound to the enzyme, presumably in a non-covalent manner. The resulting UV-vis spectrum shares very similar absorbance maxima to the myriocin degradation product (Figure 4-24, solid line). Following the addition of five equivalents of myriocin, K265A AmSPT responds in in a similar manner to wild-type AmSPT (Figure 4-24, dotted line). Both initial PLP internal aldimine peaks are replaced by one large absorbance at 425 nm, which is now known to correspond to the PLP:myriocin external aldimine. Surprisingly, when left to incubate for 16 hours the PLP:myriocin external

aldimine does not degrade (Figure 4-24, dashed and dotted lines). The longevity of the 425 nm peak (PLP:myriocin external aldimine) under the same conditions but with single amino acid substitution demonstrates the essential involvement of the active-site lysine 265 in the degradation pathway.

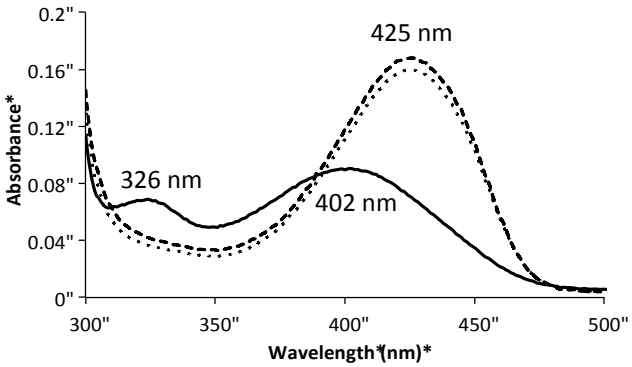

Figure 4-24 UV−vis analysis of K265A AmSPT
After de-salting K265A AmSPT (40 μM) showed two absorbance maxima at 326 and 402 nm (solid line). Upon addition of 200 μM myriocin, an immediate shift to a single peak at 425 nm occurred (dotted line), indicating the formation of a PLP-myriocin aldimine complex. Over 16 hours this spectrum remains unchanged (dashed line), indicating that the PLP-myriocin aldimine complex is not degraded by this mutant enzyme.

Combining the formation of a new species, as observed in the UV-vis spectrum, after prolonged incubation of myriocin and SPT with the continued SPT inhibition it was hypothesised that the PLP:myriocin aldimine degraded over time to produce a second inhibitory species. As the degradation product(s) also inhibit SPT the nature of the inhibition of SPT by myriocin was probed both before and after 16 hours of incubation. To test the reversibility of the inhibition, the PLP:myriocin aldimine and degradation product were first generated by incubation of SPT with the inhibitor for 10 minutes and 16 hours respectively at 25 °C. After this incubation period the temperature was lowered to 4 °C to stop further conversion and extensive dialysis against buffer containing 25 μM fresh PLP was performed for 24 hours. Aliquots were removed from the dialysate at specific time points (0, 3 and 24 hours) and assayed for SPT activity. (Figure 4-25)

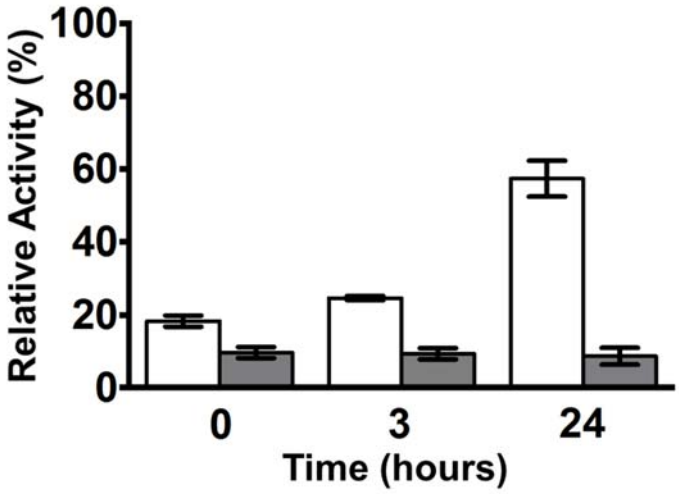

Figure 4-25 Relative enzymatic activity after removal of inhibiting species by dialysis
40 μM SPT was inhibited with 200 μM myriocin and incubated for 10 minutes (white bars) or 16 hours (grey bars) at 25 °C before removal of myriocin by extensive dialysis. The enzymatic activity was then determined at 0 hours, 3 hours, and 24 hours after dialysis.

For the enzyme incubated with myriocin for the shorter time (10 mins), then dialysed for 3 hours, no significant activity was recovered; however, dialysis for 24 hours recovered 60% enzymatic activity (Figure 4-25, white bars). This regain in enzymatic activity was also accompanied by a change in the UV-vis spectrum back to the internal aldimine form (λmax 333 and 420 nm). Taken together, this data from short, 10 minute incubations of SPT with myriocin is consistent with the formation of an initial enzyme-inhibitor complex which is non-covalent in nature and reversible, albeit with a very slow off rate (k_{off}). This provides evidence to support our assignment of the PLP:myriocin aldimine as the initial inhibitory species. In contrast, for the enzyme pre-incubated with myriocin for 16 hours, no detectable regain in activity was observed after dialysis either at 3 or 24 hours (Figure 4-25, grey bars); indicating that this second, newly-formed species acts as an irreversible inhibitor of SPT.

Analysis of the vast PLP literature reveals PLP is capable of catalysing many varying reactions with the end product being dictated not only by the substrate but also the protein scaffold that composes the active-site. Although most PLP enzymes have a conserved PLP binding pocket there is significant variation in proximal amino acids. This variation allows different hydrogen bonds and electrostatic interactions to exist in different enzymes producing differing propensities to form one product over another. An investigation of PLP catalysed reactions revealed serine hydroxymethyltransferase (SHMT) and cholerae autoinducer-1 synthase (CqsA) to

have mechanisms that could be applied to the breakdown of the PLP:myriocin external aldimine (Figure 4-26).[12, 166-167] CqsA is a PLP dependent synthase responsible for the condensation of either L-threonine, L-2-aminobutyric acid or S-adenosylmethionine and decanoyl-coenzyme A to synthesise a precursor of the cholera autoinducer-1, an important molecule in quorum sensing. The hydroxyl group on the β–□□□□□□□□□□□□□□□□□□□□ to both of the above examples and is also present in the PLP:myriocin external aldimine (Figure 4-17).

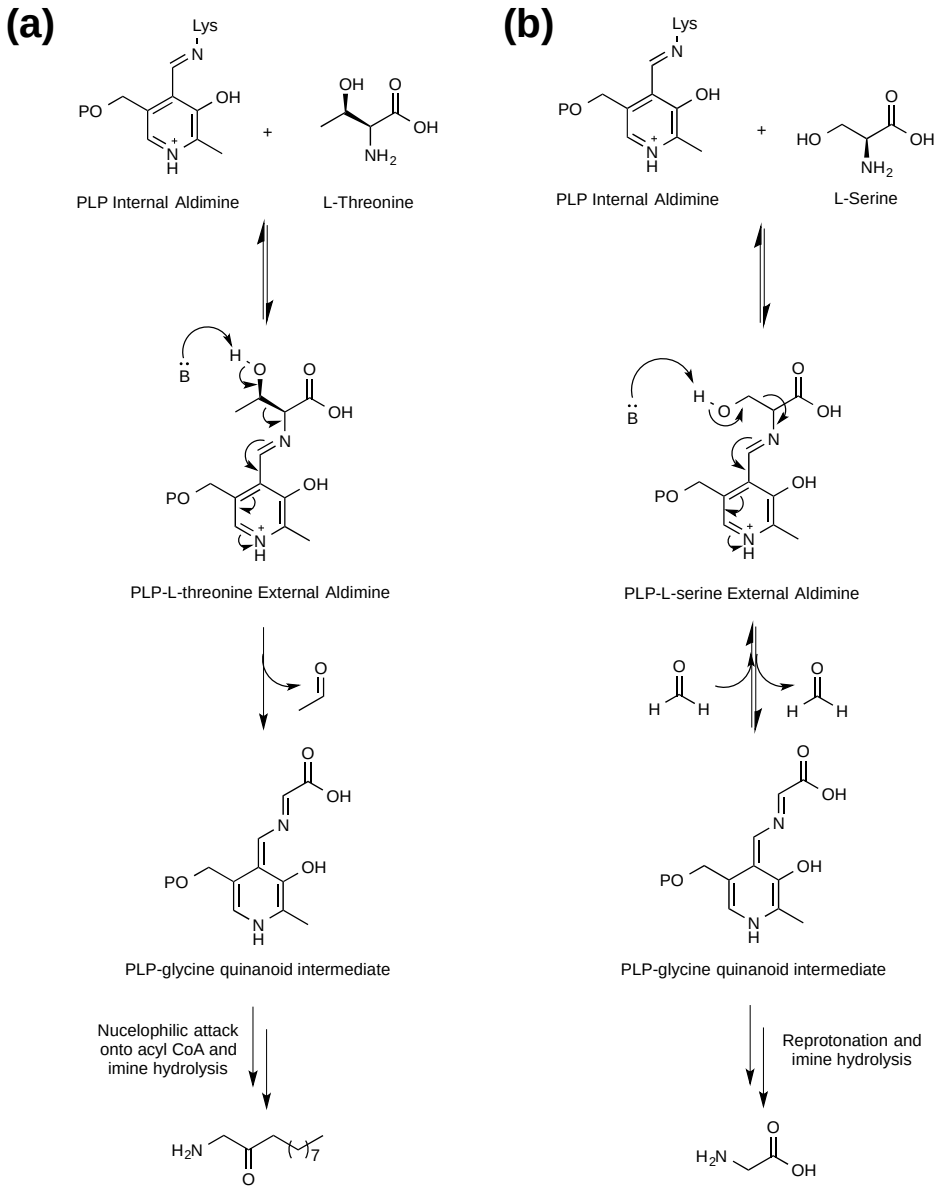

Figure 4-26 CqsA and Serine hydroxymethyltransferase mechanisms
(a) - CqsA mechanism shown for simplicity with L-threonine as the substrate. Deprotonation, formation of a carbonyl and then cleavage of the Cα-Cβ bond. (**a)** - Serine hydroxymethyltransferase mechanism detailing deprotonation, formation of a carbonyl and then cleavage of the Cα-Cβ bond.

The cleavage of the Cα-Cβ bond via hydroxyl deprotonation and carbonyl formation is named a "retro-aldol" like reaction. The possibility that the PLP:myriocin aldimine undergoes a retro-aldol reaction would produce a long chain aldehyde and a PLP:D-serine aldimine. The proposed mechanism a retro-aldol degradation of the PLP:myriocin aldimine is shown in Figure 4-27.

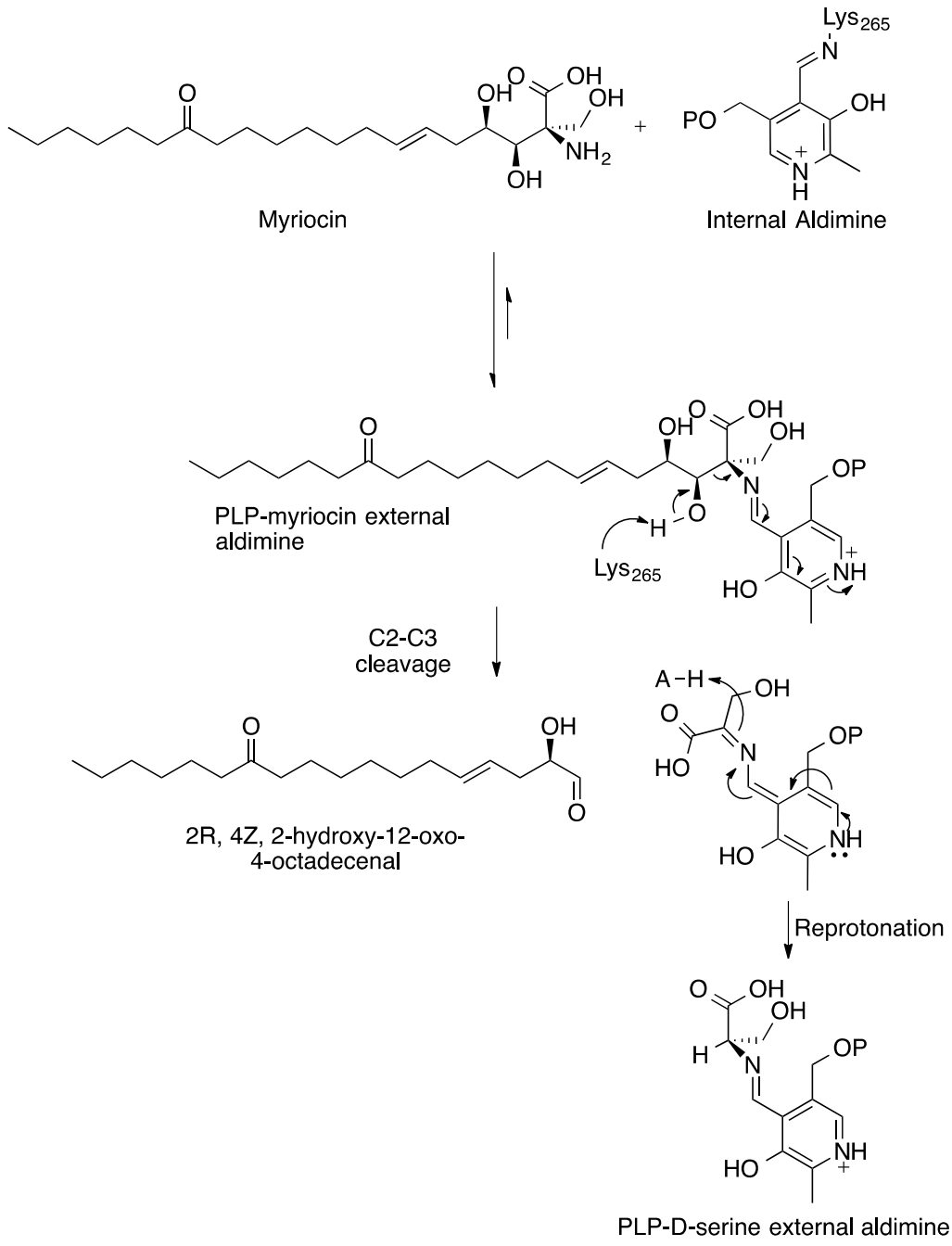

Figure 4-27 The proposed "retro-aldol like" mechanism for the observed degradation of the PLP-myriocin aldimine

Myriocin, undergoes fast transamination with the internal aldimine, releasing Lys265 and forming the PLP-myriocin aldimine inhibitory complex. This inhibitory complex is slowly degraded by deprotonation of the myriocin C_3-hydroxyl with C2-C3 bond cleavage and movement of electrons into the pyridine ring of PLP. This results in the formation of a 2-hydroxyl-C_{18} aldehyde species and a PLP-D-serine aldimine.

To test this hypothetical breakdown mechanism, evidence of one of the products was sought. As any PLP:D-serine aldimine would immediately dissociate in solution due to the relatively high D-serine K_d (10 mM) quantification of the long chain aldehyde was attempted. Unequivocal identification was attempted via mass spectrometry with the potential aldehyde functionality being utilised through the use of hydrazides. Initially derivatisation of the aldehyde with 2,4-dinitrophenylhydrazine (Figure 4-28) was attempted but repeated reactions, extractions and analysis showed no masses corresponding to a hydrazone being formed from the putative 18-carbon aldehyde.

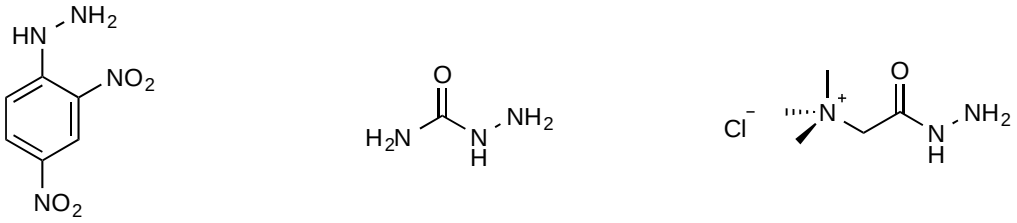

2,4-Dinitrophenylhydrazine Semicarbazide Girard's Reagent T

Figure 4-28 Aldehyde derivatisation agents.

Following the work of Berdyshev *et al.* with the S1PL and his quantification of the product hexadecenal using semicarbazide (Figure 4-28) and mass spectrometry a similar approach was attempted.[168-169] Multiple permutations of the published method all failed to yield any results. After discussion with Professor Al Merrill (Georgia Tech, USA), an expert in sphingolipid mass spectrometry, Girard's reagent T was used as a derivatisation agent prior to mass spectrometry analysis.[170] Girard developed two quaternary ammonium salts for derivatisation of aldehydes prior to crystallisation in order to aid separation (Figure 4-28). More recently the same reagents have been used to add a charged moiety to aldehydes to aid ionisation.[171] Again this method failed to produce any ions attributable to the derivative of the putative 18-carbon aldehyde. Failure to detect any aldehyde suggested it either didn't exist or was not free in solution ready to facilitate derivatisation. Focussing on the later hypothesis intact protein mass spectrometry was undertaken based on the knowledge that long chain aldehydes are relatively reactive and could potentially covalently modify any nucleophilic residues. Comparison of the mass spectrum before and 16 hours after myriocin addition showed a clear proportion of protein with a 278 Da mass increase (Figure 4-29). The mass difference of 278 Da

corresponds exactly to the condensation product of the C18 aldehyde product that would be formed from a retro-aldol type degradation of myriocin.

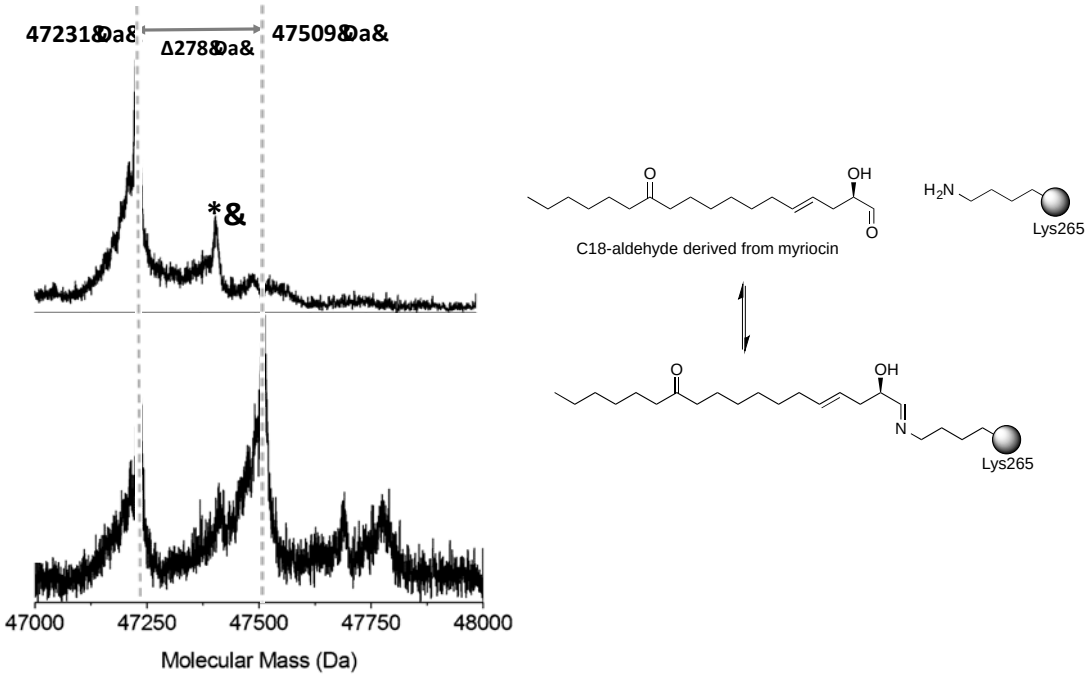

Figure 4-29 Mass spectrometry analysis of the myriocin-derived covalent modification of SPT **Left** - Intact protein mass spectrometry of AmSPT (40 μM) before (*top*) and after (*bottom*) 16 hour treatment with 200 μM myriocin at 25 °C. SPT displays an average neutral mass of 47231 Da. After myriocin treatment a prominent new species of average mass 47509 is observed (Δmass +278 Da). Minor peaks highlighted by * arise from α-*N*-gluconoylation of the His-tag. **Right** - The myriocin-derived modification.

In an attempt to increase the proportion of the modified protein in the sample, attempts were made to reduce the highly likely imine bond attachment of the myriocin fragment to SPT. Sodium borohydride was used to convert the labile imine to the more stable secondary amine. Mass analysis observed the modified mass had increased to Δ282.24 Da after the reduction with sodium borohydride. The difference of 4 Da is most likely due to both the reduction of the octadecenal-protein imine bond and the reduction of the ketone on carbon-12 of the myriocin fragment (Figure 4-30B).

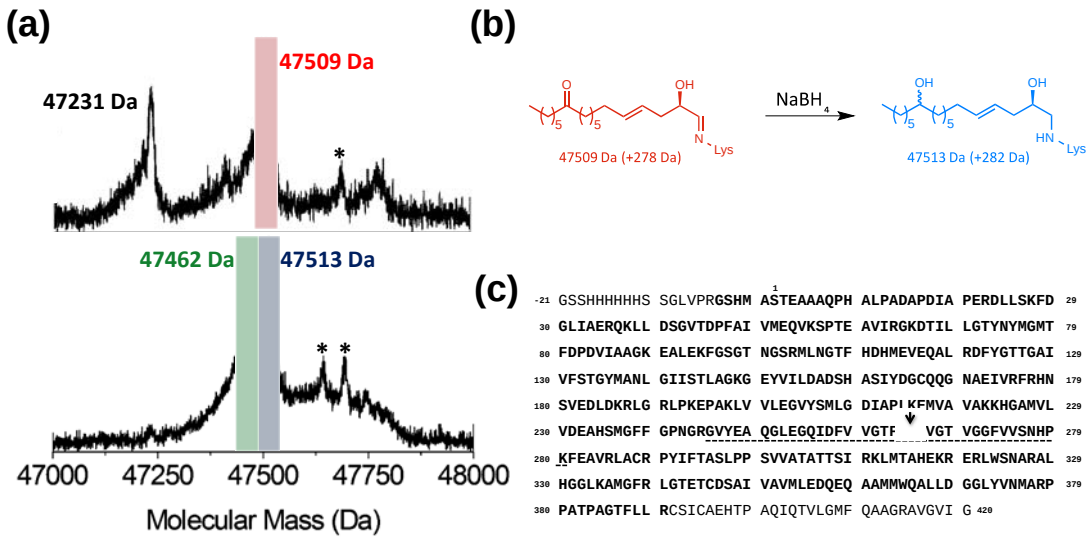

Figure 4-30 Chemical reduction of the covalent adduct formed by myriocin degradation
(a) - Top, deconvoluted intact protein mass spectrum after incubation with myriocin for 18 hours at 25 °C. The MS displays two species - 47,231 Da, consistent with apo-SPT; and the unknown myriocin-derived covalent adduct at 47,509 Da (Δmass +278 Da). **Bottom,** deconvoluted intact protein mass spectrum after chemical reduction with 10 mM $NaBH_4$. The MS displays two new species – 47,462 Da (Δmass +231 Da), which is consistent with the reduced SPT-PLP internal aldimine; and 47,513 Da (Δmass +282 Da). Peaks highlighted by * arise from α-N-Gluconoylation of the His-tag. **(b)** - Proposed chemistry occurring upon reduction of the myriocin-induced SPT covalent adduct. Octadecenal, condensation with Lys265 produces the imine species (Δmass 278 Da; $+C_{18}H_{30}O_2$). Chemical reduction then produces the observed hydroxy-amine adduct (Δmass +282 Da; $+C_{18}H_{34}O_2$). **(c)** - Sequence coverage achieved when analysing myriocin-modified SPT enzyme. Amino acids highlighted in bold were observed in the peptide mass fingerprint (Appendix 2). The myriocin derived modification was isolated to a single site between Glu245 and Lys280 (underlined); this sequence contains a single internal lysine residue, Lys265 (highlighted by the arrow).

After reduction, the protein mass spectrum displayed two peaks. One corresponding to the doubly reduced modification (Figure 4-30A blue peak) and an unknown Δmass +231 Da species. Literature consultation later showed the Δ231 Da species to arise from reduction of PLP:lysine internal aldimine to the enzyme. The location of the modification was determined by trypsin digestion followed by peptide analysis. After formation of the aldehyde sodium borohydride was again added to reduce the imine linkage before trypsin was used to digest SPT into fragments for mass spectrometry analysis. Analysis achieved overall sequence coverage of 89%, with three peptides assigned as containing the Δmass 282.24 Da modification ($+C_{18}H_{34}O_2$) (Figure 4-30C). All three modified peptides covered the region around lysine265. Comparison of the modified peptides determined the active site lysine265 as site of modification.

The detection of a covalently linked octadecenal on lysine265 of SPT supports the suggested retro-aldol mechanism. The changes in the UV-vis spectrum (Figure 4-22)

are now known to show the disappearance of the PLP:myriocin aldimine and the formation of PLP:D-serine aldimine. The shifted 333 and 400 nm λmax would not usually be expected to arise from a PLP:D-serine aldimine but the difference can be attributed to the presence of the lysine modification. The covalent modification of the active site lysine also explains the prolonged and irreversible inhibition observed after the myriocin incubation (Figure 4-25).

The turnover of myriocin in the active site was believed to be a contributing factor in previously unsuccessful myriocin-SPT co-crystal trials. The knowledge that myriocin is broken down via a retro-aldol mechanism can be utilised to probe the effect of myriocin turnover on crystallisation. All retro-aldol reactions initially require a base to deprotonate the hydroxyl group. Analysis of the SPT active site from previous crystal structures places lysine265 in the ideal position, therefore co-crystallisation of myriocin and the K265A SPT mutant was attempted. The stability of the PLP:myriocin aldimine for longer than 16 hours when formed with the K265A AmSPT also confirms the involvement of the active site lysine. Based on this increased stability of the myriocin complex crystal trials were attempted with K265A AmSPT and myriocin. Working with Professor Jim Naismith and Dr Stephen McMahon extensive crystal trials with both commercial and in-house precipitant screens were undertaken. Following an initial hit, screen optimisation determined the optimal conditions to be 32% PEG MME 2000, 0.1 M HEPES pH 7.5 and a protein:precipitant ratio of 1:1. Using these conditions crystals were grown by vapour drop diffusion at 20 °C over the course of 2 weeks and are readily reproducible. Several data sets were collected but only the highest resolution (1.6 Å) structure was completely refined. The structure was solved by molecular replacement using an already published SPT-PLP internal aldimine structure (PDB code 2JG2)[100] and contained a canonical dimer in the asymmetric unit (Table 4-3 and Figure 4-31).

Data Collection	
Space Group	P 2_1 2_1 2_1
Cell dimensions	
a, b, c (Å)	61.9, 98.7, 133.2
α, β, γ (°)	90, 90, 90
Resolution (Å)*	56.14 – 1.62
(high resolution)	(1.66 - 1.62)
R_{merge}	0.067 (0.497)
I/σ(I)	10.8 (2.3)
Completeness (%)	98.9 (99.7)
Average Redundancy	3.6 (3.8)
V_m ($Å^3$/Da)	2.25
Solvent (%)	45.2
Refinement	
Unique reflections	103044
R_{work} / R_{free}	19.0 / 21.2
Geometric deviations	
Bonds (Å) / Angles (°)	0.009 / 1.43
No. atoms	
Protein	5967
Water	567
Glycerol	12
PLP-Myriocin Aldimine	56
B factors ($Å^2$)	
Protein	19.3
Water	27.9
PLP-Myriocin Aldimine	33.3
Glycerol	32.8
Ramachandran	
Allowed / disallowed (%)	97.3 / 0
Molprobity score / centile	1.25 / 97
PDB code	4BMK
*Values in parentheses refer to the highest resolution shell	

Table 4-3 Crystallographic statistics for SPT K265A PLP-decarboxymyriocin

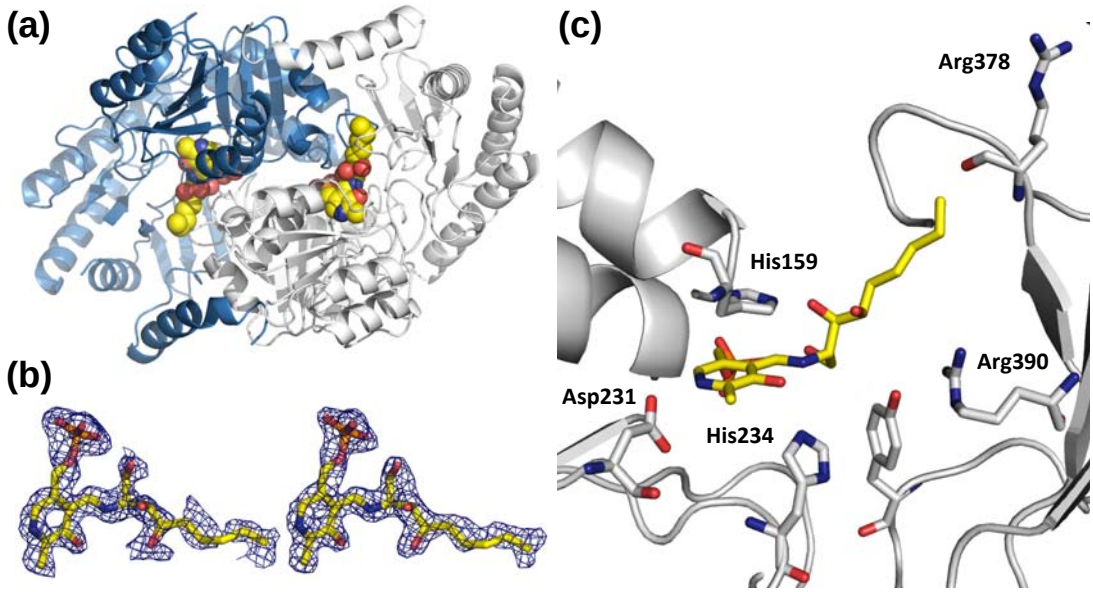

Figure 4-31 The structure of SPT K265A PLP-decarboxymyriocin aldimine inhibitory complex
A - The biological SPT dimer of the decarboxylated myriocin complex. The protein is shown as a cartoon with one subunit coloured blue and the other white. The PLP external aldimine of the decarboxylated myriocin is shown in space fill with carbons coloured yellow, nitrogen blue, oygen red and phosphorous orange. **B - Left**, The Fo-Fc map (blue chicken wire contoured at 1.8σ, carve radius 1.5Å) calculated from a model which had never contained either PLP or myriocin. Atoms are coloured as in **A**. **Right**, the final Fo-Fc map contoured at 0.85σ with a carve radius 1.8Å. **C** - Detailed representation of the active site interactions, carbon atoms are coloured yellow and shown in sticks for the PLP-decarboxymyriocin aldimine. Carbon atoms in protein side chains are shown as white sticks, others atoms are coloured as in **A**. The hydrocarbon chain of the myriocin inserts into a hydrophobic pocket.

The mobility/flexibility of the acyl chain prevented the assignment of a structure beyond carbon 9 of myriocin. Nevertheless difference electron density revealed a PLP:myriocin aldimine complex had formed (Figure 4-31B). The myriocin stereochemistry is retained - the *Z* configuration of the double bond at position C6 and *cis* diol geometry at positions C3 and C4. It was surprising to discover that the density indicates that myriocin had undergone loss of the carboxylate from the C2 position to form a PLP:decarboxymyriocin aldimine. The model was built reasoning the replacement of the carboxylate with a proton (sp^3 hybridised carbon) but the resolution on its own is not sufficient to distinguish an sp^3 from an sp^2 carbon (Figure 4-31B). As had been noted previously, residues from both SPT subunits are involved in PLP binding and the active site is at the dimer interface.[29] Comparison of this complex with the wild type SPT:PLP-L-serine external aldimine complex (PDB code 2W8J)[29] reveals essentially the same positioning of the PLP rings in both structures (Figure 4-32).

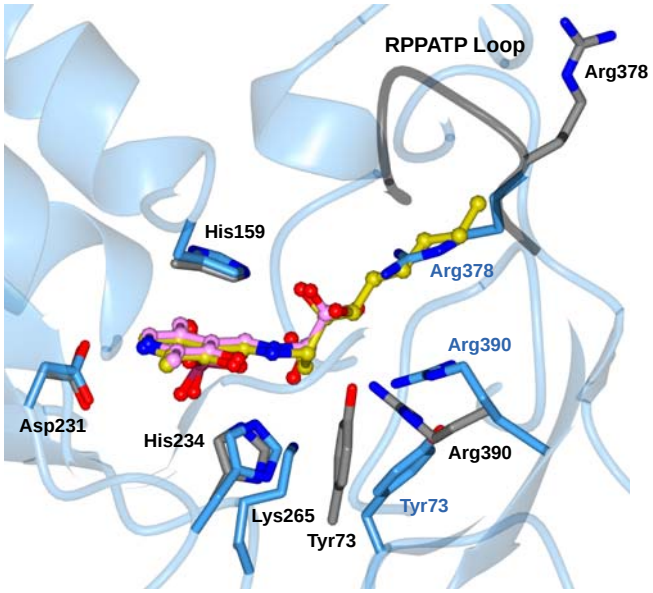

Figure 4-32 Overlay of myriocin K265A AmSPT and PLP-L-ser spSPT
Superposition of the PLP-decarboxymyriocin external aldimine (key sidechains and secondary structure rendered in grey and the aldimine coloured yellow) with the PLP-L-serine external aldimine 2W8J (key sidechains and secondary structure rendered in blue and the aldimine carbons coloured pink) The key catalytic Lys265 residue is mutated to Ala in the decarboxylated myriocin complex.

Moreover, many key active site residues (His159, Asp231, His234) adopt similar positions. However Arg378, which is involved in a key electrostatic interaction with the carboxylate of L-serine in the SPT:PLP-L-serine external aldimine structure, is swung out of the active site with concomitant change in the important mobile loop 378-RPPATP-383; both the loop and Arg378 are partially disordered in the new complex. These changes are presumably the result of accommodating the extended hydrophobic tail of myriocin. Also Arg390, a conserved residue that is required for product formation in the SPT catalytic cycle, adjusts its side chain conformation and makes interactions with both Tyr73 and the C4 hydroxyl of myriocin.[172] Modelling the SPT K265A PLP:myriocin external aldimine complex places the carboxylate perpendicular to the PLP ("Dunathan conformation") that would allow decarboxylation by the mechanism proposed in Figure 4-33.

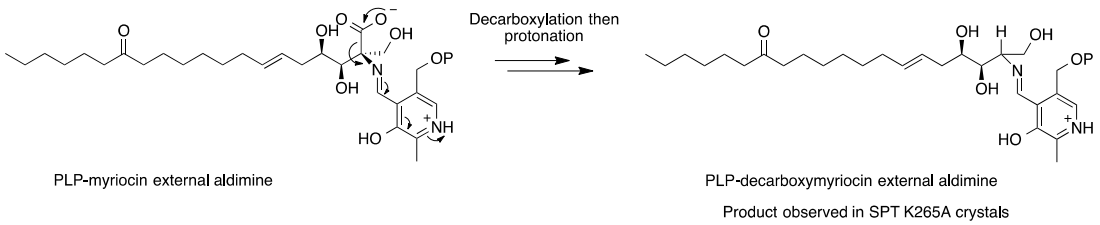

Figure 4-33 Decarboxylation mechanism
Proposed mechanism to account for the PLP-decarboxymyriocin external aldimine observed in the crystal structure of SPT K265A.

However, its extreme slowness relative to *bona fide* PLP-dependent decarboxylases, cautions that the PLP-myriocin aldimine in K265A is not optimally aligned for this reaction. Evidence of the decarboxylation was initially only ever discovered following the two-week crystallisation process. In an attempt to produce the PLP:decaroxylatedmyriocin aldimine in solution the K265A mutant was incubated with myriocin and then stored at 25 ^{o}C. Periodic mass spectrometry analysis showed the PLP:decaroxylatedmyriocin aldimine only formed after 7 days incubation thus emphasising the extremely slow nature of the reaction most likely arising from the sub-optimal alignment (Figure 4-34).

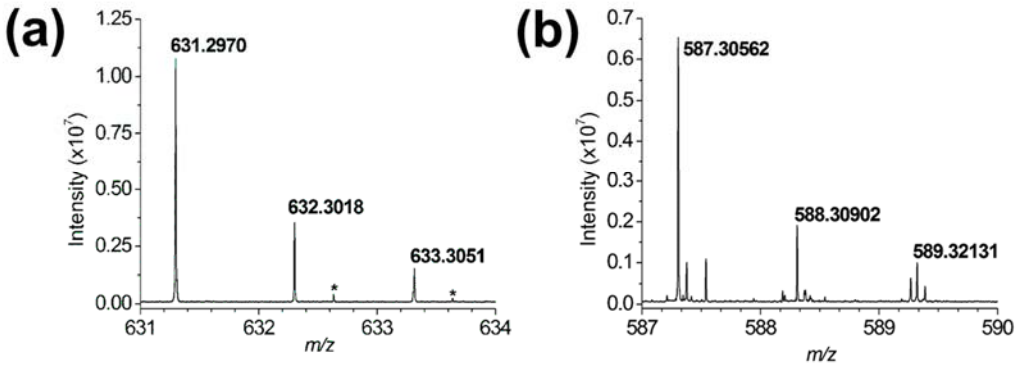

Figure 4-34 Mass spectrometry analysis of the reaction between SPT K265A and myriocin
(a) Detection of the PLP-myriocin aldimine (11) in the SPT K265A mutant by LC-MS. MS obtained by summing the spectra between t = 8-12 minutes. ($[M+H]^+$ $C_{29}H_{48}N_2O_{11}P$; predicted *m/z* 631.29902; observed error 3.2ppm). * denotes a contaminant.
(b) Detection of the PLP-decarboxymyriocin aldimine (15) in the SPT K265A mutant by LC-MS. This species was only observed after incubation of myriocin (200 µM) with SPT K265A (40 µM) for 7 days at room temperature. MS obtained by summing the spectra between t = 10-12 minutes. ($[M+H]^+$ $C_{28}H_{48}N_2O_9P$; predicted *m/z* 587.30919; observed error 6.1ppm).

It is worth noting that the precise orientation of the PLP:myriocin aldimine required for decarboxylation may not be achievable in the wild type enzyme. In the wild type SPT the side chain of K265 would be very close to or perhaps clash with the carboxylate, distorting it out of the Dunathan conformation or stabilising the carboxylate by an ionic interaction. In previous studies of the SPT:PLP-L-serine external aldimine complex of S. *paucimobilis* SPT it was revealed that the carboxylate group is held in a specific orientation by salt bridges with Arg378 and His159.[29, 172] In this arrangement decarboxylation is not favoured, rather

deprotonation of the L-serine at Cα by K265 is achieved only upon a conformational change caused by palmitoyl-CoA binding.[29, 115] The CH_2OH head group of myriocin interacts with the 5′-phosphate of PLP in the same manner as the hydroxyl group from L-serine (Figure 4-35).[28] The 5'-phosphate of PLP interacts with both ligand and protein residues (side chain and backbone) in what is termed a "phosphate cup."

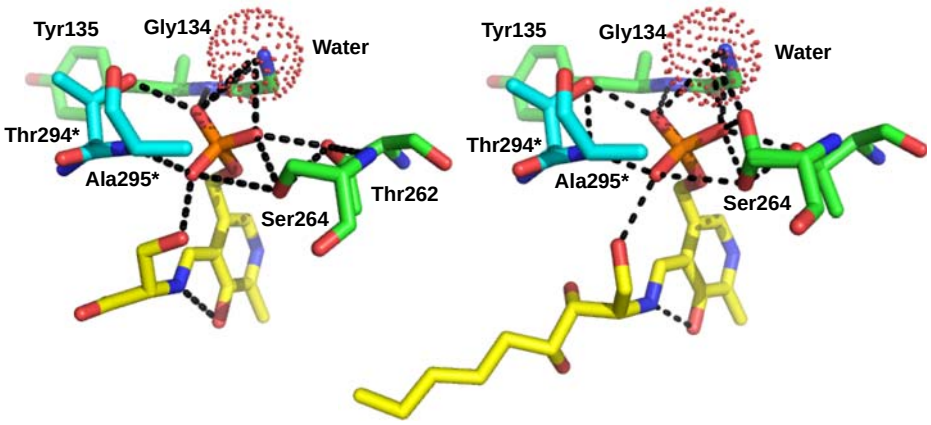

Figure 4-35 Analysis of the PLP phosphate binding via visualisation of the "phosphate cup" **Left.** PLP-L-serine aldimine (PDB code 2W8J) showing residues from monomer A (green) and monomer B (blue) involved in binding the 5'-phosphate of PLP. **Right.** PLP-decarboxymyriocin aldimine showing residues from monomer A (green) and monomer B (blue) involved in binding the phosphate of PLP. Despite the opposite stereochemistry of myriocin at Cα compared with L-serine, the C1 hydroxyl still hydrogen bonds to the 5'-phosphate of PLP.

Elsewhere the 3,4-*cis* diol of decarboxymyriocin makes hydrogen bonds to the protein, notably the 3-hydroxy of myriocin with the important catalytic residue His159; this interaction would be expected to be preserved in the wild type SPT:myriocin complex. Some insight into the binding of myriocin can be inferred from the literature but most of the published structure activity studies involving myriocin were concerned with myriocin's immunosuppressant properties which were later shown not to arise from its ability to inhibit SPT. Therefore, it is unknown at which point in the selective removal of the functional groups from myriocin as part of the process of developing FTY720 that SPT inhibition was lost, as it has now been confirmed that FTY720 does not inhibit SPT.[147, 173] However, the published work probing the SAR of sphingofungin B suggests an electron rich oxygen is required at carbon-14 but not necessarily as part of a carbonyl moiety and that the stereochemistry at the α, β and γ carbons are crucial to SPT inhibition.[133, 174] The hydrogen bond network that surrounds and includes the 4-hydroxy of

decarboxymyriocin may be changed by the presence of Lys265 but at least some of the same network seems certain to persist. This network involves the same residues that interact with the carboxylate of the PLP:L-serine external aldimine. These interactions rationalise the competitive inhibition with L-serine. Accompanying these interactions are movements of the side-chains of Tyr73, Arg378 and Arg390 as well as a displacement of a key conserved stretch of amino acids (RPPATP). The carbon tail of myriocin binds in a similar orientation to the decanoyl-tail of the PLP-product external aldimine observed bound in the crystal structure of the related AOS enzyme CqsA from *Vibrio cholera* consistent with our hypothesis that myriocin mimics the condensation intermediate (Figure 4-36).[166]

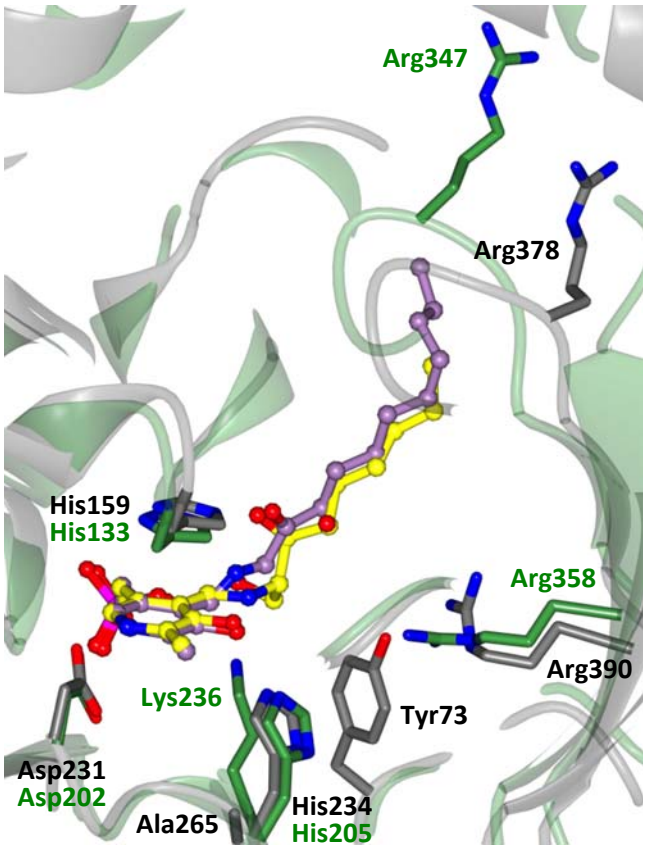

Figure 4-36 Overlay of myriocin K265A AmSPT and PLP-deconyl CqsA
Active site geometry of the PLP-decarboxymyriocin external aldimine structure (key sidechains and secondary structure rendered in grey; PBD 4BMK) with the V. cholera CqsA enzyme with the trapped product external aldimine bound (key sidechains and secondary structure rendered in green; PBD 2WKA). The PLP-decarboxymyriocin aldimine (yellow) overlays extremely well with the C10-product external aldimine in the CqsA active site (lilac). It is clear that both species occupy the same hydrophobic pocket.

As well as SHMT and CqsA the proposed mechanism for myriocin degradation is also reminiscent of the mechanism of the PLP-dependent S1PL. S1PL is the terminal enzyme of sphingolipid biosynthesis (Figure 1-9) and catalyses the breakdown of

S1P.[51] During the catalytic cycle of S1PL, the C3 hydroxyl group of the key PLP:S1P external aldimine is deprotonated, which leads to C2-C3 bond cleavage and production of hexadecenal and phosphoethanolamine. The similarity of the long chain aldehyde product of S1PL to the suicide-inhibitor produced by SPT-catalysed breakdown of myriocin is striking. This suggested a possible feedback mechanism whereby the end product of the sphingolipid pathway, hexadecenal, may regulate sphingolipid biosynthesis by inhibiting SPT, the enzyme that catalyses the first step in *de novo* sphingolipid synthesis. Indeed, in exciting preliminary in vitro studies, it was found that hexadecanal inhibits SPT with an IC_{50} of 144 μM (Figure 4-37).

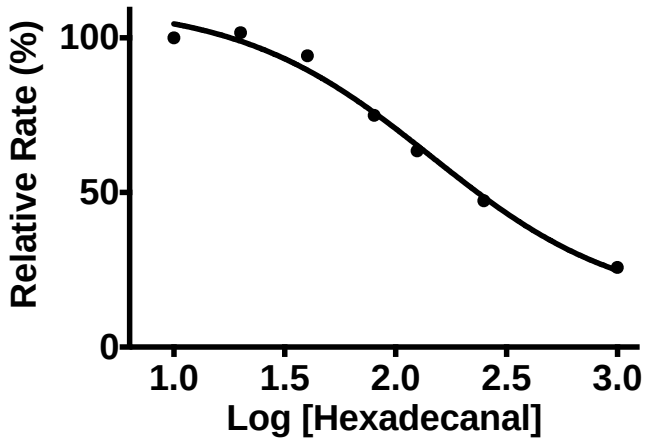

Figure 4-37 Dose response curve showing changes in relative rate versus the log of hexadecanal concentration.
Activity was quantified by monitoring the reaction of the co-product CoASH with DTNB. The reaction was performed on a 250 μL scale, SPT (200 nM) was incubated with L-serine (20 mM) in the presence of varying hexadecanal concentrations (20, 40, 80, 125, 250, 500 and 1000 μM). The reaction was started by the addition of the second substrate palmitoyl-CoA (250 μM).

Following the success of the myriocin crystal trials and the availability of the newly optimised conditions, crystal trials were attempted with compounds provided in a collaborative PhD agreement by Dr Howard Broughton at Lilly Pharmaceuticals. Lilly were interested in inhibition of human SPT but acknowledged that the bacterial SPT would provide a good model and provided 40 of their lead SPT inhibitors (Appendix 3). Lilly had access to both a bacterial and human SPT assay with some of these compounds showing low nanomolar inhibition. Based upon their IC_{50} values and the priority level given to the compounds by Lilly, four inhibitors were taken forward into crystal trials (Figure 4-38).

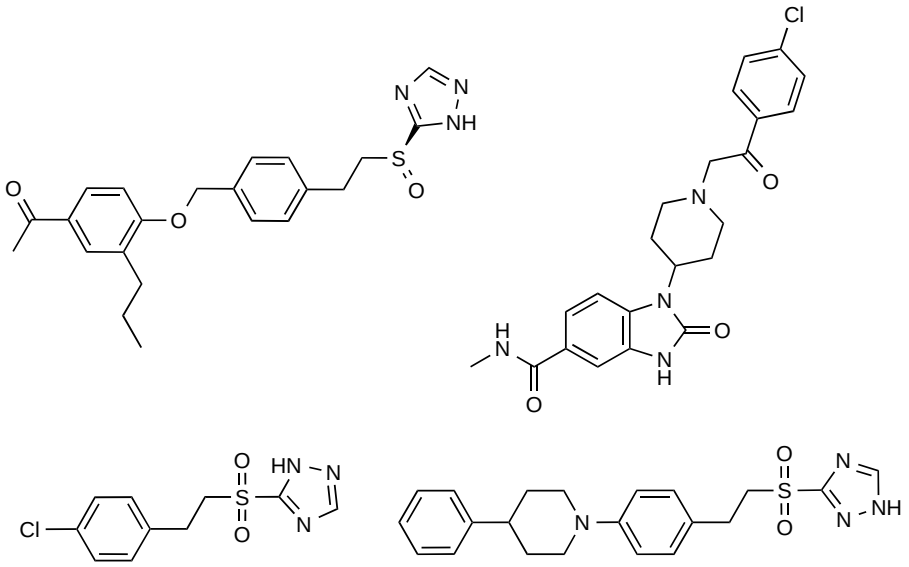

Figure 4-38 Selected Lilly inhibitors taken forward for crystal trials

As inhibition data was already available and a co-crystal structure would yield the most relevant information for a drug development programme the four compounds were solely committed to crystal trials. Unlike myriocin, no degradation of the inhibitor was expected and to gain maximum structural information co-crystallisation was attempted with WT AmSPT. Initial screens centred around the optimal conditions determined for myriocin but this yielded no results. Starting the screening process afresh for each of the four compounds also provided no viable crystals. Due to time constraints, the success of the myriocin study and limited access to the crystallography lab in St. Andrews no further work was undertaken with these compounds.

The initial aim of the work with myriocin was to delineate the structural and mechanistic details of how myriocin inhibits SPT, and in doing so it has revealed unexpected and hitherto unprecedented chemistry (summarized in Figure 4-39).

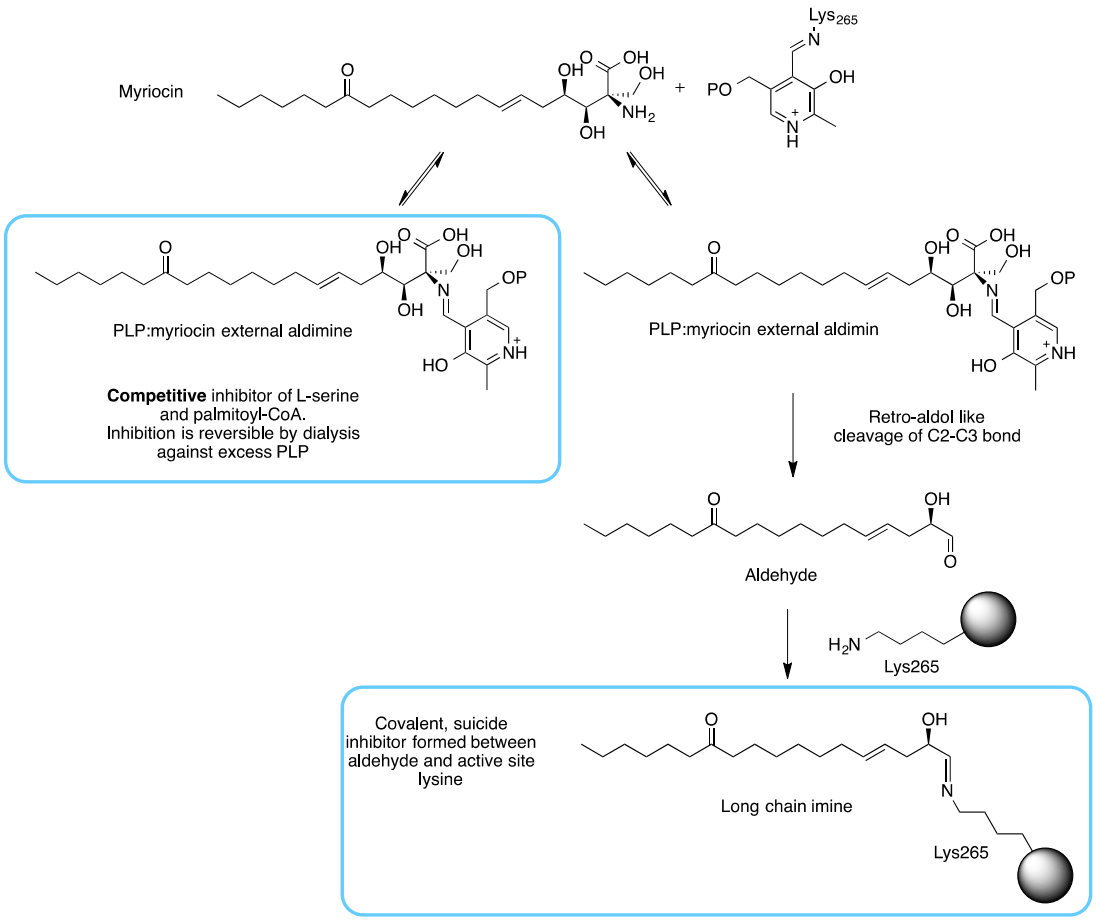

Figure 4-39 Summary of myriocin's dual mode of action. (Inhibitory species highlighted in boxes)

Left: myriocin reacts with PLP in the active site to form the inhibitory PLP:myriocin aldimine, this species is stable for greater than 1 h at physiological temperature with inhibition being reversible upon addition of excess PLP. **Right:** PLP-myriocin aldimine decomposes over 16 h, at physiological temperature, to produce a long chain aldehyde that reacts with the active site lysine to form an imine, thus rendering the enzyme inactive. This covalent modification can be classed as suicide inhibition.

These results demonstrate that, as predicted, myriocin acts as a classical intermediate mimic inhibitor with nanomolar affinity for its target. However, once bound in the active site the inhibitory species is broken down by the enzyme to generate a reactive product which acts as a suicide inhibitor by covalent modification of a key active site residue conserved in all SPTs.

The PLP-catalyzed retro-aldol reaction that breaks down the myriocin calls to mind other important PLP-dependent enzymes that use the cofactor to catalyze carbon-carbon bond cleavage. SHMT, which is involved in one carbon metabolism, and CqsA, which produces quorum sensing molecules, both use a proposed retro-aldol mechanism to generate glycine from L-serine and L-threonine, respectively. Furthermore, the proposed mechanism for myriocin degradation is reminiscent of the

mechanism of the PLP-dependent S1PL, the terminal enzyme of sphingolipid biosynthesis that catalyzes the breakdown of S1P.

The high sequence homology between the SPTs from bacteria and other higher order species suggests that the mechanism of myriocin inhibition is conserved and indeed studies on the human enzyme are already under way within the Campopiano group. The unprecedented combination of tight binding and mechanism-based inactivation within a single molecule described herein, has the potential to inform the design of a new class of inhibitors for SPT and other PLP-dependent enzymes.

4.3 SPT Fusions

The main difference between SPTs from eukaryotic species (such as humans, plants and yeast) and bacteria was, until recently, believed to be the existence of two distinct but structurally similar subunits that come together to form a heterodimer in humans. Moreover, small subunits such as Tsc3p, ssSPT and ORMs act as either positive or negative regulators of SPT activity in these organisms and can provide a mechanism to control sphingolipid biosynthesis/metabolic flux when demand is either high or low. In contrast, bacterial SPT consist of only one subunit that forms a homodimeric complex with no small regulatory subunits involved. An interesting discovery made by our group was that the SPT from *S. wittichii* is coded in the same open reading frame as an unusual acyl-carrier protein (ACP) possibly suggesting its substrate is an acyl-ACP rather than an acyl-CoA.[175] ACPs play key roles in fatty acid biosynthesis so this may allow regulation of sphingolipid biosynthesis by linking it to fatty acid metabolism. Since bacterial SPTs are relatively simple compared with their eukaryotic counterparts the utility of bacterial SPT as a structural model for the human protein was relatively limited, but still extensively utilised due to the intractability of human SPT to current biochemical methods. Following the discovery of a natural viral SPT fusion in the *Coccolithovirus* in 2005,[108] the concept of synthetic SPT fusions quickly developed and led to the publication of both synthetic yeast and human fusions by Dunn and colleagues in 2006.[109] Interestingly, another natural AOS fusion has been discovered in fumonisin biosynthesis, where Fum8p consists of two distinct domains that each show high sequence homologoy to lcb1 or lcb2.[176] This natural fusion condenses L-alanine to stearoyl-ACP to form a key intermediate in fumonisin biosynthesis and further proves the validity of fusion proteins.

Unfortunately the fusing of the two yeast proteins by Dunn *et al.* caused a 70% drop in activity with the added deleterious effect of causing a change in substrate specificity from C-16 to C-14.[109] This change in substrate specificity suggests the folding of the two regions has somehow impeded the active-site and highlights the problems of creating synthetic fusions. Ferreira and colleagues have studied the structure and mechanism of the AOS family member ALAS involved in heme biosynthesis.[177] They found that an ALAS fusion (2xALAS) was more active than the wild-type ALAS enzyme possibly by reducing the impact of rate limiting steps in

the mechanism.[178] They have also generated ALAS/AONS fusions to study the possibility that subunits from different AOS families can interact with each other with limited success. The fusion work of Dunn and Ferreira highlights the advantages to fusion proteins, mainly the ability to circumvent the difficulty in over expressing and purifying stoichiometric quantities of each subunit. The advantage of any bacterial fusion would hopefully be in increased solubility leading to the ability to purify the enzyme therefore allowing robust kinetic analysis. In an attempt to make a more realistic model of the human protein complex from the bacterial enzyme our aim was to prepare a fusion that had one LCB1-like subunit lacking PLP-binding residues and the other mimicking LCB2. If it folded as a "monomer" it would be predicted to only have one PLP-binding active site. The PLP binding residues that had been naturally evolved out of the human lcb1 subunit were mapped to spSPT and mutated (Figure 4-40, Top). The four key PLP binding residues His159, Asp231, His234 and Lys265 were mutated to the corresponding amino acids from lcb1 before the quadruple mutant is fused to a second active spSPT (Figure 4-40, Bottom C). As a control a fusion that had two wild-type SPTs linked together with two complete PLP binding sites was also generated.

```
Human lcb1          MATATEQWVLVEMVQALYEAPAYHLILEGILILWIIRLLFSKTYKLQERSDLTVKEKEEL 60
spSPT               ---------MTEAAAQPHALPADAPDIA------------PERDLLSKFDGLIAERQKL 38
                           :.* .   :  **    :                .* .: *  : *:::*
Human lcb1          IEEWQPEPLVPPVPKDHPALNYNIVSGPPSHKTVVNGKECINFASFNFLGLLDNPRVKAA 120
spSPT               LDSGVTDPFAIVMEQVKSPT----------EAVIRGKDTILLGTYNYMGMTFDPDVIAA 87
                    ::.  .:*:.  : : :..           ::*:.**: * :.::*::*:  :* * **
Human lcb1          ALASLKKYGVGTCGPRGFYGTFDVHLDLEDRLAKFMKTEEAIIYSYGFATIASAIPAYSK 180
spSPT               GKEALEKFGSGTNGSRMLNGTFHDHMEVEQALRDFYGTTGAIVFSTGYMANLGIISTLAG 147
                    .  :*:*:* ** *.* : ***. *:::*: * .*  *  **::* *: :  . *.: :
Human lcb1          RGDIVFVDRAACFAIQKGLQASRSDIKLFKHNDMADLERLLKEQEIEDQKNPRKARVTRR 240
spSPT               KGEYVILDADSHASIYDGCQQGNAEIVRFRHNSVEDLDKRLG----------RLPKEPAK 197
                    :*: *::*  :  :* .* * ..::*  *:**.: **:: *          * .: . :
Human lcb1          FIVVEGLYMNTGTICPLPELVKLKYKYKARIFLEESLSFGVLGEHGRGVTEHYGINIDDI 300
spSPT               LVVLEGVYSMLGDIAPLKEMVAVAKKHGAMVLVDEAHSMGFFGPNGRGVYEAQGLEG-QI 256
                    ::*:**:*   * *.** *:* :  *: * ::::*: *:*.:* :**** *  *::  :*
Human lcb1          DLISANMENALASIGGFCCGRSFVIDHQRLSGQGYCFSASLPPLLAAAAIEALNIMEENP 360
spSPT               DFVVGTFSKSVGTVGGFVVSNHPKFEAVRLACRPYIFTASLPPSVVATATTSIRKLMTAH 316
                    *:: ..:.:::.::***  ..   ::  **: : * *:***** :.*:*  ::. :
Human lcb1          GIFAVLKEKCGQIHKALQGISGLKVVGESLSPAFHLQLEESTGSREQDVRLLQEIVDQCM 420
spSPT               EKRERLWSNARALHGGLKAMG-FRLGTETCDSAIVAVMLE---DQEQAAMMWQALLDGGL 372
                         * .:.  :* .*:.:. :::  *: ..*:   : *   .:** . : * ::*  :
Human lcb1          NRSIALTQARYLEKEEKCLPPPSIRVVVTVEQTEEELERAASTIKEVAQAVLL-- 473
spSPT               YVNMARPPATPAG------TFLLRCSICAEHTPAQIQTVLGMFQAAGRAVGVIG 420
                      .:* . *           .  :*  : .*:*  ::: . . :: ..:** :
```

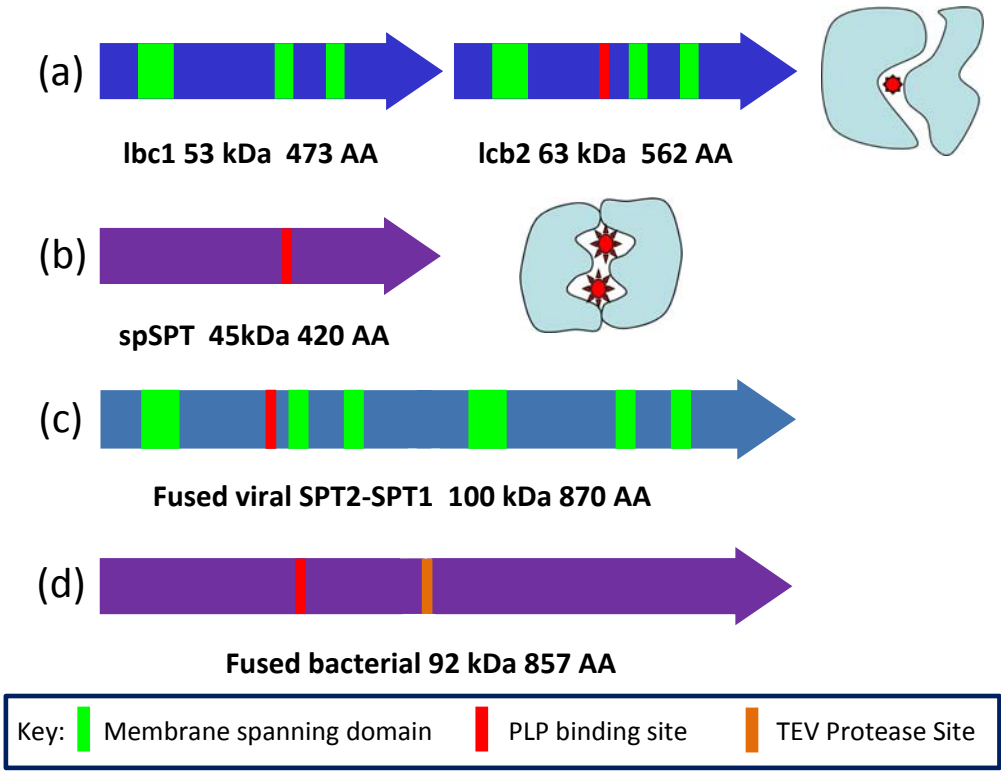

Figure 4-40 Top - Amino acid sequence alignment of human lcb1 and spSPT. Bottom - Cartoon representation of the fusion project

Top - Mutated residues are higlihghted in blue. Key - * (asterisk) indicates positions which have fully conserved residues, : (colon) indicates conservation between groups of strongly similar properties and . (full stop) indicates conservation between groups of weakly similar properties.

Bottom (a) - Two subunits of human SPT showing membrane spanning domains, the PLP binding site and the heterodimeric nature of the complex **(b) -** Bacterial spSPT showing the only subunit and homodimeric nature of the soluble complex. **(c) -** The natural Coccolithovirus fusion arranged with the PLP binding protein first. **(d) -** The proposed arrangement of the bacterial fusion.

The two bacterial subunits will be arranged in a similar manner as the viral fusion with the PLP binding; lcb2 like, subunit being at the N-terminus followed by the inactive, lcb1 like, subunit (Figure 4-40).

The production of a plasmid with two identical 1200 base pair sequences had previously caused problems, mostly likely from recombination of the plasmid construct and loop formation. The ability to combine two DNA sequences encoding for the same protein into one plasmid was only made possible by using two sequences that utilised different codons for the same amino acids. AmSPT had been gifted to the lab from Professor Teresa Dunn and was originally synthesised as a synthetic gene codon optimised for Arabidopsis expression. The fusion project had been previously started within the laboratory by Dr Marine Raman and resulted in a wild type fusion, two fused wild type SPT subunits, already being available. The two subunits of SPT were linked by Tobacco Etch Virus (TEV) protease site with the intention of cleaving the fusion after purification to check the fidelity of the individual monomers. Monomeric spSPT had previously been produced with three of the four desired PLP binding mutations, D231E, H234L and K265N. Site direct mutagenesis (for primers see Table 3-4) was used to make the final targeted fourth mutation, H159C. A double Age1 and Xho1 digest was then used to add the mutated portion of spSPT to the reciprocally cut WT fusion to generate a quadruple mutant SPT fusion (x4M SPT fusion) shown in Figure 4-41 (DNA and protein sequence are shown in Appendix 1).

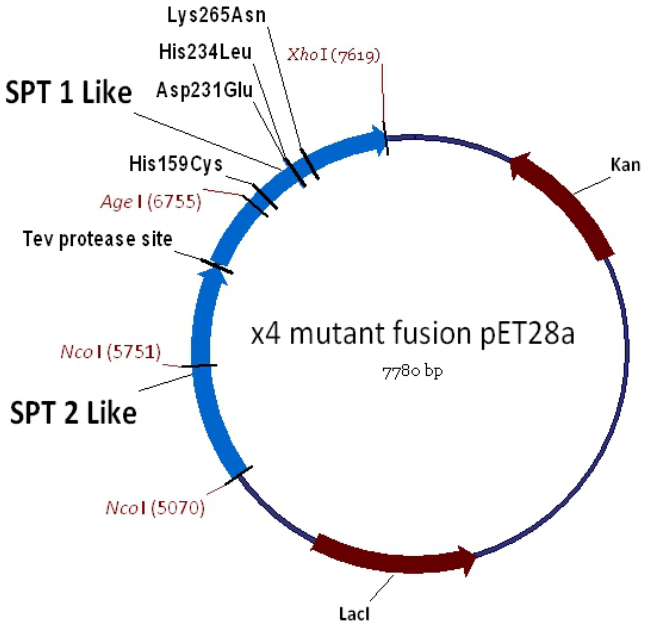

Figure 4-41 Plasmid map of x4M SPT fusion

Both the WT and x4M fusion plasmids were sequenced and found to be correct. Test expressions revealed the WT fusion to be easier to express at scale. The x4M fusion

required expression to be induced with 1 mM IPTG for 5 hours at 30 °C to produce the quantity of protein required for visualisation by SDS PAGE, a band at 92 kDa was observed and matched our prediction for the size of the fusion protein. Nickel affinity chromatography purified both proteins well (Figure 4-42 and Figure 4-43). Size exclusion chromatography showed the WT fusion to exist in a single form with an elution volume of 168 mL corresponding to roughly 92 kDa (Figure 4-42).

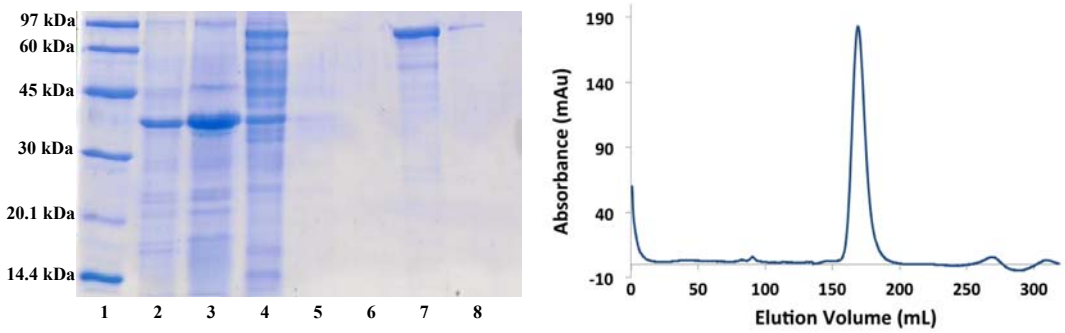

Figure 4-42 Optimised purification of WT SPT Fusion
Left - Lane 1: Low molecular weight marker, Lane 2: Pellet, Lane 3: Supernatant, Lane 4: Flow through, Lane 5: Wash 1 - 30 mM Imidazole wash, Lane 6: Wash 2 - 30 mM Imidazole, Lane 7: Elution 1 - 300 mM Imidazole, Lane 8: Elution 2 – 300 mM Imidazole. **Right** - Elution profile from Sephacryl 26/60 S300 size exclusion column, blue line showing absorbance at 280 nm.

The same size exclusion chromatography for the x4M fusion showed it had aggregated in solution (Figure 4-43). The elution profile displayed a peak with a broad shoulder eluting in the void volume and therefore corresponding to aggregates greater or equal to 1.5 MDa. The two subsequent peaks correspond to 270 kDa (trimer) and the 92 kDa monomer. The small proportion of isolatable monomer allowed the process to be scaled and monomer isolated preferentially. Unsurprisingly the removal of a complete PLP binding site had affected protein folding but not abolished it completely. In an attempt to aid the proportion of monomer by more successful protein folding both the expression temperature and IPTG concentration were lowered with the aim of slowing protein expression and allowing more time for the protein to fold correctly. Cofactors are also known to increase protein folding efficiency but addition of pyridoxal to the growth media failed to yield a greater proportion of the fusion monomer.[179] Mass spectrometry was attempted to confirm the identity of both fusion proteins but the large 92 kDa mass made this unsuccessful with the equipment available.

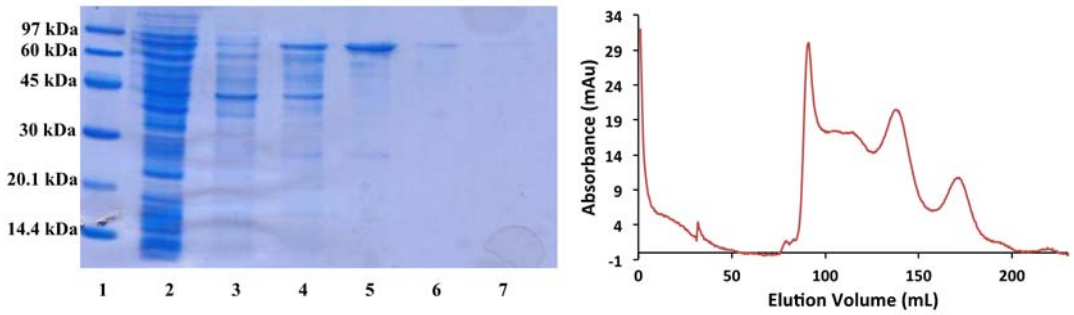

Figure 4-43 Optimised purification of x4M SPT Fusion
Left - Lane 1: Low molecular weight marker, Lane 2: Pellet, Lane 3: Supernatant, Lane 4: Wash 1 - 30 mM Imidazole, Lane 5: Elution 1 - 150 mM Imidazole, Lane 6: Elution 2 – 150 mM Imidazole, Lane 7: Elution 3 – 300 mM Imidazole. **Right** - Elution profile from Sephacryl 26/60 S300 size exclusion column, red line showing absorbance at 280 nm.

The UV-vis spectrum of the WT fusion closely matched the monomeric spSPT spectrum demonstrating that PLP is bound to the enzyme in both the enolimine (333 nm) and the ketoenamine (415 nm) forms (Figure 4-44). Addition of 20 mM L-serine also elicited the characteristic increase in the ketoenamine form, providing strong evidence that the enzyme has bound L-serine and formed a PLP:L-serine external aldimine.

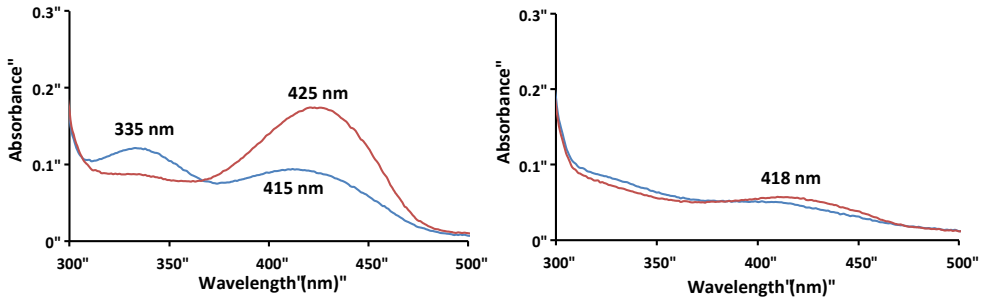

Figure 4-44 Exogenous UV-vis analysis of fusion proteins
Left – 40 μM WT Fusion before (Blue) and after 20 mM L-serine addition (Red). **Right** - 40 μM x4M Fusion before (Blue) and after 20 mM L-serine addition (Red).

In contrast to the WT SPT fusion the x4M SPT fusion showed no UV-vis evidence of binding exogenous PLP. The addition of L-serine further proved the lack of PLP by the inability to form the characteristically large ketoenamine peak generated from the formation of the PLP-L-serine external aldimine. Dialysis of the x4M fusion against a high (25 μM) PLP buffer for 18 hours did induce limited PLP binding and allowed the titration of L-serine standards. (Figure 4-45A)

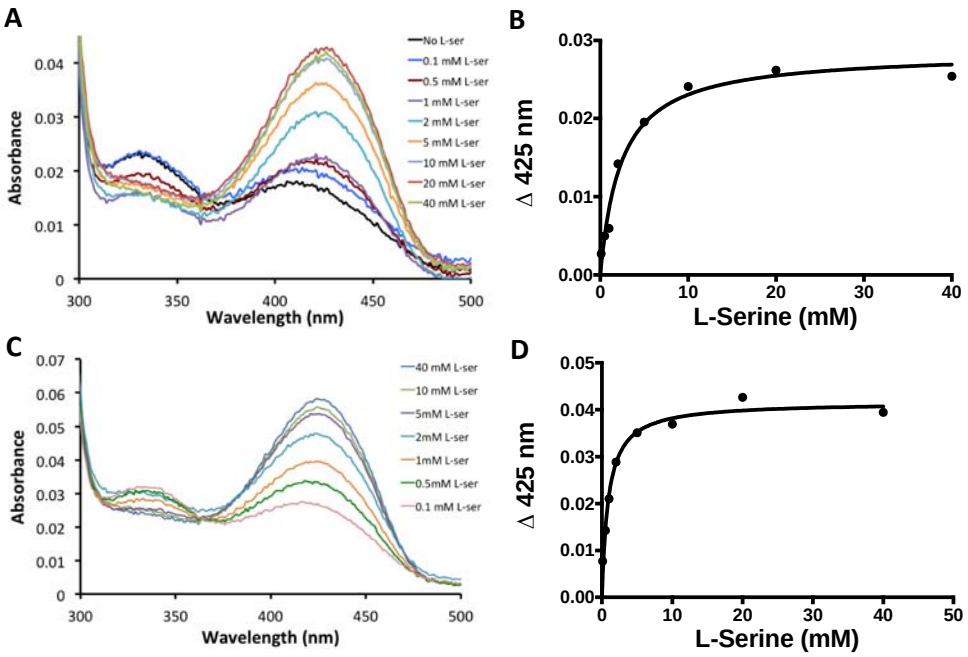

Figure 4-45 UV-vis spectrum and kinetic analysis of fusion proteins
A - Addition of 0.1, 0.5, 1, 2, 5, 10, 20 and 40 mM L-Serine to 10 μM x4M SPT fusion. **B** - Michaelis-Menten analysis of L-Serine binding to x4M SPT fusion. **C** - Addition of 0.1, 0.5, 1, 2, 5, 10 and 40 mM L-Serine to 10 μM WT SPT fusion. **D** - Michaelis-Menten analysis of L-Serine binding to WT SPT fusion.

Analysis of the absorbance differences at 425 nm over several L-serine concentrations produces an L-serine K_d for the x4M SPT fusion of 2.4 ± 0.4 mM (Figure 4-45A and B). The same analysis of the WT SPT fusion gave a L-serine K_d of 0.9 ± 0.1 mM, comparable to the monomeric spSPT (1.4 mM) (Figure 4-45C and D). The similarity between the monomeric and the WT SPT fusion binding coefficients is evidence that the head-to-tail attachment of two SPTs has no detrimental effect of L-serine binding. The roughly 50% drop in binding efficiency in the x4M SPT fusion could arise from the lack of a PLP binding site in one monomer causing a long range subtle conformational change in the second active site. Alternatively the large-scale aggregation seen via the size exclusion chromatography could also cause sub-optimal substrate binding.

Unfortunately, the progress of the fusion project was continually hampered by the tendency of the x4M SPT fusion to aggregate both during expression and after size exclusion chromatography. Relatively pure monomer was isolated from the size exclusion procedure but aggregated again within hours. The ability to express pure

monomeric WT SPT fusion was also unreproducible. The original growth, expression and purification conditions were repeated diligently but the size exclusion chromatography always revealed a multimeric mixture. Lowering the expression temperature, addition of pyridoxal to the media and changing the media were all attempted to aid protein folding but yielded no results. The inability to purify the control, WT SPT fusion, or large quantities of the x4M SPT fusion rendered the project difficult to continue to full structural studies.

These results and the work of Dunn and Ferreira suggest that the production of unnatural fusion proteins are possible. It is worth noting that no artificial bacterial fusion will ever be a 100% accurate model for the human SPT complex so any data produced from such a fusion will always be questioned. Therefore efforts may be better directed developing conditions to express and purify the challenging multimeric membrane bound human SPT complex. However, if the usefulness of a bacterial SPT fusion warrants further work, a similar approach to that of Ferreira *et al.*[178] could be adopted. In this work a powerful *in vivo* complementation activity screen was developed by using *E. coli* cells deficient in 5-aminolevulinate synthase activity. They can therefore only grow when transformed with a functioning ALAS or ALAS fusion. If a sphingolipid producing bacterium could be made auxotrophic for sphingolipid biosynthesis then this could be used to screen plasmids for a functioning SPT fusion. A classic model system developed by Dunn and others is the use of yeast lcb1 and lcb2 knockouts to test the activity of SPT homologs – this would be a good test system. Moreover, recent work that identified the SPT involved in *Bacteroides fragilis* sphingolipid biosynthesis has suggested that this organism may also be an ideal model to test the ability of SPT fusions and SPT homologs from other species to complement an SPT-deficient *B. fragilis* strain.[180]

Chapter 5:
Conclusions and Future Work

5 Conclusions and future work

Both initial aims of the myriocin project have been fulfilled. The inhibition of SPT by myriocin has now been shown to be competitive for both substrates, L-serine and palmitoyl-CoA. The K_i was determined to be 967 ± 98 nm and the initial inhibitory species was identified to be a myriocin-PLP external aldimine. Moreover, myriocin was shown to inhibit SPT via two divergent pathways. Firstly myriocin formed an aldimine with PLP and bound tightly into the active site blocking substrate turnover. This binding of the myriocin-PLP external aldimine was non-covalent and could be removed through extensive dialysis. The second mode of inhibition arose from the myriocin-PLP external aldimine degrading in the active-site via a "retro-aldol" type mechanism to form a reactive long chain aldehyde which then went on to covalently modify the active-site lysine and again render the enzyme inactive. The classical initial non-covalent inhibition and the second suicide inhibition mechanism have been proved independently of each other through the use of mass spectrometry, UV-vis spectroscopy and protein crystallography. The elucidation of two inhibition mechanisms greatly enhances the myriocin/SPT inhibition literature and gives rise to new opportunities for drug development. At best, this work gives rise to the possibility of aiding the development of a drug that inhibits SPT by being designed to degrade in the active site and covalently modify the enzyme. At the very least, the myriocin crystal structure can aid future drug development by being used in computer modelling. The compounds provided by Lilly can be taken forward into crystal trials with renewed optimism following the success of producing an SPT-myriocin co-crystal structure.

Through both truncation and extension of the N-terminus it has been shown that the as yet unknown function of the N-terminus cannot be underestimated. Both the removal of the first 21 amino acids and extension of the termini proved detrimental to the enzyme activity. Unfortunately the lack of any structural data pertaining to the position of the N-terminus prevents extrapolation or conjecture about its function. Therefore all that can be categorically stated from this work is its essential nature for full catalytic activity. The failure to visualise the N-terminus in either our structure or previously published work suggests it has a high degree of flexibility and is therefore incompatible with protein crystallography therefore, perhaps future advances in NMR structure determination will someday elucidate its mechanistic role.

The impressive and technically demanding work others have undertaken to develop fusion proteins laid a strong foundation for our work with SPT. Combining this previous knowledge with the proof of concept provided by Nature in the *Coccolithovirus* led to the development of two, active, SPT fusion proteins. Unfortunately aggregation/solubility issues dogged the development of the quadruple mutant fusion from the onset and in the end also hampered the characterisation of the WT fusion. Nevertheless, the concept of fusing proteins together is not without merit and could now be employed as a purification aid for the membrane bound multimeric human SPT complex. Fusion proteins could provide solutions to both the solubility issues arising from the membrane bound nature of the complex and aid the production of equimolar quantities of a multimeric complex which could later be separated, after purification, through the use of proteases.

References

1. Raboni, S.; Spyrakis, F.; Campanini, B.; Amadasi, A.; Bettati, S.; Peracchi, A.; Mozzarelli, A.; Contestabile, R.; Lew, M.; Hung-Wen, L., Pyridoxal 5'-Phosphate-Dependent Enzymes: Catalysis, Conformation, and Genomics. *Comprehensive Natural Products II* **2010**, 273-350.

2. Espaillat, A.; Carrasco-Lopez, C.; Bernardo-Garcia, N.; Pietrosemoli, N.; Otero, L. H.; Alvarez, L.; de Pedro, M. A.; Pazos, F.; Davis, B. M.; Waldor, M. K.; Hermoso, J. A.; Cava, F., Structural basis for the broad specificity of a new family of amino-acid racemases. *Acta crystallographica. Section D, Biological crystallography* **2014,** *70* (Pt 1), 79-90.

3. Percudani, R.; Peracchi, A., A genomic overview of pyridoxal-phosphate-dependent enzymes. *EMBO Rep* **2003,** *4* (9), 850-854.

4. Garrido-Franco, M., Pyridoxine 5′-phosphate synthase: de novo synthesis of vitamin B6 and beyond. *Biochim. Biophys Acta - Proteins and Proteomics* **2003,** *1647* (1–2), 92-97.

5. Ehrenshaft, M.; Bilski, P.; Li, M. Y.; Chignell, C. F.; Daub, M. E., A highly conserved sequence is a novel gene involved in de novo vitamin B6 biosynthesis. *Proc. Natl. Acad. Sci. U.S.A.* **1999,** *96* (16), 9374-9378.

6. Leuendorf, J.; Mooney, S.; Chen, L.; Hellmann, H., Arabidopsis thaliana PDX1.2 is critical for embryo development and heat shock tolerance. *Planta* **2014,** *240* (1), 137-146.

7. Fitzpatrick, T. B.; Amrhein, N.; Kappes, B.; Macheroux, P.; Tews, I.; Raschle, T., Two independent routes of de novo vitamin B6 biosynthesis: not that different after all. *The Biochemical journal* **2007,** *407* (1), 1-13.

8. Hanes, J. W.; Keresztes, I.; Begley, T. P., 13C NMR snapshots of the complex reaction coordinate of pyridoxal phosphate synthase. *Nat. Chem. Biol.* **2008,** *4* (7), 425-430.

9. Burns, K. E.; Xiang, Y.; Kinsland, C. L.; McLafferty, F. W.; Begley, T. P., Reconstitution and Biochemical Characterization of a New Pyridoxal-5'-Phosphate Biosynthetic Pathway. *J. Am. Chem. Soc.* **2005,** *127* (11), 3682-3683.

10. Smith, M. A.; Mack, V.; Ebneth, A.; Moraes, I.; Felicetti, B.; Wood, M.; Schonfeld, D.; Mather, O.; Cesura, A.; Barker, J., The Structure of Mammalian Serine Racemase: Evidence for conformational changes upon inhibitor binding. *J. Biol. Chem.* **2010,** *285* (17), 12873-12881.

11. Tramonti, A.; John, R. A.; Bossa, F.; De Biase, D., Contribution of Lys276 to the conformational flexibility of the active site of glutamate decarboxylase from Escherichia coli. *Eur. J. Biochem.* **2002,** *269* (20), 4913-4920.

12. Florio, R.; di Salvo, M. L.; Vivoli, M.; Contestabile, R., Serine hydroxymethyltransferase: A model enzyme for mechanistic, structural, and evolutionary studies. *Biochim. Biophys. Acta - Proteins and Proteomics* **2011,** *1814* (11), 1489-1496.

13. Kirsch, J. F.; Eichele, G.; Ford, G. C.; Vincent, M. G.; Jansonius, J. N.; Gehring, H.; Christen, P., Mechanism of action of aspartate aminotransferase proposed on the basis of its spatial structure. *J. Mol. Biol.* **1984,** *174* (3), 497-525.

14. Sun, L.; Bartlam, M.; Liu, Y.; Pang, H.; Rao, Z., Crystal structure of the pyridoxal-5'-phosphate-dependent serine dehydratase from human liver. *Protein Sci.* **2005,** *14* (3), 791-798.

15. Mozzarelli, A.; Bettati, S.; Campanini, B.; Salsi, E.; Raboni, S.; Singh, R.; Spyrakis, F.; Kumar, V. P.; Cook, P. F., The multifaceted pyridoxal 5′-phosphate-dependent O-acetylserine sulfhydrylase. *Biochim. Biophys. Acta - Proteins and Proteomics* **2011,** *1814* (11), 1497-1510.

16. Stipanuk, M. H., Sulfur amino acid metabolism: pathways for production and removal of homocysteine and cysteine. *Annu. Rev. Nutr.* **2004,** *24*, 539-577.

17. Aitken, S. M.; Kim, D. H.; Kirsch, J. F., Escherichia coli Cystathionine γ-Synthase Does Not Obey Ping-Pong Kinetics. Novel Continuous Assays for the Elimination and Substitution Reactions. *Biochemistry* **2003,** *42* (38), 11297-11306.

18. Shiraiwa, Y.; Ikushiro, H.; Hayashi, H., Multifunctional Role of His159in the Catalytic Reaction of Serine Palmitoyltransferase. *J. Biol. Chem.* **2009,** *284* (23), 15487-15495.

19. Toney, M. D., Controlling reaction specificity in pyridoxal phosphate enzymes. *Biochim. Biophys. Acta - Proteins and Proteomics* **2011,** *1814* (11), 1407-1418.

20. Metzler, D. E.; Snell, E. E., Some Transamination Reactions Involving Vitamin B61. *J. Am. Chem. Soc.* **1952,** *74* (4), 979-983.

21. Matsushima, Y.; Martell, A. E., Pyridoxal Analogs. X. Zinc(II)-Chelate Catalysis of Transamination in Methanol Solution. *J. Am. Chem. Soc.* **1967,** *89* (6), 1331-1335.

22. Miles, E. W.; Metzler, D. E., Esmond Emerson Snell (1914–2003). *J. Nutr.* **2004,** *134* (11), 2907-2910.

23. Christen, P.; Metzler, D. E., *Transaminases*. Wiley: 1985.

24. Metzler, D. E.; Ikawa, M.; Snell, E. E., A General Mechanism for Vitamin B6-catalyzed Reactions. *J. Am. Chem. Soc.* **1954,** *76* (3), 648-652.

25. Zabinski, R. F.; Toney, M. D., Metal Ion Inhibition of Nonenzymatic Pyridoxal Phosphate Catalyzed Decarboxylation and Transamination. *J. Am. Chem. Soc.* **2000,** *123* (2), 193-198.

26. Felten, A. E.; Zhu, G.; Aron, Z. D., Simplifying Pyridoxal: Practical Methods for Amino Acid Dynamic Kinetic Resolution. *Org. Lett.* **2010,** *12* (9), 1916-1919.

27. Dunathan, H. C., Conformation and reaction specificity in pyridoxal phosphate enzymes. *Proc. Natl. Acad. Sci. U.S.A.* **1966,** *55* (4), 712-716.

28. Beattie, A. E.; Clarke, D. J.; Wadsworth, J. M.; Lowther, J.; Sin, H.-L.; Campopiano, D. J., Reconstitution of the pyridoxal 5'-phosphate (PLP) dependent enzyme serine palmitoyltransferase (SPT) with pyridoxal reveals a crucial role for the phosphate during catalysis. *Chem. Commun.* **2013,** *49* (63), 7058-7060.

29. Raman, M. C. C.; Johnson, K. A.; Yard, B. A.; Lowther, J.; Carter, L. G.; Naismith, J. H.; Campopiano, D. J., The External Aldimine Form of Serine Palmitoyltransferase. *J. Biol. Chem.* **2009,** *284* (25), 17328-17339.

30. Metzler, D. E.; Metzler, C. M., *Biochemistry: The Chemical Reactions of Living Cells. Vol. 1*. Harcourt/Academic Press: 2003.

31. Richard, J. P.; Amyes, T. L.; Crugeiras, J.; Rios, A., Pyridoxal 5′-phosphate: electrophilic catalyst extraordinaire. *Curr. Opin. Chem. Biol.* **2009,** *13* (4), 475-483.

32. Crugeiras, J.; Rios, A.; Riveiros, E.; Amyes, T. L.; Richard, J. P., Glycine Enolates: The Effect of Formation of Iminium Ions to Simple Ketones on α-Amino Carbon Acidity and a Comparison with Pyridoxal Iminium Ions. *J. Am. Chem. Soc.* **2008,** *130* (6), 2041-2050.

33. Tidwell, T. T., Hugo (Ugo) Schiff, Schiff Bases, and a Century of β-Lactam Synthesis. *Angew. Chem. Int. Ed.* **2008,** *47* (6), 1016-1020.

34. Griswold, W. R.; Toney, M. D., Role of the Pyridine Nitrogen in Pyridoxal 5′-Phosphate Catalysis: Activity of Three Classes of PLP Enzymes Reconstituted with Deazapyridoxal 5′-Phosphate. *J. Am. Chem. Soc.* **2011,** *133* (37), 14823-14830.

35. Alexander, F. W.; Sandmeier, E.; Mehta, P. K.; Christen, P., Evolutionary relationships among pyridoxal-5′-phosphate-dependent enzymes. *Eur. J. Biochem.* **1994,** *219* (3), 953-960.

36. Schneider, G.; Käck, H.; Lindqvist, Y., The manifold of vitamin B6 dependent enzymes. *Structure* **2000,** *8* (1), R1-R6.

37. Christen, P.; Mehta, P. K., From cofactor to enzymes. The molecular evolution of pyridoxal-5′-phosphate-dependent enzymes. *Chem. Rec.* **2001,** *1* (6), 436-447.

38. Thudichum, J. L. W., *A treatise on the chemical constitution of the brain*. Baillière, Tindall and Cox: London, 1884; p 262.

39. Carter, H. E.; Glick, F. J.; Norris, W. P.; Phillips, G. E., The Structure of Sphingosine. *J. Biol. Chem.* **1942,** *142* (1), 449-450.

40. Carter, H. E.; Glick, F. J.; Norris, W. P.; Phillips, G. E., Biochemistry of the Sphingolipides: III. Structure of Sphingosine. *J. Biol. Chem.* **1947,** *170* (1), 285-294.

41. Hanada, K., Serine palmitoyltransferase, a key enzyme of sphingolipid metabolism. *Biochim. Biophys. Acta - Molecular and Cell Biology of Lipids* **2003,** *1632* (1-3), 16-30.

42. Lowther, J.; Naismith, J. H.; Dunn, T. M.; Campopiano, D. J., Structural, mechanistic and regulatory studies of serine palmitoyltransferase. *Biochem. Soc. Trans.* **2012,** *40* (3), 547-554.

43. Mandon, E. C.; van Echten, G.; Birk, R.; Schmidt, R. R.; Sandhoff, K., Sphingolipid biosynthesis in cultured neurons. *Eur. J. Biochem.* **1991,** *198* (3), 667-674.

44. Han, G.; Gupta, S. D.; Gable, K.; Niranjanakumari, S.; Moitra, P.; Eichler, F.; Brown, R. H.; Harmon, J. M.; Dunn, T. M., Identification of small subunits of mammalian serine palmitoyltransferase that confer distinct acyl-CoA substrate specificities. *Proc. Natl. Acad. Sci. U.S.A.* **2009,** *106* (20), 8186-8191.

45. Hornemann, T.; Penno, A.; Rütti, M. F.; Ernst, D.; Kivrak-Pfiffner, F.; Rohrer, L.; von Eckardstein, A., The SPTLC3 Subunit of Serine Palmitoyltransferase Generates Short Chain Sphingoid Bases. *J. Biol. Chem.* **2009,** *284* (39), 26322-26330.

46. Pinto, W. J.; Wells, G. W.; Lester, R. L., Characterization of enzymatic synthesis of sphingolipid long-chain bases in Saccharomyces cerevisiae: mutant strains exhibiting long-chain-base auxotrophy are deficient in serine palmitoyltransferase activity. *J. Bacteriol.* **1992,** *174* (8), 2575-2581.

47. Stoffel, W.; Sticht, G.; LeKim, D., Metabolism of sphingosine bases. 8. Distribution, isolation and properties of D-3-oxosphinganine reductase. Stereospecificity of the NADPH-dependent reaction of 3-oxodihydrospingosine (2-amino-1-hydroxyoctadecane-3-one). *Hoppe Seyler's Z. Physiol. Chem.* **1968,** *349* (12), 1637-1644.

48. Bandhuvula, P.; Saba, J. D., Sphingosine-1-phosphate lyase in immunity and cancer: silencing the siren. *Trends in Molecular Medicine* **2007,** *13* (5), 210-217.

49. Stoffel, W.; LeKim, D.; Sticht, G., Distribution and properties of dihydrosphingosine-1-phosphate aldolase (sphinganine-1-phosphate alkanal-lyase). *Hoppe Seyler's Z. Physiol. Chem.* **1969,** *350* (10), 1233-1241.

50. Bourquin, F.; Riezman, H.; Capitani, G.; Grütter, M. G., Structure and Function of Sphingosine-1-Phosphate Lyase, a Key Enzyme of Sphingolipid Metabolism. *Structure* **2010,** *18* (8), 1054-1065.

51. Bourquin, F.; Capitani, G.; Grutter, M. G., PLP-dependent enzymes as entry and exit gates of sphingolipid metabolism. *Protein Sci.* **2011,** *20* (9), 1492-1508.

52. Serra, M.; Saba, J. D., Sphingosine 1-phosphate lyase, a key regulator of sphingosine 1-phosphate signaling and function. *Adv. Enzyme Regul.* **2010,** *50* (1), 349-362.

53. Kariya, Y.; Kihara, A.; Ikeda, M.; Kikuchi, F.; Nakamura, S.; Hashimoto, S.; Choi, C.-H.; Lee, Y.-M.; Igarashi, Y., Products by the sphingosine kinase/sphingosine 1-phosphate (S1P) lyase pathway but not S1P stimulate mitogenesis. *Genes to Cells* **2005,** *10* (6), 605-615.

54. Reiss, U.; Oskouian, B.; Zhou, J.; Gupta, V.; Sooriyakumaran, P.; Kelly, S.; Wang, E.; Merrill, A. H.; Saba, J. D., Sphingosine-phosphate Lyase Enhances Stress-induced Ceramide Generation and Apoptosis. *J. Biol. Chem.* **2004,** *279* (2), 1281-1290.

55. Saba, J., Sphingosine-1-Phosphate Lyase. In *Sphingolipid Biology*, Hirabayashi, Y.; Igarashi, Y.; Merrill, A., Jr., Eds. Springer Japan: 2006; pp 219-230.

56. Fahy, E.; Subramaniam, S.; Murphy, R. C.; Nishijima, M.; Raetz, C. R. H.; Shimizu, T.; Spener, F.; van Meer, G.; Wakelam, M. J. O.; Dennis, E. A., Update of the LIPID MAPS comprehensive classification system for lipids. *J. Lipid Res.* **2009,** *50* (Supplement), S9-S14.

57. Merrill, A. H., Sphingolipid and Glycosphingolipid Metabolic Pathways in the era of Sphingolipidomics. *Chem. Rev.* **2011,** *111* (10), 6387-6422.

58. Livingston, P. O.; Natoli, E. J.; Calves, M. J.; Stockert, E.; Oettgen, H. F.; Old, L. J., Vaccines containing purified GM2 ganglioside elicit GM2 antibodies in melanoma patients. *Proc. Natl. Acad. Sci. U.S.A.* **1987,** *84* (9), 2911-2915.

59. Igdoura, S. A.; Mertineit, C.; Trasler, J. M.; Gravel, R. A., Sialidase-Mediated Depletion of GM2 Ganglioside in Tay-Sachs Neuroglia Cells. *Hum. Mol. Gen.* **1999,** *8* (6), 1111-1116.

60. Pike, L. J., The challenge of lipid rafts. *J. Lipid Res.* **2009,** *50* (Supplement), S323-S328.

61. Spiegel, S.; Milstien, S., Sphingosine-1-phosphate: an enigmatic signalling lipid. *Nat. Rev. Mol. Cell. Biol.* **2003,** *4* (5), 397-407.

62. Pyne, N. J.; Pyne, S., Sphingosine 1-phosphate and cancer. *Nat. Rev. Cancer* **2010,** *10* (7), 489-503.

63. Summers, S. A.; Nelson, D. H., A Role for Sphingolipids in Producing the Common Features of Type 2 Diabetes, Metabolic Syndrome X, and Cushing's Syndrome. *Diabetes* **2005,** *54* (3), 591-602.

64. Kanety, H.; Hemi, R.; Papa, M. Z.; Karasik, A., Sphingomyelinase and Ceramide Suppress Insulin-induced Tyrosine Phosphorylation of the Insulin Receptor Substrate-1. *J. Biol. Chem.* **1996,** *271* (17), 9895-9897.

65. Sonnino, S.; Chigorno, V., Ganglioside molecular species containing C18- and C20-sphingosine in mammalian nervous tissues and neuronal cell cultures. *Biochim. Biophys. Acta - Reviews on Biomembranes* **2000,** *1469* (2), 63-77.

66. Sonnino, S.; Bassi, R.; Chigorno, V.; Tettamanti, G., Further studies on the changes of chicken brain gangliosides during prenatal and postnatal life. *J. Neurochem.* **1990,** *54* (5), 1653-1660.

67. van Echten-Deckert, G.; Walter, J., Sphingolipids: Critical players in Alzheimer's disease. *Prog. Lipid Res.* **2012,** *51* (4), 378-393.

68. Kracun, I.; Kalanj, S.; Talan-Hranilovic, J.; Cosovic, C., Cortical distribution of gangliosides in Alzheimer's disease. *Neurochem. Int.* **1992,** *20* (3), 433-438.

69. Katsel, P.; Li, C.; Haroutunian, V., Gene Expression Alterations in the Sphingolipid Metabolism Pathways during Progression of Dementia and Alzheimer's Disease: A Shift Toward Ceramide Accumulation at the Earliest Recognizable Stages of Alzheimer's Disease? *Neurochem. Res.* **2007,** *32* (4-5), 845-856.

70. Yanagisawa, K.; Odaka, A.; Suzuki, N.; Ihara, Y., GM1 ganglioside-bound amyloid β-protein (Aβ): A possible form of preamyloid in Alzheimer's disease. *Nat. Med.* **1995,** *1* (10), 1062-1066.

71. Mahfoud, R.; Garmy, N.; Maresca, M.; Yahi, N.; Puigserver, A.; Fantini, J., Identification of a Common Sphingolipid-binding Domain in Alzheimer, Prion, and HIV-1 Proteins. *J. Biol. Chem.* **2002,** *277* (13), 11292-11296.

72. Yang, Y.; Uhlig, S., The role of sphingolipids in respiratory disease. *Ther. Adv. Respir. Dis.* **2011,** *5* (5), 325-344.

73. Breslow, D. K.; Collins, S. R.; Bodenmiller, B.; Aebersold, R.; Simons, K.; Shevchenko, A.; Ejsing, C. S.; Weissman, J. S., Orm family proteins mediate sphingolipid homeostasis. *Nature* **2010,** *463* (7284), 1048-1053.

74. Moffatt, M. F.*, et al.*, Genetic variants regulating ORMDL3 expression contribute to the risk of childhood asthma. *Nature* **2007,** *448* (7152), 470-473.

75. Tafesse, F. G.; Holthuis, J. C. M., Cell biology: A brake on lipid synthesis. *Nature*\ **2010,** *463*\ (7284\), 1028\-1029\.

76. Snell, E. E.; Dimari, S. J.; Brady, R. N., Biosynthesis of sphingosine and dihydrosphingosine by cell-free systems from Hansenula ciferri. *Chem. Phys. Lipids* **1970,** *5* (1), 116-138.

77. Stoffel, W., Studies on the biosynthesis and degradation of sphingosine bases. *Chem. Phys. Lipids* **1970,** *5* (1), 139-158.

78. Williams, R. D.; Wang, E.; Merrill, A. H., Enzymology of long-chain base synthesis by liver: Characterization of serine palmitoyltransferase in rat liver microsomes. *Arch. Biochem. Biophys.* **1984,** *228* (1), 282-291.

79. Braun, P. E.; Morell, P.; Radin, N. S., Synthesis of C18- and C20-Dihydrosphingosines, Ketodihydrosphingosines, and Ceramides by Microsomal Preparations from Mouse Brain. *J. Biol. Chem.* **1970,** *245* (2), 335-341.

80. Kanfer, J.; Bates, S., Sphingolipid metabolism II. The biosynthesis of 3-keto-dihydrosphingosine by a partially-purified enzyme from rat brain. *Lipids* **1970,** *5* (8), 718-720.

81. Wells, G. B.; Lester, R. L., The isolation and characterization of a mutant strain of Saccharomyces cerevisiae that requires a long chain base for growth and for synthesis of phosphosphingolipids. *J. Biol. Chem.* **1983,** *258* (17), 10200-10203.

82. Nagiec, M. M.; Baltisberger, J. A.; Wells, G. B.; Lester, R. L.; Dickson, R. C., The LCB2 gene of Saccharomyces and the related LCB1 gene encode subunits of serine palmitoyltransferase, the initial enzyme in sphingolipid synthesis. *Proc. Natl. Acad. Sci. U.S.A.* **1994,** *91* (17), 7899-7902.

83. Buede, R.; Rinker-Schaffer, C.; Pinto, W. J.; Lester, R. L.; Dickson, R. C., Cloning and characterization of LCB1, a Saccharomyces gene required for biosynthesis of the long-chain base component of sphingolipids. *J. Bacteriol.* **1991,** *173* (14), 4325-4332.

84. Weiss, B.; Stoffel, W., Human and Murine Serine-Palmitoyl-CoA Transferase. *Eur. J. Biochem.* **1997,** *249* (1), 239-247.

85. Hanada, K.; Hara, T.; Fukasawa, M.; Yamaji, A.; Umeda, M.; Nishijima, M., Mammalian Cell Mutants Resistant to a Sphingomyelin-directed Cytolysin. *J. Biol. Chem.* **1998,** *273* (50), 33787-33794.

86. Yasuda, S.; Nishijima, M.; Hanada, K., Localization, Topology, and Function of the LCB1 Subunit of Serine Palmitoyltransferase in Mammalian Cells. *J. Biol. Chem.* **2003,** *278* (6), 4176-4183.

87. Chen, J. K.; Lane, W. S.; Schreiber, S. L., The identification of myriocin-binding proteins. *Chem. Biol.* **1999,** *6* (4), 221-235.

88. Hanada, K.; Hara, T.; Nishijima, M., Purification of the Serine Palmitoyltransferase Complex Responsible for Sphingoid Base Synthesis by Using Affinity Peptide Chromatography Techniques. *J. Biol. Chem.* **2000,** *275* (12), 8409-8415.

89. Roelants, F. M.; Breslow, D. K.; Muir, A.; Weissman, J. S.; Thorner, J., Protein kinase Ypk1 phosphorylates regulatory proteins Orm1 and Orm2 to control sphingolipid homeostasis in Saccharomyces cerevisiae. *Proc. Natl. Acad. Sci. U.S.A.* *108* (48), 19222-19227.

90. Gable, K.; Slife, H.; Bacikova, D.; Monaghan, E.; Dunn, T. M., Tsc3p Is an 80-Amino Acid Protein Associated with Serine Palmitoyltransferase and Required for Optimal Enzyme Activity. *J. Biol. Chem.* **2000,** *275* (11), 7597-7603.

91. Braun, P. E.; Snell, E. E., The biosynthesis of dihydrosphingosine in cell-free preparations of Hansenula ciferri. *Proc. Natl. Acad. Sci. U.S.A.* **1967,** *58* (1), 298-303.

92. Han, S.; Lone, M. A.; Schneiter, R.; Chang, A., Orm1 and Orm2 are conserved endoplasmic reticulum membrane proteins regulating lipid homeostasis and protein quality control. *Proc. Natl. Acad. Sci. U.S.A.* **2010,** *107* (13), 5851-5856.

93. Schuldiner, M.; Collins, S. R.; Thompson, N. J.; Denic, V.; Bhamidipati, A.; Punna, T.; Ihmels, J.; Andrews, B.; Boone, C.; Greenblatt, J. F.; Weissman, J. S.; Krogan, N. J., Exploration of the Function and Organization of the Yeast Early Secretory Pathway through an Epistatic Miniarray Profile. *Cell* **2005,** *123* (3), 507-519.

94. Siow, D. L.; Wattenberg, B. W., Mammalian ORMDL Proteins Mediate the Feedback Response in Ceramide Biosynthesis. *J. Biol. Chem.* **2012,** *287* (48), 40198-40204.

95. Harmon, J. M.; Bacikova, D.; Gable, K.; Gupta, S. D.; Han, G.; Sengupta, N.; Somashekarappa, N.; Dunn, T. M., Topological and Functional Characterization of the ssSPTs, Small Activating Subunits of Serine Palmitoyltransferase. *J. Biol. Chem.* **2013,** *288* (14), 10144-10153.

96. Olsen, I.; Jantzen, E., Sphingolipids in Bacteria and Fungi. *Anaerobe* **2001,** *7* (2), 103-112.

97. Stoffel, W.; Dittmar, K.; Wilmes, R., Sphingolipid metabolism in Bacteroideaceae. *Hoppe Seyler's Z. Physiol. Chem.* **1975,** *356* (6), 715-25.

98. Lev, M.; Milford, A. F., The 3-ketodihydrosphingosine synthetase of Bacteroides melaninogenicus: Partial purification and properties. *Arch. Biochem. Biophys.* **1981,** *212* (2), 424-431.

99. Ikushiro, H.; Hayashi, H.; Kagamiyama, H., A Water-soluble Homodimeric Serine Palmitoyltransferase from Sphingomonas paucimobilis EY2395T Strain. *J. Biol. Chem.* **2001,** *276* (21), 18249-18256.

100. Yard, B. A.; Carter, L. G.; Johnson, K. A.; Overton, I. M.; Dorward, M.; Liu, H.; McMahon, S. A.; Oke, M.; Puech, D.; Barton, G. J.; Naismith, J. H.; Campopiano, D. J., The Structure of Serine Palmitoyltransferase; Gateway to Sphingolipid Biosynthesis. *J. Mol. Biol.* **2007,** *370* (5), 870-886.

101. Webster, S. P.; Alexeev, D.; Campopiano, D. J.; Watt, R. M.; Alexeeva, M.; Sawyer, L.; Baxter, R. L., Mechanism of 8-Amino-7-oxononanoate Synthase: Spectroscopic, Kinetic, and Crystallographic Studies. *Biochemistry* **2000,** *39* (3), 516-528.

102. Schmidt, A.; Sivaraman, J.; Li, Y.; Larocque, R.; Barbosa, J. A. R. G.; Smith, C.; Matte, A.; Schrag, J. D.; Cygler, M., Three-Dimensional Structure of 2-Amino-3-ketobutyrate CoA Ligase from Escherichia coli Complexed with a PLP−Substrate Intermediate: Inferred Reaction Mechanism. *Biochemistry* **2001,** *40* (17), 5151-5160.

103. Astner, I.; Schulze, J. O.; van den Heuvel, J.; Jahn, D.; Schubert, W.-D.; Heinz, D. W., Crystal structure of 5-aminolevulinate synthase, the first enzyme of heme biosynthesis, and its link to XLSA in humans. *EMBO J.* **2005,** *24* (18), 3166-3177.

104. Beattie, A. E.; Gupta, S. D.; Frankova, L.; Kazlauskaite, A.; Harmon, J. M.; Dunn, T. M.; Campopiano, D. J., The pyridoxal 5'-phosphate (PLP)-dependent enzyme serine palmitoyltransferase (SPT): effects of the small subunits and insights from bacterial mimics of human hLCB2a HSAN1 mutations. *Biomed. Res. Int.* **2013,** *2013*, 194371.

105. Lowther, J.; Beattie, A. E.; Langridge-Smith, P. R. R.; Clarke, D. J.; Campopiano, D. J., L-Penicillamine is a mechanism-based inhibitor of serine palmitoyltransferase by forming a pyridoxal-5'-phosphate-thiazolidine adduct. *Med. Chem. Comm.* **2012,** *3* (8), 1003-1008.

106. Lowther, J.; Yard, B. A.; Johnson, K. A.; Carter, L. G.; Bhat, V. T.; Raman, M. C. C.; Clarke, D. J.; Ramakers, B.; McMahon, S. A.; Naismith, J. H.; Campopiano, D. J., Inhibition of the PLP-dependent enzyme serine

palmitoyltransferase by cycloserine: evidence for a novel decarboxylative mechanism of inactivation. *Molecular BioSystems* **2010,** *6* (9), 1682-1693.

107. Jeffrey, G. A., *An Introduction to Hydrogen Bonding*. Oxford University Press: 1997.

108. Wilson, W. H.; Schroeder, D. C.; Allen, M. J.; Holden, M. T. G.; Parkhill, J.; Barrell, B. G.; Churcher, C.; Hamlin, N.; Mungall, K.; Norbertczak, H.; Quail, M. A.; Price, C.; Rabbinowitsch, E.; Walker, D.; Craigon, M.; Roy, D.; Ghazal, P., Complete Genome Sequence and Lytic Phase Transcription Profile of a Coccolithovirus. *Science* **2005,** *309* (5737), 1090-1092.

109. Han, G.; Gable, K.; Yan, L.; Allen, M. J.; Wilson, W. H.; Moitra, P.; Harmon, J. M.; Dunn, T. M., Expression of a novel marine viral single-chain serine palmitoyltransferase and construction of yeast and mammalian single-chain chimera. *J. Biol. Chem.* **2006,** *281* (52), 39935-39942.

110. Zabin, I.; Mead, J. F., The Biosynthesis of Sphingosine. *J. Biol. Chem.* **1953,** *205* (1), 271-277.

111. Brady, R. O.; Koval, G. J., The Enzymatic Synthesis of Sphingosine. *J. Biol. Chem.* **1958,** *233* (1), 26-31.

112. Sprinson, D. B.; Coulon, A. e., The Precursors of Sphingosine in Brain Tissue. *J. Biol. Chem.* **1954,** *207* (2), 585-592.

113. Weiss, B., The Biosynthesis of Sphingosine: I. A Study of the Reacrtion with Tritium-Labelled Serine. *J. Biol. Chem.* **1963,** *238* (6), 1953-1959.

114. Krisnangkura, K.; Sweeley, C. C., Studies on the mechanism of 3-ketosphinganine synthetase. *J. Biol. Chem.* **1976,** *251* (6), 1597-602.

115. Ikushiro, H.; Fujii, S.; Shiraiwa, Y.; Hayashi, H., Acceleration of the Substrate Cα Deprotonation by an Analogue of the Second Substrate Palmitoyl-CoA in Serine Palmitoyltransferase. *J. Biol. Chem.* **2008,** *283* (12), 7542-7553.

116. Penno, A.; Reilly, M. M.; Houlden, H.; Laurá, M.; Rentsch, K.; Niederkofler, V.; Stoeckli, E. T.; Nicholson, G.; Eichler, F.; Brown, R. H.; von Eckardstein, A.; Hornemann, T., Hereditary Sensory Neuropathy Type 1 Is Caused by the Accumulation of Two Neurotoxic Sphingolipids. *J. Biol. Chem.* **2010,** *285* (15), 11178-11187.

117. Strettoi, E.; Gargini, C.; Novelli, E.; Sala, G.; Piano, I.; Gasco, P.; Ghidoni, R., Inhibition of ceramide biosynthesis preserves photoreceptor structure and function in a mouse model of retinitis pigmentosa. *Proc. Natl. Acad. Sci. U.S.A.* **2010,** *107* (43), 18706-18711.

118. Vercelli, D., Discovering susceptibility genes for asthma and allergy. *Nat. Rev. Immunol.* **2008,** *8* (3), 169-182.

119. Tatematsu, K.; Tanaka, Y.; Sugiyama, M.; Sudoh, M.; Mizokami, M., Host sphingolipid biosynthesis is a promising therapeutic target for the inhibition of hepatitis B virus replication. *J. Med. Virol.* **2011,** *83* (4), 587-593.

120. Amemiya, F.; Maekawa, S.; Itakura, Y.; Kanayama, A.; Matsui, A.; Takano, S.; Yamaguchi, T.; Itakura, J.; Kitamura, T.; Inoue, T.; Sakamoto, M.; Yamauchi, K.; Okada, S.; Yamashita, A.; Sakamoto, N.; Itoh, M.; Enomoto, N., Targeting Lipid Metabolism in the Treatment of Hepatitis C Virus Infection. *J. Infect. Dis.* **2008,** *197* (3), 361-370.

121. Ciesek, S.; Steinmann, E.; Manns, M. P.; Wedemeyer, H.; Pietschmann, T., The Suppressive Effect That Myriocin Has on Hepatitis C Virus RNA Replication Is Independent of Inhibition of Serine Palmitoyl Transferase. *J. Infect. Dis.* **2008,** *198* (7), 1091-1093.

122. Schiffmann, S.; Sandner, J.; Birod, K.; Wobst, I.; Angioni, C.; Ruckhäberle, E.; Kaufmann, M.; Ackermann, H.; Lötsch, J.; Schmidt, H.; Geisslinger, G.; Grösch, S., Ceramide synthases and ceramide levels are increased in breast cancer tissue. *Carcinogenesis* **2009,** *30* (5), 745-752.

123. Knapp, P.; Baranowski, M.; Knapp, M.; Zabielski, P.; Błachnio-Zabielska, A. U.; Górski, J., Altered sphingolipid metabolism in human endometrial cancer. *Prostaglandins & Other Lipid Mediators* **2010,** *92* (1–4), 62-66.

124. Lee, Y.-S.; Choi, K.-M.; Lee, S.; Sin, D.-M.; Yoo, K.-S.; Lim, Y.; Lee, Y.-M.; Hong, J.-T.; Yun, Y.-P.; Yoo, H.-S., Myriocin, a serine palmitoyltransferase inhibitor, suppresses tumor growth in a murine melanoma model by inhibiting de novo sphingolipid synthesis. *Cancer Biol. Ther.* **2012,** *13* (2), 92-100.

125. Schmitz-Peiffer, C., Targeting Ceramide Synthesis to Reverse Insulin Resistance. *Diabetes* **2010,** *59* (10), 2351-2353.

126. Schmitz-Peiffer, C.; Craig, D. L.; Biden, T. J., Ceramide Generation Is Sufficient to Account for the Inhibition of the Insulin-stimulated PKB Pathway in C2C12 Skeletal Muscle Cells Pretreated with Palmitate. *J. Biol. Chem.* **1999,** *274* (34), 24202-24210.

127. Holland, W. L.; Brozinick, J. T.; Wang, L.-P.; Hawkins, E. D.; Sargent, K. M.; Liu, Y.; Narra, K.; Hoehn, K. L.; Knotts, T. A.; Siesky, A.; Nelson, D. H.; Karathanasis, S. K.; Fontenot, Greg K.; Birnbaum, M. J.; Summers, S. A., Inhibition of Ceramide Synthesis Ameliorates Glucocorticoid-, Saturated-Fat-, and Obesity-Induced Insulin Resistance. *Cell Metabolism* **2007,** *5* (3), 167-179.

128. Yuyama, K.; Mitsutake, S.; Igarashi, Y., Pathological roles of ceramide and its metabolites in metabolic syndrome and Alzheimer's disease. *Biochim. Biophys. Acta - Molecular and Cell Biology of Lipids 1841* (5), 793–798.

129. Cheng, J.; Park, T. S.; Fischl, A. S.; Ye, X. S., Cell cycle progression and cell polarity require sphingolipid biosynthesis in Aspergillus nidulans. *Mol. Cell. Biol.* **2001,** *21* (18), 6198-6209.

130. Bolton, G. L.; Hutchings, R. H.; Kohrt, J. T.; Park, W. K. C.; Van, H. C. A. Inhibitors of serine palmitoyltransferase. WO2008084300, 2008.

131. Kossida, S. Regulation of human serine palmitoyltransferase. WO 2002048325, 2002.

132. Nestor, J. J. Compounds and methods of treating metabolic syndrome and inflammation. 20080139455, 2008.

133. Kobayashi, S.; Furuta, T.; Hayashi, T.; Nishijima, M.; Hanada, K., Catalytic Asymmetric Syntheses of Antifungal Sphingofungins and Their Biological Activity as Potent Inhibitors of Serine Palmitoyltransferase (SPT). *J. Am. Chem. Soc.* **1998,** *120* (5), 908-919.

134. VanMiddlesworth, F.; Giacobbe, R. A.; Lopez, M.; Garrity, G.; Bland, J. A.; Bartizal, K.; Fromtling, R. A.; Polishook, J.; Zweerink, M.; Edison, A. M.; et al., Sphingofungins A, B, C, and D; a new family of antifungal agents. I. Fermentation, isolation, and biological activity. *J. Antibiot.* **1992,** *45* (6), 861-867.

135. Zweerink, M. M.; Edison, A. M.; Wells, G. B.; Pinto, W.; Lester, R. L., Characterization of a novel, potent, and specific inhibitor of serine palmitoyltransferase. *J. Biol. Chem.* **1992,** *267* (35), 25032-25038.

136. Mandala, S. M.; Thornton, R. A.; Frommer, B. R.; Dreikorn, S.; Kurtz, M. B., Viridiofungins, novel inhibitors of sphingolipid synthesis. *J. Antibiot.* **1997,** *50* (4), 339-343.

137. Mandala, S. M.; Frommer, B. R.; Thornton, R. A.; Kurtz, M. B.; Young, N. M.; Cabello, M. A.; Genilloud, O.; Liesch, J. M.; Smith, J. L.; Horn, W. S., Inhibition of serine palmitoyl-transferase activity by lipoxamycin. *J. Antibiot.* **1994,** *47* (3), 376-379.

138. Kluepfel, D.; Bagli, J.; Baker, H.; Charest, M. P.; Kudelski, A., Myriocin, a new antifungal antibiotic from Myriococcum albomyces. *J. Antibiot.* **1972,** *25* (2), 109-115.

139. Aragozzini, F.; Manachini, P. L.; Craveri, R.; Rindone, B.; Scolastico, C., Isolation and structure determination of a new antifungal α-hydroxymethyl-α-amino acid. *Tetrahedron* **1972,** *28* (21), 5493-5498.

140. Bagli, J.; Kluepfel, D.; St.-Jacques, M., Elucidation of structure and stereochemistry of myriocin. Novel antifungal antibiotic. *J. Org. Chem.* **1973,** *38* (7), 1253-1260.

141. Destro, R.; Colombo, A., Crystal structure and relative configuration of the N-acetyl-[gamma]-lactone of the antifungal antibiotic thermozymocidin. *J. Chem. Soc., Perkin Trans. 2* **1979,** (7), 896-899.

142. Banfi, L.; Beretta, M. G.; Colombo, L.; Gennari, C.; Scolastico, C., Total synthesis of (+)-thermozymocidin (myriocin) from D-fructose. *J. Chem. Soc., Chem. Commun.* **1982,** (9), 488-490.

143. Jones, M. C.; Marsden, S. P., Total Synthesis of the Immunosuppressants Myriocin and 2-epi-Myriocin. *Org. Lett.* **2008,** *10* (18), 4125-4128.

144. Fujita, T.; Inoue, K.; Yamamoto, S.; Ikumoto, T.; Sasaki, S.; Toyama, R.; Chiba, K.; Hoshino, Y.; Okumoto, T., Fungal metabolites. Part 11. A potent immunosuppressive activity found in Isaria sinclairii metabolite. *J. Antibiot.* **1994,** *47* (2), 208-215.

145. Miyake, Y.; Kozutsumi, Y.; Nakamura, S.; Fujita, T.; Kawasaki, T., Serine Palmitoyltransferase Is the Primary Target of a Sphingosine-like Immunosuppressant, ISP-1/Myriocin. *Biochem. Biophys. Res. Commun.* **1995,** *211* (2), 396-403.

146. Fujita, T.; Inoue, K.; Yamamoto, S.; Ikumoto, T.; Sasaki, S.; Toyama, R.; Yoneta, M.; Chiba, K.; Hoshino, Y.; Okumoto, T., Fungal metabolites. Part 12. Potent immunosuppressant, 14-deoxomyriocin, (2S,3R,4R)-(E)-2-amino-3,4-dihydroxy-2-hydroxymethyleicos-6-enoic acid and structure-activity relationships of myriocin derivatives. *J. Antibiot.* **1994,** *47* (2), 216-224.

147. Strader, C. R.; Pearce, C. J.; Oberlies, N. H., Fingolimod (FTY720): A Recently Approved Multiple Sclerosis Drug Based on a Fungal Secondary Metabolite. *J. Nat. Prod.* **2011,** *74* (4), 900-907.

148. Adachi, K.; Kohara, T.; Nakao, N.; Arita, M.; Chiba, K.; Mishina, T.; Sasaki, S.; Fujita, T., Design, synthesis, and structure-activity relationships of 2-substituted-2-amino-1,3-propanediols: Discovery of a novel immunosuppressant, FTY720. *Bioorg. Med. Chem. Lett.* **1995,** *5* (8), 853-856.

149. Paugh, S. W.; Payne, S. G.; Barbour, S. E.; Milstien, S.; Spiegel, S., The immunosuppressant FTY720 is phosphorylated by sphingosine kinase type 2. *FEBS Lett.* **2003,** *554* (1–2), 189-193.

150. Hanada, K.; Nishijima, M.; Fujita, T.; Kobayashi, S., Specificity of inhibitors of serine palmitoyltransferase (SPT), a key enzyme in sphingolipid biosynthesis, in intact cells: A novel evaluation system using an SPT-defective mammalian cell mutant. *Biochem. Pharmacol.* **2000,** *59* (10), 1211-1216.

151. Medlock, K. A.; Merrill, A. H., Inhibition of serine palmitoyltransferase in vitro and long-chain base biosynthesis in intact Chinese hamster ovary cells by β-chloroalanine. *Biochemistry* **1988,** *27* (18), 7079-7084.

152. Liu, H.; Naismith, J., An efficient one-step site-directed deletion, insertion, single and multiple-site plasmid mutagenesis protocol. *BMC Biotechnol.* **2008,** *8* (1), 1-10.

153. Smith, P. K.; Krohn, R. I.; Hermanson, G. T.; Mallia, A. K.; Gartner, F. H.; Provenzano, M. D.; Fujimoto, E. K.; Goeke, N. M.; Olson, B. J.; Klenk, D. C., Measurement of protein using bicinchoninic acid. *Anal. Biochem.* **1985,** *150* (1), 76-85.

154. Winter, G., xia2: an expert system for macromolecular crystallography data reduction. *J. Appl. Crystallogr.* **2010,** *43* (1), 186-190.

155. McCoy, A. J.; Grosse-Kunstleve, R. W.; Adams, P. D.; Winn, M. D.; Storoni, L. C.; Read, R. J., Phaser crystallographic software. *J. Appl. Crystallogr.* **2007,** *40* (Pt 4), 658-674.

156. Schuttelkopf, A. W.; van Aalten, D. M. F., PRODRG: a tool for high-throughput crystallography of protein-ligand complexes. *Acta Crystallographica Section D* **2004,** *60* (8), 1355-1363.

157. Winn, M. D.; Isupov, M. N.; Murshudov, G. N., Use of TLS parameters to model anisotropic displacements in macromolecular refinement. *Acta Crystallogr. Sect. D* **2001,** *57* (Pt 1), 122-133.

158. Emsley, P.; Cowtan, K., Coot: model-building tools for molecular graphics. *Acta crystallographica. Section D, Biological crystallography* **2004,** *60* (Pt 12 Pt 1), 2126-2132.

159. Davis, I. W.; Leaver-Fay, A.; Chen, V. B.; Block, J. N.; Kapral, G. J.; Wang, X.; Murray, L. W.; Arendall, W. B., 3rd; Snoeyink, J.; Richardson, J. S.; Richardson, D. C., MolProbity: all-atom contacts and structure validation for proteins and nucleic acids. *Nucleic Acids Res.* **2007,** *35* (Web Server issue), W375-W383.

160. Geoghegan, K. F.; Dixon, H. B. F.; Rosner, P. J.; Hoth, L. R.; Lanzetti, A. J.; Borzilleri, K. A.; Marr, E. S.; Pezzullo, L. H.; Martin, L. B.; LeMotte, P. K.; McColl, A. S.; Kamath, A. V.; Stroh, J. G., Spontaneous α-N-6-Phosphogluconoylation of a "His Tag" in Escherichia coli:The Cause of Extra Mass of 258 or 178 Da in Fusion Proteins. *Anal. Biochem.* **1999,** *267* (1), 169-184.

161. Ikushiro, H.; Islam, M. M.; Tojo, H.; Hayashi, H., Molecular Characterization of Membrane-Associated Soluble Serine Palmitoyltransferases from Sphingobacterium multivorum and Bdellovibrio stolpii. *J. Bacteriol.* **2007,** *189* (15), 5749-5761.

162. Ikushiro, H.; Hayashi, H.; Kagamiyama, H., Reactions of Serine Palmitoyltransferase with Serine and Molecular Mechanisms of the Actions of Serine Derivatives as Inhibitors. . *Biochemistry* **2004,** *43* (4), 1082-1092.

163. Copeland, R. A., *Enzymes: A Practical Introduction to Structure, Mechanism, and Data Analysis*. Wiley: 2004.

164. Cha, S.; Agarwal, R. P.; Parks Jr, R. E., Tight-binding inhibitors—II: Non-steady state nature of inhibition of milk xanthine oxidase by allopurinol and alloxanthine and of human erythrocytic adenosine deaminase by coformycin. *Biochem. Pharmacol.* **1975,** *24* (23), 2187-2197.

165. Hanada, K.; Hara, T.; Nishijima, M., D-Serine inhibits serine palmitoyltransferase, the enzyme catalyzing the initial step of sphingolipid biosynthesis. *FEBS Lett.* **2000,** *474* (1), 63-65.

166. Jahan, N.; Potter, J. A.; Sheikh, M. A.; Botting, C. H.; Shirran, S. L.; Westwood, N. J.; Taylor, G. L., Insights into the Biosynthesis of the Vibrio cholerae Major Autoinducer CAI-1 from the Crystal Structure of the PLP-Dependent Enzyme CqsA. *J. Mol. Biol.* **2009,** *392* (3), 763-773.

167. Kelly, R. C.; Bolitho, M. E.; Higgins, D. A.; Lu, W.; Ng, W.-L.; Jeffrey, P. D.; Rabinowitz, J. D.; Semmelhack, M. F.; Hughson, F. M.; Bassler, B. L., The Vibrio cholerae quorum-sensing autoinducer CAI-1: analysis of the biosynthetic enzyme CqsA. *Nat. Chem. Biol.* **2009,** *5* (12), 891-895.

168. Berdyshev, E. V., Mass spectrometry of fatty aldehydes. *Biochim. Biophys. Acta - Molecular and Cell Biology of Lipids* **2011,** *1811* (11), 680-693.

169. Berdyshev, E. V.; Goya, J.; Gorshkova, I.; Prestwich, G. D.; Byun, H.-S.; Bittman, R.; Natarajan, V., Characterization of sphingosine-1-phosphate lyase activity by electrospray ionization–liquid chromatography/tandem mass spectrometry quantitation of (2E)-hexadecenal. *Anal. Biochem.* **2011,** *408* (1), 12-18.

170. Girard, A., Betaine Hydrazide Hydrochloride. *Org. Synth.* **1938,** *18*, 10.

171. Kim, Y.-G.; Harvey, D. J.; Yang, Y.-H.; Park, C.-G.; Kim, B.-G., Mass spectrometric analysis of the glycosphingolipid-derived glycans from miniature pig endothelial cells and islets: identification of NeuGc epitope in pig islets. *J. Mass Spectrom.* **2009,** *44* (10), 1489-1499.

172. Lowther, J.; Charmier, G.; Raman, M. C.; Ikushiro, H.; Hayashi, H.; Campopiano, D. J., Role of a conserved arginine residue during catalysis in serine palmitoyltransferase. *FEBS Lett.* **2011,** *585* (12), 1729-1734.

173. Kiuchi, M.; Adachi, K.; Kohara, T.; Minoguchi, M.; Hanano, T.; Aoki, Y.; Mishina, T.; Arita, M.; Nakao, N.; Ohtsuki, M.; Hoshino, Y.; Teshima, K.; Chiba, K.; Sasaki, S.; Fujita, T., Synthesis and Immunosuppressive Activity of 2-Substituted

2-Aminopropane-1,3-diols and 2-Aminoethanols1,2. *J. Med. Chem.* **2000,** *43* (15), 2946-2961.

174. Delgado, A.; Casas, J.; Llebaria, A.; Abad, J. L.; Fabrias, G., Inhibitors of sphingolipid metabolism enzymes. *Biochim. Biophys. Acta - Biomembranes* **2006,** *1758* (12), 1957-1977.

175. Raman, M. C. C.; Johnson, K. A.; Clarke, D. J.; Naismith, J. H.; Campopiano, D. J., The serine palmitoyltransferase from Sphingomonas wittichii RW1: An interesting link to an unusual acyl carrier protein. *Biopolymers 93* (9), 811-822.

176. Gerber, R.; Lou, L.; Du, L., A PLP-Dependent Polyketide Chain Releasing Mechanism in the Biosynthesis of Mycotoxin Fumonisins in Fusarium verticillioides. *J. Am. Chem. Soc.* **2009,** *131* (9), 3148-3149.

177. Zhang, J.; Cheltsov, A. V.; Ferreira, G. C., Conversion of 5-aminolevulinate synthase into a more active enzyme by linking the two subunits: Spectroscopic and kinetic properties. *Protein Sci.* **2005,** *14* (5), 1190-1200.

178. Turbeville, T. D.; Zhang, J.; Adams, W. C.; Hunter, G. A.; Ferreira, G. C., Functional asymmetry for the active sites of linked 5-aminolevulinate synthase and 8-amino-7-oxononanoate synthase. *Arch. Biochem. Biophys.* **2011,** *511* (1-2), 107-117.

179. Wittung-Stafshede, P., Role of Cofactors in Protein Folding. *Acc. Chem. Res.* **2002,** *35* (4), 201-208.

180. Wieland Brown, L. C.; Penaranda, C.; Kashyap, P. C.; Williams, B. B.; Clardy, J.; Kronenberg, M.; Sonnenburg, J. L.; Comstock, L. E.; Bluestone, J. A.; Fischbach, M. A., Production of alpha-galactosylceramide by a prominent member of the human gut microbiota. *PLoS biology* **2013,** *11* (7), e1001610.

Appendix 1

Gene sequence of spSPT as published by Ikushiro[99]

```
  ATGACCGAAG CCGCCGCTCA GCCCCACGCC CTCCCCGCCG ACGCGCCCGA
51 CATCGCGCCG GAACGCGACC TGCTCTCCAA GTTCGACGGC CTGATCGCCG
101 AGCGGCAGAA GCTGCTCGAC TCCGGCGTCA CCGATCCCTT CGCGATCGTG
151 ATGGAACAGG TGAAGTCGCC GACCGAGGCC GTGATCCGTG GCAAGGACAC
201 GATCCTGCTC GGCACGTACA ACTATATGGG CATGACCTTC GATCCGGACG
251 TGATCGCAGC GGGCAAGGAA GCGCTGGAGA AGTTCGGGTC GGGCACCAAT
301 GGCAGCCGGA TGCTCAACGG CACCTTCCAC GACCATATGG AAGTCGAACA
351 GGCGCTGCGC GATTTCTACG GCACGACCGG CGCGATCGTC TTTTCGACCG
401 GTTACATGGC CAATCTCGGC ATCATCTCAA CGCTGGCGGG CAAGGGTGAG
451 TATGTCATCC TCGACGCCGA CAGCCATGCG TCGATCTATG ACGGCTGCCA
501 GCAGGGCAAT GCCGAGATCG TCCGCTTCCG CCACAATTCG GCTGAGGATC
551 TCGACAAGCG GCTGGGCCGT CTGCCCAAGG AACCTGCCAA GCTGGTCGTG
601 CTGGAGGGCG TCTATTCGAT GCTCGGCGAC ATCGCTCCGC TGAAGGAGAT
651 GGTCGCGGTC GCCAAGAAGC ATGGCGCAAT GGTCTTGGTC GACGAAGCGC
701 ATTCGATGGG CTTTTTCGGC CCCAACGGGC GCGGCGTGTA CGAGGCGCAA
751 GGGTTGGAAG GCCAGATCGA TTTCGTCGTC GGCACCTTCT CCAAATCGGT
801 CGGCACAGTC GGCGGCTTCG TCGTGTCCFF TCATCCGAAG TTCGAGGCGG
851 TCCGCCTCGC CTGCCGTCCG TACATCTTCA CCGCCTCGCT GCCGCCCTCG
901 GTGGTAGCGA CCGCGACGAC GTCGATCCGC AAGCTGATGA CCGCGCATGA
951 AAAGCGTGAG CGGCTGTGGT CGAATGCCCG CGCGTTGCAT GGCGGGCTGA
1001 AGGCGATGGG CTTCAGGCTC GGCACCGAGA CCTGCGACAG CGCGATCGTC
1051 GCGGTCATGC TGGAGGATCA GGAACAGGCC GCGATGATGT GGCAGGCGCT
1101 GCTCGACGGC GGGCTCTACG TCAACATGGC GCGCCCGCCC GCGACCCCGG
1151 CCGGCACCTT CCTGCTGCGC TGCTCCATCT GTGCCGAGCA CACGCCGGCG
1201 CAGATCCAGA CCGTGCTGGG CATGTTCCAG GCCGCGGGCC GCGCGGTCGG
1251 CGTCATCGGC
```

Amino acid sequence of spSPT as published by Ikushiro[99]

```
  MTEAAAQPHA LPADAPDIAP ERDLLSKFDG LIAERQKLLD SGVTDPFAIV
51 MEQVKSPTEA VIRGKDTILL GTYNYMGMTF DPDVIAAGKE ALEKFGSGTN
101 GSRMLNGTFH DHMEVEQALR DFYGTTGAIV FSTGYMANLG IISTLAGKGE
151 YVILDADSHA SIYDGCQQGN AEIVRFRHNS VEDLDKRLGR LPKEPAKLVV
201 LEGVYSMLGD IAPLKEMVAV AKKHGAMVLV DEAHSMGFFG PNGRGVYEAQ
251 GLEGQIDFVV GTFSKSVGTV GGFVVSNHPK FEAVRLACRP YIFTASLPPS
301 VVATATTSIR KLMTAHEKRR ERLWSNARAL HGGLKAMGFR LTETCDSAIV
351 AVMLEDQEQA AMMWQALLDG GLYVNMARPP ATPAGTFLLR CSICAEHTPA
401 QIQTVLGMFQ AAGRAVGVIG
```

MW = 45140
ε = 24780

Gene sequence of spSPT

```
   ATGACCGAAG CCGCCGCTCA GCCCCACGCC CTCCCCGCCG ACGCGCCCGA
 51 CATCGCGCCG GAACGCGACC TGCTCTCCAA GTTCGACGGC CTGATCGCCG
101 AGCGGCAGAA GCTGCTCGAC TCCGGCGTCA CCGATCCCTT CGCGATCGTG
151 ATGGAACAGG TGAAGTCGCC GACCGAGGCC GTGATCCGTG GCAAGGACAC
201 GATCCTGCTC GGCACGTACA ACTATATGGG CATGACCTTC GATCCGGACG
251 TGATCGCAGC GGGCAAGGAA GCGCTGGAGA AGTTCGGGTC GGGCACCAAT
301 GGCAGCCGGA TGCTCAACGG CACCTTCCAC GACCATATGG AAGTCGAACA
351 GGCGCTGCGC GATTTCTACG GCACGACCGG CGCGATCGTC TTTTCGACCG
401 GTTACATGGC CAATCTCGGC ATCATCTCAA CGCTGGCGGG CAAGGGTGAG
451 TATGTCATCC TCGACGCCGA CAGCCATGCG TCGATCTATG ACGGCTGCCA
501 GCAGGGCAAT GCCGAGATCG TCCGCTTCCG CCACAATTCG GTCGAGGATC
551 TCGACAAGCG GCTGGGCCGT CTGCCCAAGG AACCTGCCAA GCTGGTCGTG
601 CTGGAGGGCG TCTATTCGAT GCTCGGCGAC ATCGCTCCGC TGAAGGAGAT
651 GGTCGCGGTC GCCAAGAAGC ATGGCGCAAT GGTCTTGGTC GACGAAGCGC
701 ATTCGATGGG CTTTTTCGGC CCCAACGGGC GCGGCGTGTA CGAGGCGCAA
751 GGGTTGGAAG GCCAGATCGA TTTCGTCGTC GGCACCTTCT CCAAATCGGT
801 CGGCACAGTC GGCGGCTTCG TCGTGTCCAA TCATCCGAAG TTCGAGGCGG
851 TCCGCCTCGC CTGCCGTCCG TACATCTTCA CCGCCTCGCT GCCGCCCTCG
901 GTGGTAGCGA CCGCGACGAC GTCGATCCGC AAGCTGATGA CCGCGCATGA
951 AAAGCGTGAG CGGCTGTGGT CGAATGCCCG CGCGTTGCAT GGCGGGCTGA
1001AGGCGATGGG CTTCAGGCTC GGCACCGAGA CCTGCGACAG CGCGATCGTC
1051GCGGTCATGC TGGAGGATCA GGAACAGGCC GCGATGATGT GGCAGGCGCT
1101GCTCGACGGC GGGCTCTACG TCAACATGGC GCGCCCGCCC GCGACCCCGG
1151CCGGCACCTT CCTGCTGCGC TGCTCCATCT GTGCCGAGCA CACGCCGGCG
1201CAGATCCAGA CCGTGCTGGG CATGTTCCAG GCCGCGGGCC GCGCGGTCGG
1251CGTCATCGGC CTCGAGCACC ACCACCACCA CCAC
```

Amino acid sequence of spSPT

```
  MTEAAAQPHA LPADAPDIAP ERDLLSKFDG LIAERQKLLD SGVTDPFAIV
 51 MEQVKSPTEA VIRGKDTILL GTYNYMGMTF DPDVIAAGKE ALEKFGSGTN
101GSRMLNGTFH DHMEVEQALR DFYGTTGAIV FSTGYMANLG IISTLAGKGE
151YVILDADSHA SIYDGCQQGN AEIVRFRHNS VEDLDKRLGR LPKEPAKLVV
201LEGVYSMLGD IAPLKEMVAV AKKHGAMVLV DEAHSMGFFG PNGRGVYEAQ
251GLEGQIDFVV GTFSKSVGTV GGFVVSNHPK FEAVRLACRP YIFTASLPPS
301VVATATTSIR KLMTAHEKRE RLWSNARALH GGLKAMGFRL GTETCDSAIV
351AVMLEDQEQA AMMWQALLDG GLYVNMARPP ATPAGTFLLR CSICAEHTPA
401QIQTVLGMFQ AAGRAVGVIG LEHHHHHH
```

MW = 46104 Da
ε = 24780

Gene sequence of AmSPT

```
   ATGGGCAGCA GCCATCATCA TCATCATCAC AGCAGCGGCC TGGTGCCGCG
  51 CGGCAGCCAT ATGGCTAGCA CAGAGGCTGC CGCTCAGCCG CACGCCCTGC
 101 CTGCAGACGC GCCTGACATT GCTCCTGAAC GTGATTTGTT AAGTAAATTT
 151 GATGGCCTAA TCGCCGAAAG ACAAAAACTA CTCGATTCAG GTGTAACAGA
 201 TCCTTTTGCC ATCGTTATGG AGCAAGTTAA GTCTCCAACT GAAGCTGTGA
 251 TACGAGGAAA AGATACAATC CTGCTCGGAA CTTATAATTA CATGGGAATG
 301 ACCTTTGATC CGGACGTAAT TGCAGCAGGT AAGGAAGCAT TGGAGAAATT
 351 TGGTAGCGGT ACTAATGGTA GCAGAATGCT GAACGGGACC TTTCATGATC
 401 ATATGGAAGT TGAACAAGCC TTGCGTGATT TCTACGGTAC GACGGGAGCT
 451 ATTGTCTTTT CAACTGGTTA CATGGCAAAC CTTGGAATCA TATCAACACT
 501 TGCGGGTAAA GGTGAGTATG TTATTTTGGA TGCAGACTCT CATGCTTCTA
 551 TCTACGATGG CTGTCAACAA GGAAACGCGG AAATCGTAAG ATTCCGGCAC
 601 AACTCAGTGG AGGATCTTGA TAAGAGACTT GGTAGGCTTC CAAAGGAACC
 651 AGCTAAACTC GTTGTTTTGG AAGGCGTTTA TTCGATGCTT GGTGATATTG
 701 CTCCTCTCAA GGAGATGGTT GCTGTGGCCA AGAAGCATGG AGCCATGGTG
 751 CTTGTCGACG AGGCACATTC TATGGGCTTC TTCGGACCAA ATGGTAGAGG
 801 AGTGTACGAA GCTCAGGGAC TCGAAGGACA GATAGACTTC GTCGTCGGCA
 851 CTTTCTCTAA GTCTGTTGGA ACTGTTGGCG GGTTTGTTGT GAGCAATCAT
 901 CCAAAATTCG AGGCGGTGAG GTTAGCTTGT AGGCCATATA TATTCACCGC
 951 TAGTTTGCCC CCGAGTGTCG TAGCTACAGC TACCACATCT ATACGAAAAC
1001 TTATGACAGC GCACGAGAAA CGGGAGAGAT TATGGTCTAA TGCAAGAGCA
1051 CTGCATGGAG GGCTTAAGGC TATGGGGTTT AGGTTAGGAA CGGAGACTTG
1101 CGACTCCGCT ATTGTAGCTG TGATGCTTGA GGATCAGGAA CAAGCTGCTA
1151 TGATGTGGCA GGCCTTGTTA GATGGTGGAC TATATGTTAA CATGGCAAGA
1201 CCTCCTGCAA CCCCTGCTGG TACGTTTCTC CTACGTTGTT CCATTTGCGC
1251 TGAACACACT CCCGCACAAA TCCAGACTGT TTTGGGGATG TTTCAAGCTG
1301 CGGGACGCGC AGTCGGGGTT ATTGGT
```

Amino acid sequence of AmSPT

```
  MGSSHHHHHH SSGLVPRGSH MASTEAAAQP HALPADAPDI APERDLLSKF
 51 DGLIAERQKL LDSGVTDPFA IVMEQVKSPT EAVIRGKDTI LLGTYNYMGM
101 TFDPDVIAAG KEALEKFGSG TNGSRMLNGT FHDHMEVEQA LRDFYGTTGA
151 IVFSTGYMAN LGIISTLAGK GEYVILDADS HASIYDGCQQ GNAEIVRFRH
201 NSVEDLDKRL GRLPKEPAKL VVLEGVYSML GDIAPLKEMV AVAKKHGAMV
251 LVDEAHSMGF FGPNGRGVYE AQGLEGQIDF VVGTFSKSVG TVGGFVVSNH
301 PKFEAVRLAC RPYIFTASLP PSVVATATTS IRKLMTAHEK RERLWSNARA
351 LHGGLKAMGF RLGTETCDSA IVAVMLEDQE QAAMMWQALL DGGLYVNMAR
401 PPATPAGTFL LRCSICAEHT PAQIQTVLGM FQAAGRAVGV IG
```

MW = 47363
ε = 24780

Gene sequence of Δ21 spSPT

```
  ATGGCACGCG ACGTGCTCTC CAAGTTCGAC GGCCTGATCG CCGAGCGGCA
 50 GAAGCTGCTC GACTCCGGCG TCACCGATCC CTTCGCGATC GTGATGGAAC
101 AGGTGAAGTC GCCGACCGAG GCCGTGATCC GTGGCAAGGA CACGATCCTG
151 CTCGGCACGT ACAACTATAT GGGCATGACC TTCGATCCGG ACGTGATCGC
201 AGCGGGCAAG GAAGCGCTGG AGAAGTTCGG GTCGGGCACC AATGGCAGCC
251 GGATGCTCAA CGGCACCTTC CACGACCATA TGGAAGTCGA ACAGGCGCTG
301 CGCGATTTCT ACGGCACGAC CGGCGCGATC GTCTTTTCGA CCGGTTACAT
351 GGCCAATCTC GGCATCATCT CAACGCTGGC GGGCAAGGGT GAGTATGTCA
401 TCCTCGACGC CGACAGCCAT GCGTCGATCT ATGACGGCTG CCAGCAGGGC
451 AATGCCGAGA TCGTCCGCTT CCGCCACAAT TCGGTCGAGG ATCTCGACAA
501 GCGGCTGGGC CGTCTGCCCA AGGAACCTGC CAAGCTGGTC GTGCTGGAGG
551 GCGTCTATTC GATGCTCGGC GACATCGCTC CGCTGAAGGA GATGGTCGCG
601 GTCGCCAAGA AGCATGGCGC AATGGTCTTG GTCGACGAAG CGCATTCGAT
651 GGGCTTTTTC GGCCCCAACG GGCGCGGCGT GTACGAGGCG CAAGGGTTGG
701 AAGGCCAGAT CGATTTCGTC GTCGGCACCT TCTCCAAATC GGTCGGCACA
751 GTCGGCGGCT TCGTCGTGTC CAATCATCCG AAGTTCGAGG CGGTCCGCCT
801 CGCCTGCCGT CCGTACATCT TCACCGCCTC GCTGCCGCCC TCGGTGGTAG
851 CGACCGCGAC GACGTCGATC CGCAAGCTGA TGACCGCGCA TGAAAAGCGT
901 GAGCGGCTGT GGTCGAATGC CCGCGCGTTG CATGGCGGGC TGAAGGCGAT
951 GGGCTTCAGG CTCGGCACCG AGACCTGCGA CAGCGCGATC GTCGCGGTCA
1001 TGCAGGAGGA TCAGGAACAG GCCGCGATGA TGTGGCAGGC GCTGCTCGAC
1051 GGCGGGCTCT ACGTCAACAT GGCGCGCCCG CCCGCGACCC CGGCCGGCAC
1101 CTTCCTGCTG CGCTGCTCCA TCTGTGCCGA GCACACGCCG GCGCAGATCC
1151 AGACCGTGCT GGGCATGTTC CAGGCCGCGG GCCGCGCGGT CGGCGTCATC
1201 GGCCTCGAGC ACCACCACCA CCACCAC
```

Amino acid sequence of Δ21 spSPT

```
  MARDVLSKFD GLIAERQKLL DSGVTDPFAI VMEQVKSPTE AVIRGKDTIL
 51 LGTYNYMGMT FDPDVIAAGK EALEKFGSGT NGSRMLNGTF HDHMEVEQAL
101 RDFYGTTGAI VFSTGYMANL GIISTLAGKG EYVILDADSH ASIYDGCQQG
151 NAEIVRFRHN SVEDLDKRLG RLPKEPAKLV VLEGVYSMLG DIAPLKEMVA
201 VAKKHGAMVL VDEAHSMGFF GPNGRGVYEA QGLEGQIDFV VGTFSKSVGT
251 VGGFVVSNHP KFEAVRLACR PYIFTASLPP SVVATATTSI RKLMTAHEKR
301 ERLWSNARAL HGGLKAMGFR LGTETCDSAI VAVMQEDQEQ AAMMWQALLD
351 GGLYVNMARP PATPAGTFLL RCSICAEHTP AQIQTVLGMF QAAGRAVGVI
401 GLEHHHHHH
```

Amino acids highlighted in yellow are different from spSPT.

MW = 44211 Da
ε = 26150

Gene sequence of x4M SPT fusion

```
   ATGGGATCCG AGGCTGCCGC TCAGCCGCAC GCCCTGCCTG CAGACGCGCC
51 TGACATTGCT CCTGAACGTG ATTTGTTAAG TAAATTTGAT GGCCTAATCG
101 CCGAAAGACA AAAACTACTC GATTCAGGTG TAACAGATCC TTTTGCCATC
151 GTTATGGAGC AAGTTAAGTC TCCAACTGAA GCTGTGATAC GAGGAAAAGA
201 TACAATCCTG CTCGGAACTT ATAATTACAT GGGAATGACC TTTGATCCGG
251 ACGTAATTGC AGCAGGTAAG GAAGCATTGG AGAAATTTGG TTCGGGAACT
301 AATGGTAGCA GAATGCTGAA CGGGACCTTT CATGATCATA TGGAAGTTGA
351 ACAAGCCTTG CGTGATTTCT ACGGTACGAC GGGAGCTATT GTCTTTTCAA
401 CTGGTTACAT GGCAAACCTT GGAATCATAT CAACACTTGC GGGTAAAGGT
451 GAGTATGTTA TTTTGGATGC AGACTCTCAT GCTTCTATCT ACGATGGCTG
501 TCAACAAGGA AACGCGGAAA TCGTAAGATT CCGGCACAAC TCAGTGGAGG
551 ATCTTGATAA GAGACTTGGT AGGCTTCCAA AGGAACCAGC TAAACTCGTT
601 GTTTTGGAAG GCGTTTATTC GATGCTTGGT GATATTGCTC CTCTCAAGGA
651 GATGGTTGCT GTGGCCAAGA AGCATGGAGC CATGGTGCTT GTCGACGAGG
701 CACATTCTAT GGGCTTCTTC GGACCAAATG GTAGAGGAGT GTACGAAGCT
751 CAGGGACTCG AAGGACAGAT AGACTTCGTC GTCGGCACTT TCTCTAAGTC
801 TGTTGGAACT GTTGGCGGGT TTGTTGTGAG CAATCATCCA AAATTCGAGG
851 CGGTGAGGTT AGCTTGTAGG CCATATATAT TCACCGCTAG TTTGCCCCCG
901 AGTGTCGTAG CTACAGCTAC CACATCTATA CGAAAACTTA TGACAGCGCA
951 CGAGAAACGG GAGAGATTAT GGTCTAATGC AAGAGCACTG CATGGAGGGC
1001 TTAAGGCTAT GGGGTTTAGG TTAGGAACGG AGACTTGCGA CTCCGCTATT
1051 GTAGCTGTGA TGCTTGAGGA TCAGGAACAA GCTGCTATGA TGTGGCAGGC
1101 CTTGTTAGAT GGTGGACTAT ATGTTAACAT GGCAAGACCT CCTGCAACCC
1151 CTGCTGGTAC GTTTCTCCTA CGTTGTTCCA TTTGCGCTGA ACACACTCCC
1201 GCACAAATCC AGACTGTTTT GGGGATGTTT CAAGCTGCGG GACGCGCAGT
1251 CGGGGTTATT GGTGCTAGCG AAAACCTGTA TTTTCAGGGC ACCGAAGCCG
1301 CCGCTCAGCC CCACGCCCTC CCCGCCGACG CGCCCGACAT CGCGCCGGAA
1351 CGCGACCTGC TCTCCAAGTT CGACGGCCTG ATCGCCGAGC GGCAGAAGCT
1401 GCTCGACTCC GGCGTCACCG ATCCCTTCGC GATCGTGATG GAACAGGTGA
1451 VAGTCGCCGA CCGAGGCCGT GATCCGTGGC AAGGACACGA TCCTGCTCGG
1501 CACGTACAAC TATATGGGCA TGACCTTCGA TCCGGACGTG ATCGCAGCGG
1551 GCAAGGAAGC GCTGGAGAAG TTCGGGTCGG GCACCAATGG CAGCCGGATG
1601 CTCAACGGCA CCTTCCACGA CCATATGGAA GTCGAACAGG CGCTGCGCGA
1651 TTTCTACGGC ACGACCGGCG CGATCGTCTT TTCGACCGGT TACATGGCCA
1701 ATCTCGGCAT CATCTCAACG CTGGCGGGCA AGGGTGAGTA TGTCATCCTC
1751 GACGCCGACA GCTGTGCGTC GATCTATGAC GGCTGCCAGC AGGGCAATGC
1801 CGAGATCGTC CGCTTCCGCC ACAATTCGGT CGAGGATCTC GACAAGCGGC
1851 TGGGCCGTCT GCCCAAGGAA CCTGCCAAGC TGGTCGTGCT GGAGGGCGTC
1901 TATTCGATGC TCGGCGACAT CGCTCCGCTG AAGGAGATGG TCGCGGTCGC
1951 CAAGAAGCAT GGCGCAATGG TCTTGGTCGA AGAAGCGCTT TCGATGGGCT
2001 TTTTCGGCCC CAACGGGCGC GGCGTGTACG AGGCGCAAGG GTTGGAAGGC
2051 CAGATCGATT TCGTCGTCGG CACCTTCTCC AACTCGGTCG GCACAGTCGG
2101 CGGCTTCGTC GTGTCCAATC ATCCGAAGTT CGAGGCGGTC CGCCTCGCCT
2151 GCCGTCCGTA CATCTTCACC GCCTCGCTGC CGCCCTCGGT GGTAGCGACC
2201 GCGACGACGT CGATCCGCAA GCTGATGACC GCGCATGAAA AGCGTGAGCG
2251 GCTGTGGTCG AATGCCCGCG CGTTGCATGG CGGGCTGAAG GCGATGGGCT
2301 TCAGGCTCGG CACCGAGACC TGCGACAGCG CGATCGTCGC GGTCATGCTG
2351 GAGGATCAGG AACAGGCCGC GATGATGTGG CAGGCGCTGC TVCGACGGCG
2401 GGCTCTACGT CAACATGGCG CGCCCGCCCG CGACCCCGGC CGGCACCTTC
2451 CTGCTGCGCT GCTCCATCTG TGCCGAGCAC ACGCCGGCGC AGATCCAGAC
2501 CGTGCTGGGC ATGTTCCAGG CCGCGGGCCG CGCGGTCGGC GTCATCGGCC
2551 TCGAGCACCA CCACCACCAC CAC
```

Amino acid sequence of x4M SPT fusion

MGSEAAAQPH ALPADAPDIA PERDLLSKFD GLIAERQKLL DSGVTDPFAI
51VMEQVKSPTE AVIRGKDTIL LGTYNYMGMT FDPDVIAAGK EALEKFGSGT
101NGSRMLNGTF HDHMEVEQAL RDFYGTTGAI VFSTGYMANL GIISTLAGKG
151EYVILDADSH ASIYDGCQQG NAEIVRFRHN SVEDLDKRLG RLPKEPAKLV
201VLEGVYSMLG DIAPLKEMVA VAKKHGAMVL VDEAHSMGFF GPNGRGVYEA
251QGLEGQIDFV VGTFSKSVGT VGGFVVSNHP KFEAVRLACR PYIFTASLPP
301SVVATATTSI RKLMTAHEKR ERLWSNARAL HGGLKAMGFR LGTETCDSAI
351VAVMLEDQEQ AAMMWQALLD GGLYVNMARP PATPAGTFLL RCSICAEHTP
401AQIQTVLGMF QAAGRAVGVI GASENLYFQG TEAAAQPHAL PADAPDIAPE
451RDLLSKFDGL IAERQKLLDS GVTDPFAIVM EQVKSPTEAV IRGKDTILLG
501TYNYMGMTFD PDVIAAGKEA LEKFGSGTNG SRMLNGTFHD HMEVEQALRD
551FYGTTGAIVF STGYMANLGI ISTLAGKGEY VILDADSCAS IYDGCQQGNA
601EIVRFRHNSV EDLDKRLGRL PKEPAKLVVL EGVYSMLGDI APLKEMVAVA
651KKHGAMVLVE EALSMGFFGP NGRGVYEAQG LEGQIDFVVG TFSNSVGTVG
701GFVVSNHPKF EAVRLACRPY IFTASLPPSV VATATTSIRK LMTAHEKRER
751LWSNARALHG GLKAMGFRLG TETCDSAIVA VMLEDQEQAA MMWQALLDGG
801LYVNMARPPA TPAGTFLLRC SICAEHTPAQ IQTVLGMFQA AGRAVGVIGL
851EHHHHH

MW = 92477 DA
ε = 49560

TEV Protease site highlighted in green.
Mutated PLP binding residues highlighted in yellow.

Appendix 2

Peptide mass fingerprinting of the myriocin-modified SPT. Table of peptides assigned after LC-MS analysis of the trypsin digest of the myriocin-modified SPT enzyme. SPT was treated with 200 μM myriocin and incubated at 25 °C overnight. Before MS analysis the sample was reduced with 10 mM $NaBH_4$. Overall sequence coverage observed was 89%. Three species were assigned as tryptic peptides containing the mass 282.24 Da modification ($+C_{18}H_{34}O_2$) - these are listed in **bold**. All three of these peptides span the region of the protein containing Lys265 (highlighted in red).

Mass [M+H] (Da)	Start*	End*	Sequence
2711.2842	-4	22	(R)GSHMASTEAAAQPHALPADAPDIAPER(D)
2711.2842	-4	22	(R)GSHMASTEAAAQPHALPADAPDIAPER(D)
3267.6063	-4	27	(R)GSHMASTEAAAQPHALPADAPDIAPERDLLSK(F)
3267.6063	-4	27	(R)GSHMASTEAAAQPHALPADAPDIAPERDLLSK(F)
4169.072	-4	35	(R)GSHMASTEAAAQPHALPADAPDIAPERDLLSKFDGLIAER(Q)
4425.2256	-4	37	(R)GSHMASTEAAAQPHALPADAPDIAPERDLLSKFDGLIAERQK(L)
7221.6987	-4	63	(R)GSHMASTEAAAQPHALPADAPDIAPERDLLSKFDGLIAERQKLLDSGVTDPFAIVMEQVKSPTEAVIR(G)
11427.7389	-4	103	(R)GSHMASTEAAAQPHALPADAPDIAPERDLLSKFDGLIAERQKLLDSGVTDPFAIVMEQVKSPTEAVIRGKDTILLGTYNYMGMTFDPDVIAAGKEALEKFGSGTNGSR(M)
1476.8057	23	35	(R)DLLSKFDGLIAER(Q)
920.4836	28	35	(K)FDGLIAER(Q)
2218.1788	36	55	(R)QKLLDSGVTDPFAIVMEQVK(S)
5843.9948	36	89	(R)QKLLDSGVTDPFAIVMEQVKSPTEAVIRGKDTILLGTYNYMGMTFDPDVIAAGK(E)
2218.1788	36	55	(R)QKLLDSGVTDPFAIVMEQVK(S)
1962.0252	38	55	(K)LLDSGVTDPFAIVMEQVK(S)
2815.491	38	63	(K)LLDSGVTDPFAIVMEQVKSPTEAVIR(G)
6158.1426	38	94	(K)LLDSGVTDPFAIVMEQVKSPTEAVIRGKDTILLGTYNYMGMTFDPDVIAAGKEALEK(F)
1962.0252	38	55	(K)LLDSGVTDPFAIVMEQVK(S)
2815.491	38	63	(K)LLDSGVTDPFAIVMEQVKSPTEAVIR(G)
872.4836	56	63	(K)SPTEAVIR(G)
3644.8339	56	89	(K)SPTEAVIRGKDTILLGTYNYMGMTFDPDVIAAGK(E)
4215.1352	56	94	(K)SPTEAVIRGKDTILLGTYNYMGMTFDPDVIAAGKEALEK(F)
2791.3681	64	89	(R)GKDTILLGTYNYMGMTFDPDVIAAGK(E)
3361.6694	64	94	(R)GKDTILLGTYNYMGMTFDPDVIAAGKEALEK(F)
4225.058	64	103	(R)GKDTILLGTYNYMGMTFDPDVIAAGKEALEKFGSGTNGSR(M)
2606.2517	66	89	(K)DTILLGTYNYMGMTFDPDVIAAGK(E)
1452.7077	90	103	(K)EALEKFGSGTNGSR(M)
2027.9426	104	120	(R)MLNGTFHDHMEVEQALR(D)

2923.3527	149	175	(K)GEYVILDADSHASIYDGCQQGNAEIVR(F)
1515.7663	176	187	(R)FRHNSVEDLDKR(L)
3735.1315	188	222	(R)LGRLPKEPAKLVVLEGVYSMLGDIAPLKEMVAVAK(K)
3863.2265	188	223	(R)LGRLPKEPAKLVVLEGVYSMLGDIAPLKEMVAVAKK(H)
3735.1315	188	222	(R)LGRLPKEPAKLVVLEGVYSMLGDIAPLKEMVAVAK(K)
3408.9249	191	222	(R)LPKEPAKLVVLEGVYSMLGDIAPLKEMVAVAK(K)
3537.0198	191	223	(R)LPKEPAKLVVLEGVYSMLGDIAPLKEMVAVAKK(H)
3070.6931	194	222	(K)EPAKLVVLEGVYSMLGDIAPLKEMVAVAK(K)
1917.0765	198	215	(K)LVVLEGVYSMLGDIAPLK(E)
2645.4656	198	222	(K)LVVLEGVYSMLGDIAPLKEMVAVAK(K)
2773.5606	198	223	(K)LVVLEGVYSMLGDIAPLKEMVAVAKK(H)
1917.0765	198	215	(K)LVVLEGVYSMLGDIAPLK(E)
2645.4656	198	222	(K)LVVLEGVYSMLGDIAPLKEMVAVAK(K)
747.4069	216	222	(K)EMVAVAK(K)
2357.1278	223	244	(K)KHGAMVLVDEAHSMGFFGPNGR(G)
1484.7856	266	280	(K)SVGTVGGFVVSNHPK(F)
2635.4276	286	310	(R)LACRPYIFTASLPPSVVATATTSIR(K)
2635.4276	286	310	(R)LACRPYIFTASLPPSVVATATTSIR(K)
11427.8736	286	390	(R)LACRPYIFTASLPPSVVATATTSIRKLMTAHEKRERLWSNARALHGGLKAMGFRLGTETCDSAIVAVML EDQEQAAMMWQALLDGGLYVNMARPPATPAGTFLLR(C)
1398.7634	311	321	(R)KLMTAHEKRER(L)
3992.2908	**245**	**280**	**(R)GVYEAQGLEGQIDFVVGTFSKSVGTVGGFVVSNHPK(F)**
4594.6672	**245**	**285**	**(R)GVYEAQGLEGQIDFVVGTFSKSVGTVGGFVVSNHPKFEAVR(L)**
7211.2697	**245**	**310**	**(R)GVYEAQGLEGQIDFVVGTFSKSVGTVGGFVVSNHPKFEAVRLACRPYIFTASLPPSVVATATTSIR(K)**

* Start and End residues are given for wild-type (without the N-terminal His-tag and extension) SPT protein.

Appendix 3

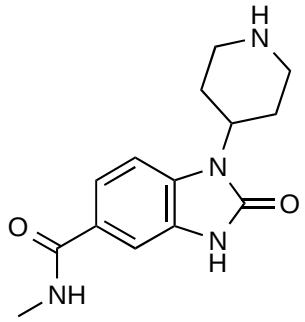

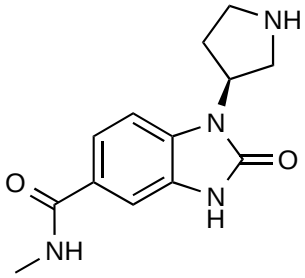

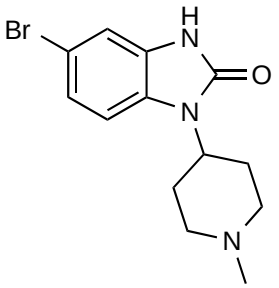

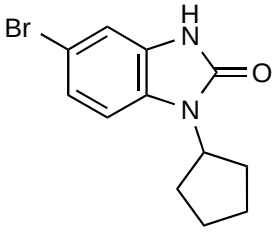

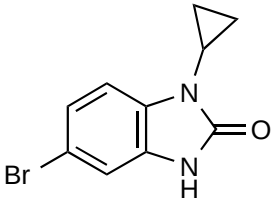

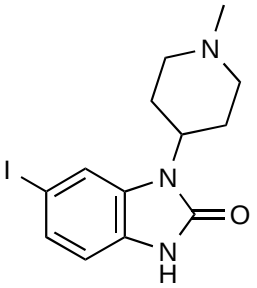

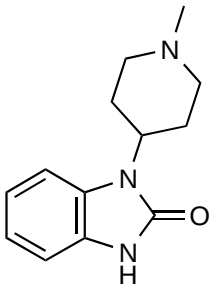

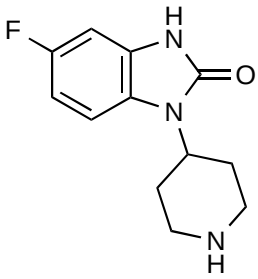

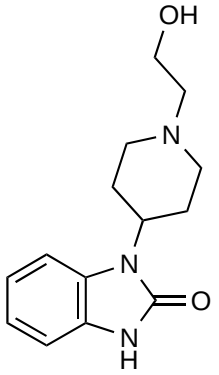

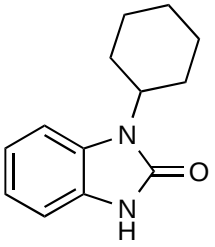

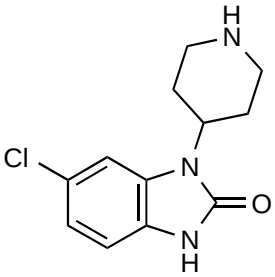

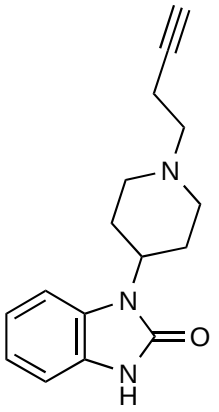

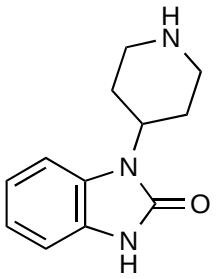

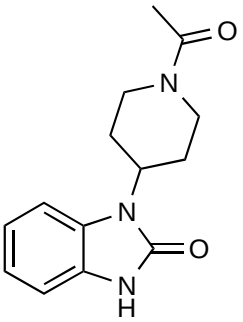

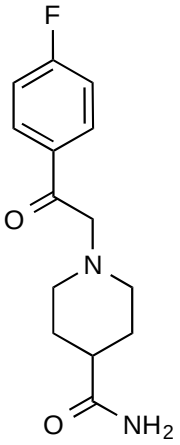

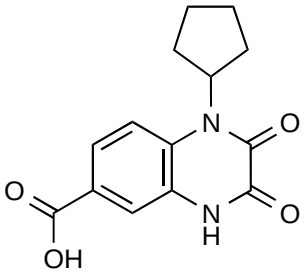

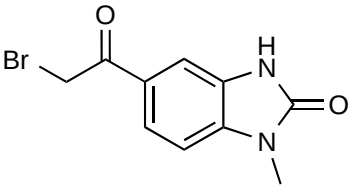

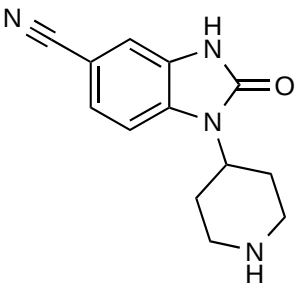

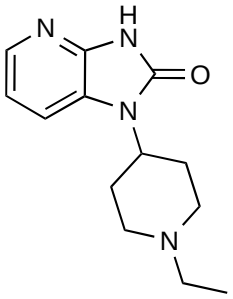

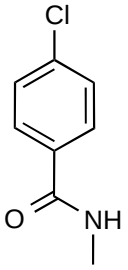

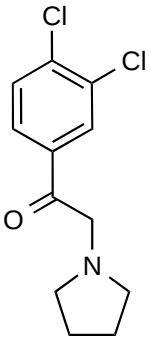

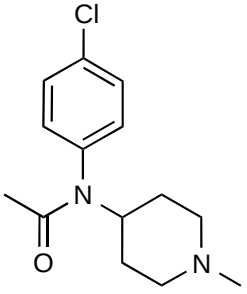

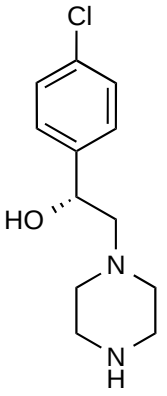

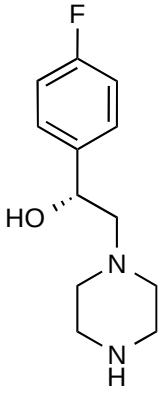

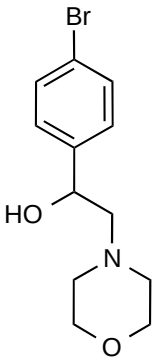
Br
HO
N
O

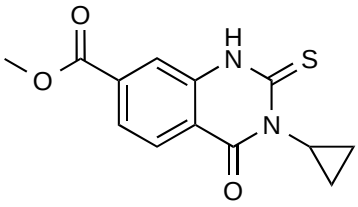
O
O
H
N
S
N
O

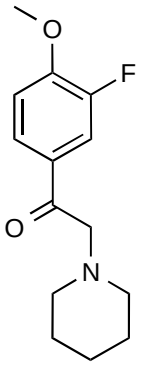
O
F
O
N

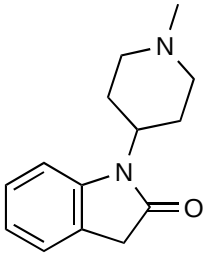
N
N
O

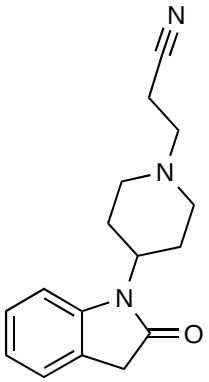
N
N
N
O

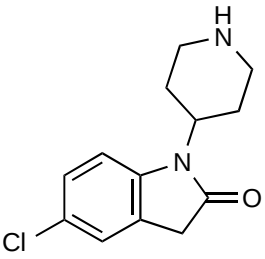
H
N
N
O
Cl

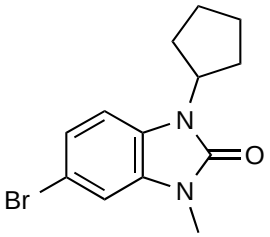
N
O
Br
N

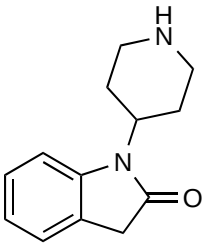
H
N
N
O

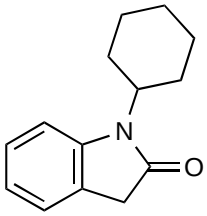
N
O

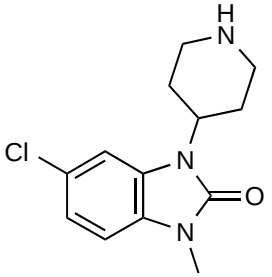
H
N
Cl
N
O
N

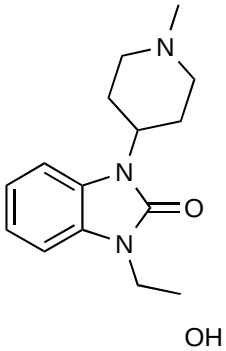
N
N
O
N
OH

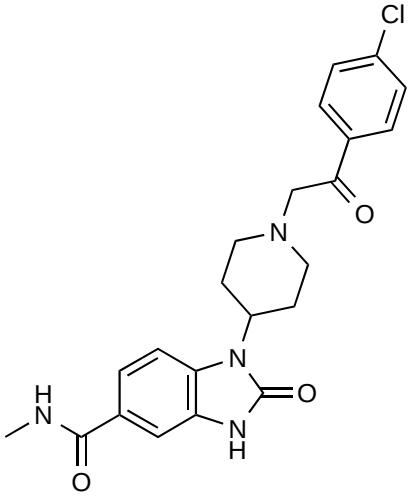
Cl
O
N
N
O
H
N
N
H
O

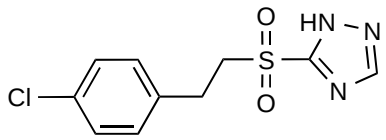
Cl
O
S
O
HN
N
N

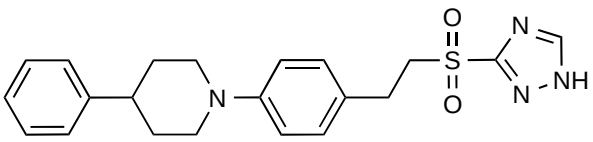
N
O
S
O
N
N
NH

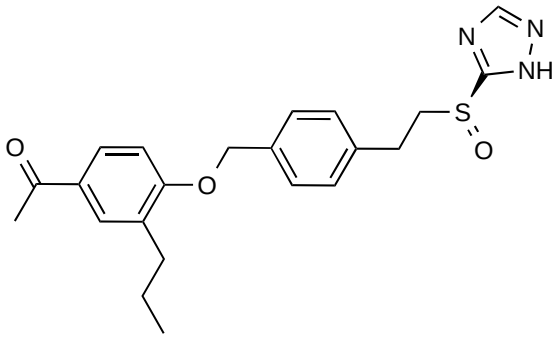
O
O
N
N
NH
S
O

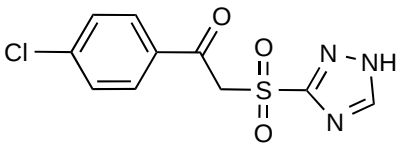
Cl
O
O
S
O
N
NH
N

Publications